Nanoparticle-based delivery of efflux pump inhibitors and antibiotics to treat mycobacterial infections

Reducing thioridazine toxicity to potentiate anti-tuberculosis therapy

Carina Beatrice Vibe

Department of Molecular Biosciences
Faculty of Mathematics and Natural Sciences
UNIVERSITY OF OSLO

September 2014

2014

Nanoparticle-based delivery of efflux pump inhibitors and antibiotics to treat mycobacterial infections

Carina Vibe

http://www.duo.uio.no

Print: Reprosentralen, University of Oslo

Acknowledgements

First of all I would like to thank Gareth Griffiths for including me in his group and encouraging me to pursue an academic career. I would also like to give a big thanks to my co-supervisor Jon Hildahl for our constructive discussions and his willingness to help me succeed. Thanks to Federico Fenaroli for his humor and for teaching me the art of nanoparticle-making, to Lilia Ulanova who taught me zebrafish microinjection and to Martin Speth who helped me with cell and bacterial culture. I am also grateful to all the remaining members of the Griffiths group for their help and support, Urska Repnik, Lasse Evensen, Shahla Bagherifam, Bård Mathiesen, Tone Lian, Patrick Johansen, Eva Berger, Signe Løvmo, Raja Kalluru and Håkon Høgseth. Thanks to Jørgen Benjaminsen for teaching me to keep zebrafish and Ana Tavara for her kindness and advice about zebrafish husbandry.

We would not have been able to set up the luciferase assay without the kind help of Marte Singsås Dragset and Trude Flo. I am also indebted to Marianne Arnemo for valuable help and advice in setting up the luciferase protocol. Thanks to our collaborators in Portugal, notably Miguel Viveiros for encouraging comments, Elsa Anes and David Pires for their advice and for testing our nanoparticles in human cells infected with *Mycobacterium tuberculosis*. I would also like to thank Max Gutierrez, who was very helpful in giving us his advice on primary macrophage BCG infection. A big thanks is owed to Steven Wilson and Dorna Mishagian from the chemistry department for their help with HPLC and nanoparticle characterization. I would also like to thank Carl Henrik Knutsen for sharing his knowledge of statistics, and Catherine Heyward for teaching me how to use the confocal microscope.

Thanks to all my friends, especially Øyvind Ødegård, my first lab partner who for the last five years has helped me with his insight and constructive comments, and Trond Vigtel, for his help and enthusiasm for statistics and coffee. Special thanks to my wonderful boyfriend Thorbjørn Diesen, who has helped and supported me these last four years. Last but not least, a warm thanks to my family for always believing in me, my parents Anita and Johan, my grandmother Leonor and my sisters and brothers Maria Christina, Cecilia, Christopher, Michael, Lucy and especially my twin sister Rosanna.

Oslo, September 2014
Carina Vibe

Abstract

Tuberculosis (TB), caused by *Mycobacterium tuberculosis*, has been treated with the same arsenal of antibiotics since the 1970's; and with an estimated one third of the world's population latently infected at the moment, new regimens are sorely needed. Treatment remains lengthy and difficult, and inappropriate dosing or administration of drugs as well as patient non-compliance is contributing to the rising threat of multi-, extensively- and now totally- drug resistant TB. Should further expansion of resistant strains become a reality it would render our current antibiotics useless. To address the need for new therapies, this thesis explores both *in vitro* and *in vivo* approaches using a novel nanoparticle-based efflux pump inhibitor-antibiotic combination treatment. Bacterial efflux pumps (EPs) are inducible membrane-based transporters that can reduce intracellular concentrations of drugs, which leaves open a window for the development of permanent genetic drug resistance. By blocking these EPs with EP inhibitors such as thioridazine (TZ), while simultaneously treating with one of the most efficient anti-TB drugs, rifampicin (RIF), we predicted a synergistic effect likely caused by an increased intracellular concentration of both drugs in the bacteria. The first aim of this study was to develop a protocol for the encapsulation of TZ in polymeric poly(lactic-co-glycolic) acid nanoparticles (PLGA NPs). Our group has previously established that PLGA NPs with RIF localize in the same cells as the bacteria, and improve therapy both *in vitro* and *in vivo* relative to free drug. Slow release from these particles and facilitated macrophage uptake could potentially lead to treatment that can be administered less frequently in a more targeted and consequently less toxic manner. This may be especially beneficial in the case of TZ, which is associated with serious dose-dependent cardiotoxicity. The second aim of the study was therefore to determine if the encapsulated form of TZ was less toxic than the free form. The third aim of this study was to explore the possible role of TZ as a potentiator of traditional anti-TB therapy. We found that encapsulating TZ in PLGA NPs reduced TZ toxicity, and had a synergistic effect when administered together with RIF. This was the case both *in vitro,* in primary murine macrophages infected with *Mycobacterium bovis* BCG, and *in vivo,* in the zebrafish model infected with *Mycobacterium marinum*.

Selected abbreviations

ABC	Adenosine triphosphate-binding cassette superfamily
ACN	Acetonitrile
ATP	Adenosine triphosphate
BCG	Bacille Calmette-Guérin
BSA	Bovine serum albumin
BSL	Biosafety level
CD14	Cluster of differentiation 14
CFU	Colony forming unit
CPZ	Chlorpromazine
DCM	Dichloromethane
DMEM	Dulbecco's modified eagle medium
DMSO	Dimethyl sulfoxide
dpf	Days post fertilization
dpt	Days post treatment
EBA	Early bactericidal activity
EM	Electron microscopy
EMB	Ethambutol
EP	Efflux pump
Fcγ	Fragment crystallizable gamma
FCS	Fetal calf serum
FDA	American food and drug administration
HPLC	High-pressure liquid chromatography
INH	Isoniazid
MATE	Multidrug and toxic compound extrusion family
M. m	*Mycobacterium marinum*
M. tb	*Mycobacterium tuberculosis*
M-CSF	Macrophage colony-stimulating factor
MDR-TB	Multi-drug resistant tuberculosis
MFS	Major facilitator superfamily
MIC	Minimum inhibitory concentration
MOI	Multiplicity of infection
NP	Nanoparticle

OD_{600}	Optical density at 600 nm
PBS	Phosphate buffered saline
PDI	Polydispersity index
PLGA	Poly(lactic-co-glycolic) acid
PS	Penicillin-streptomycin
PVA	Polyvinyl alcohol
PVP	Polyvinyl pyrrolidone
PZA	Pyrazinamide
RIF	Rifampicin
RLU	Relative light units
RND	Resistance-nodulation-division family
RPMI	Roswell park memorial institute cell medium
RT	Room temperature
SM	Streptomycin
SMR	Small multidrug resistance family
TB	Tuberculosis
TDR-TB	Totally drug resistant tuberculosis
TNF	Tumor necrosis factor
TZ	Thioridazine
VER	Verapamil
WHO	World Health Organization
w/v	Weight/volume
XDR-TB	Extensively drug resistant tuberculosis

Table of contents

1 Introduction

1.1 Tuberculosis: past and present

1.1.1 Historical context

Tuberculosis (TB) is an ancient disease whose causative agent, *Mycobacterium tuberculosis* (*M. tb*), has plagued its human host throughout known history [1]. *M. tb* and related mycobacterial species have been linked to a common progenitor species thought to have originated three million years ago. Extant representatives of this progenitor species have been found in East Africa, where they still cause human TB, suggesting that it is one of humankind's oldest infectious diseases [2]. Various strains of the bacteria from different geographical areas have also been traced back to East Africa, which implies that this is where the ancestral pathogen first emerged. This means that TB and modern humans likely originated in the same place, and it follows that the disease may have affected pre-human hominids as they evolved together [2, 3].

In 1882, Robert Koch was the first to actually link the *M. tb* pathogen to TB disease when he identified the rod-shaped bacterium in material extracted from stained human tubercules, the characteristic lesions formed in infected tissue [4]. Following Koch's discovery, attempts were made to develop a TB vaccine during the early 1900s by Calmette and Guérin at the Pasteur institute in France [1, 5]. Starting with a strain of the closely related *Mycobacterium bovis* in 1908, they spent 11 years attenuating the pathogen by serial passage, even sub-culturing throughout the outbreak of the First World War. The new vaccine was named Bacille Calmette-Guérin (BCG) after its creators and was first tested in humans in 1921. Mass production and distribution of the vaccine soon followed, especially peaking during the outbreak of TB in Asia and Europe that followed the Second World War [6]. It was later found that the attenuation of the bacilli was due to loss of several segments of DNA, notably a crucial virulence determinant coding for a secretion system (ESX-1) [7, 8].

1.1.2 Tuberculosis combination chemotherapy and vaccination

Antibiotic treatment for TB first became available with the introduction of streptomycin (SM) in 1946 [9]. However, the first clinical trial against pulmonary TB already hinted at the presence of SM-resistant bacilli [10]. To circumvent this development of resistance, treatment of bacterial diseases with a combination of two or more independently acting antimicrobial agents was introduced in 1913. During the fifties, several studies

confirmed that this multidrug treatment was less likely to result in resistance and therefore led to more efficient therapy [11]. By the 1970's isoniazid (INH), rifampicin (RIF) and pyrazinamide (PZA), and later ethambutol (EMB), were established as novel anti-tubercular drugs and were soon incorporated into the standard regimen. By using combinations of these drugs, it was found that treatment time could be shortened from twelve to six months, while reducing the rate of relapse from 29 percent to 3-8 percent [9].

According to the standard treatment recommended by the World Health Organization (WHO) today, first-time TB patients who have not been exposed to drug-resistant strains are treated in two phases that together last for a total minimum of six months. The initial phase consists of two months with daily administrations of the first line drugs INH, RIF, PZA, and EMB. This is followed by a four-month continuation phase comprising just INH and RIF [12]. In the case of drug resistance or intolerance to any of the first line drugs, a group of second-line drugs is used, which are more expensive, less efficient and more toxic. These include fluoroquinolones and injectable antimicrobials (capreomycin, kanamycin, and amikacin) [13].

The *Mycobacterium bovis* BCG vaccine continues to be the only vaccine available against TB, despite ongoing efforts to develop novel strategies [14]. In its more than 80 years of use, BCG has been delivered to more people than any other vaccine. Unfortunately, while it does protect to an appreciable degree against childhood TB (miliary and meningeal), it is not nearly as effective at protecting adults from pulmonary TB, the most prevalent form of TB today [15].

1.1.3 Current prevalence

M. tb infections can either persist in an active, infectious state associated with the clinical symptoms of TB, or a latent state where patients are asymptomatic and non-infectious. According to the WHO, in 2012 it was estimated that 12 million people had active TB, whereas one third of the world's population had latent TB [16]. Of these latently infected individuals, 5-20% will go on to develop an active, infectious form of the disease during their lifetime [16]. This progression to active disease is fueled by several circumstances, among others immunosuppression due to co-infection with HIV, malnutrition, diabetes or alcohol abuse. Although drug-sensitive TB is considered curable, in 2012 a staggering 8.6 million people contracted active TB, and 1.3 million died from the disease, a high proportion of which were HIV positive. Eastern Europe, Africa and South-East Asia are bearing the highest

burden of the disease. Among these, India and China stand out with the two highest incidence rates, while TB co-infection with HIV was highest in the African region [16].

1.2 Routes of infection and dissemination

1.2.1 Initial infection

M. tb is an intracellular pathogen that usually spreads from person to person by coughing or sneezing, resulting in airborne droplets that contain the bacteria. When these droplets are inhaled, the bacteria enter the lungs where they are ingested by alveolar macrophages [17]. Unlike extracellular pathogens, *M. tb* has developed several mechanisms to ensure macrophage uptake by phagocytosis, including non-traditional mechanisms to induce opsonization by complement factors leading to uptake by complement receptors [18]. *M. tb* can also be taken up following binding to mannose receptors, CD14 binding, scavenger receptors or Fcγ receptors [18]. Regardless of the receptors involved, phagocytosis leads to the internalization of *M. tb* in a membrane-bound phagosome. Phagosomes are normally able to interact with the endocytic pathway where they mature and fuse with lysosomes, causing a drop in pH which aids in degradation of the phago-lysosomal content [19]. To avoid this fate, *M. tb* is able to block phagosome maturation by arresting phago-lysosome fusion [19, 20]; the bacteria then remain in a phagosome with a pH of 6.4 [21]. Sheltered in this intracellular niche, the bacteria are able to exploit the host cells nutrients, such as iron from transferrin [22]. Before macrophages are activated by the adaptive immune system, they are often able to contain, but not clear the infection, allowing *M. tb* to persist intracellularly [23]. In most cases the bacteria can enter a state of prolonged dormancy, which is what characterizes a latent infection. Hidden inside an infected macrophage they can be protected from the rest of the immune system by blocking host antigen presentation and modulating cytokine production [24]. On the other hand, if the bacteria instead proliferate inside the macrophage, they can spread and cause the active, infectious form of TB [25]. Infected macrophages can then recruit healthy macrophages, which can in turn be infected when they encounter extracellular bacteria at the disease site. This starts the process of granuloma formation [26].

1.2.2 The granuloma

Often referred to as “the hallmark structure of TB”, the granuloma plays an important role in the balance between eradication and advancement of the disease. This tightly packed structure is made up of a variety of immune cells, which are clustered together in order to

contain a central core of infected and necrotic cells as well as extracellular bacteria released from dying macrophages [27]. Granuloma formation is initiated by infected alveolar macrophages, which provoke an inflammatory response capable of recruiting additional immune cells; including more macrophages, neutrophils, monocytes and dendritic cells [28]. Activated dendritic cells then drain to the lymph node [29, 30] and in turn recruit B cells and T cells which also aggregate at the infection site, aiding in bacterial killing and macrophage activation [28]. With the help of the adaptive immune system, macrophages mature, increase their microbicidal capacity and change their morphology, becoming larger with ruffled cell membranes [27]. Sustained release of the cytokine Tumor Necrosis Factor (TNF) by macrophages and T cells play a major role in recruitment of cells and granuloma maintenance [28, 31]. In addition to walling off bacterial infection, the granuloma creates a local environment tuned to restricting potentially harmful inflammation, as well as facilitating interaction between the adaptive and innate immune system [31].

1.2.3 Transmission

Despite the efforts of both the innate and adaptive immune cells to clear the *M. tb* infection, some macrophages will become overwhelmed and undergo necrosis. This leads to the formation of a characteristic necrotic core known as the caseum. The caseum can disintegrate, or "liquefy", providing an excellent medium for the extracellular growth of bacteria released from dying macrophages. Necrotic tissue surrounding the granuloma can rupture, and may subsequently spread the infection to other parts of the lung or release viable *M. tb* into the airways [17]. Subsequent coughing and expulsion of droplets allows the mycobacteria an opportunity to escape the lungs and infect other hosts, re-starting the cycle of TB [27, 28].

1.3 The emergence of resistance

1.3.1 Multi-drug resistant TB

Although the global mortality rate from TB has fallen by 45% since 1990, the emergence of multi-drug resistant TB (MDR-TB) is a growing threat. TB is considered MDR when it is resistant to RIF and INH, two of the most potent first line drugs. There were an estimated 450,000 new incidences of MDR-TB in 2012, which makes up about 5% of total incident TB cases that year. However, of the 1.3 million people that died from TB in 2012, 13% died from MDR-TB, indicating that MDR-TB is proportionally more lethal than

susceptible TB. The majority of these MDR cases were registered in Eastern Europe and Asia, notably in India, China and Russia [16]. This emerging drug-resistance has been fueled by sub-optimal dosing of antibiotics during treatment, in part caused by failure of health care providers to follow and supervise treatment and drug quality according to WHO standards. In addition, inappropriate use of antibiotics has been linked to a lack of patient compliance, made especially difficult by the long course of treatment which can be expensive, toxic and cumbersome [12, 32]. Lastly, granulomas are heterogeneous and difficult to penetrate, which can lead to inadequate accumulation of drugs at the disease site [33]. Even if efforts are made to reduce the risk of resistance by using combination therapy, sub-lethal doses of these drugs can not only allow bacteria to survive, leading to relapse, but also select for resistant bacterial genotypes [13]. In addition to the possibility for *M. tb* to acquire novel genetic resistance during treatment, MDR-TB can also be transmitted to new hosts. In fact, up to half of MDR cases occur by re-infection of previously untreated patients [34].

Mycobacteria become genetically resistant as a result of spontaneous mutations that interfere with the intended function of the antibiotics. Unlike in other bacterial species, acquired resistance is not believed to occur by horizontal gene transfer in *M. tb* due to its lack of plasmids and no documented cases of genomic DNA transfer [35]. Genetic resistance can arise through a mutation in the drug target itself, drug-deactivating enzymes or in enzymes needed for pro-drug activation [36]. In the case of TB, specific mutations have been associated with resistance to all four first-line TB drugs currently in use [35]. Since each antibiotic targets a different bacterial mechanism, each one has an independent rate of mutation. Even if genetic mutations are rare, a single resistant clone early in infection can survive antibiotic treatment and give rise to an entire population of resistant organisms [9]. The likelihood that clonal expansion of *M. tb* in an infected patient will give rise to resistance to both the independently-acting drugs INH and RIF has been placed in the range of 10^{-5} to 10^{-4} [37]. This is relatively rare in areas of low TB incidence, but seen in the context of the global TB burden, with 8.6 million new active cases in 2012 [16], the emergence of dual resistance is feasible [37]. With this in mind, using a combination of more than two different antibiotics is necessary to lower this risk and more efficiently clear the infection [38].

1.3.2 Extensively and totally drug-resistant TB

When bacteria turn MDR and become resistant to any of the first-line drugs, patients are forced to use more toxic and less efficient second- and third-line drugs. These regimens

are longer than treatment for standard TB, with a minimum duration of 18-20 months [12]. This further increases the risk of patient non-compliance, which is conducive to the development of even more resistance. These strains are known as extensively drug-resistant (XDR-TB), and have not only lost susceptibility to RIF and INH, but also to at least two second-line drugs. By the end of 2012, XDR-TB was reported by 92 countries, making up an estimated 9.6% of the MDR cases [16]. To make matters worse, strains of totally drug-resistant TB (TDR-TB) were reported in Italy in 2007 [39]. These exhibited resistance to the full range of our current first- and -second line drug regimens. There have now also been reports of TDR-TB in Iran, India and South Africa [40]. With the threat of drug resistance rendering our current antibiotics useless, it has been suggested that the "antibiotic era" is over [13]. However, even if progress is slow, there are several new classes of drugs currently being tested against TB, with 12 currently undergoing clinical trials [41].

1.4 Phenotypic resistance

1.4.1 The distinction between genetic and phenotypic resistance

While some patients respond rapidly to treatment, others have infections which appear resistant in that they do not respond to antibiotics, yet the offending bacteria are deemed susceptible to therapeutic concentrations *in vitro* [42]. These bacteria are resistant, but they have no genetic mutations in known drug targets [43, 44], implying the existence of other, non-genetic, mechanisms of resistance. Here an important distinction is brought to light: bacteria that are not considered genetically resistant to antibiotics may still be able to persist due to non-genetic mechanisms. This phenomenon is known as phenotypic resistance [45]. Until this point in the introduction, the term "resistance" has always been mentioned in the context of a genetic change. To be able to distinguish between genetic and phenotypic resistance, it is important to present clear definitions of the relevant terminology.

In the context of this work, resistance to a given drug is defined as the ability of bacteria to continue replicating in the face of a determined minimum inhibitory concentration (MIC) of drug, which normally prevents such replication. This means that resistance is relative to the defined MIC, and that the development of resistance causes an increase in the said MIC [36]. Further, such resistance is genetic when it is caused by a change in the DNA sequence of the bacterium, as described in section 1.3.1. On the other hand, resistance is considered phenotypic when it arises through other, non-genetic mechanisms stimulated by

the bacterial environment. Importantly, this kind of increase in MIC as a result of induced phenotypic resistance is not heritable, as it would be in a genetically resistant strain.

1.4.2 Phenotypic resistance in dormant cells

Phenotypic reduction in antibiotic susceptibility was first observed in dormant cells, such as those found in latent infections, in the context of many different antibiotics, including anti-TB drugs [46, 47]. This is because these drugs usually target mechanisms necessary for bacterial growth and proliferation, such as bacterial transcription in the case of RIF, or mycolic acid production in the case of INH [47]. In fact, bactericidal activity of INH is reduced 1000-fold in non-growing cultures relative to log-phase cultures of *M. tb* [48]. *M. tb* is an obligate aerobe, but can live in the hypoxic, nutrient-poor environments near the center of the granuloma where such a slow-growing state can be induced, helping it to survive treatment [49, 50]. These differences in antimicrobial susceptibility cause bacterial killing to occur in a biphasic manner. In the initial phase, the antimicrobial in question will rapidly kill the metabolically active, susceptible sub-population of bacilli (quantified as the early bactericidal activity, EBA, of this drug) [51]. In the second phase, the remaining persistent bacteria, which are more difficult to sterilize, necessitate longer treatment in order to get complete clearance of the infection [51, 52]. The dormant bacilli remain as a latent infection and may lead to relapse if treatment is too short, whereas the replicating bacilli cause the symptoms of active disease [52].

1.4.3 The role of efflux pumps

Until recently, most models explaining phenotypic resistance in *M. tb*, and consequently efforts to find novel drug targets, have built on the assumption of dormancy [53]. In contrast to this, newer models suggest that non-heritable multi-drug phenotypic resistance can also be found in actively replicating *M. tb*, as shown by Adams *et al.* [53] in the zebrafish model. In this study, phenotypic resistance was linked to the action of efflux pumps (EPs), which can reduce drug efficacy by limiting its intracellular accumulation [54].

EPs are highly conserved, membrane-associated transporters important for the active removal of toxic substances from the bacterial cell. These pumps can either be very specific or recognize a variety of substrates, such as toxins from the environment, including antibiotics or host-derived substances, or intracellular metabolites to maintain homeostasis [54, 55]. EPs can be found in both eukaryotic cells and a wide variety of bacteria and are

subdivided into five distinct families according to their structure and function. These are the adenosine-triphosphate-binding cassette (ABC) superfamily, the major facilitator superfamily (MFS), the small multidrug resistance (SMR) family, the resistance-nodulation-division (RND) family and the multidrug and toxic compound extrusion (MATE) family [54]. Nearly 50 putative EPs have been identified in *M. tb* [56]. Furthermore, *M. tb* knock-outs of EPs from the ABC, MFS and SMR families conferred an increase in susceptibility to several antibiotics, including the first-line TB drugs RIF, INH and EMB and the second-line TB drugs kanamycin and amikacin [57]. In mycobacteria, it has been suggested that up-regulation of EPs precedes genetic mutations in drug target genes following exposure to anti-TB drugs [58]. The up-regulation of such pumps works to counter intracellular drug accumulation, allowing bacteria to keep replicating in the face of treatment. This continued replication opens the possibility for accumulation of mutations, which can lead to permanent genetic resistance [58].

Constitutively expressed EPs also contribute to intrinsic resistance in mycobacteria [59]. Intrinsic resistance is the inherent ability of a given bacterial species to tolerate a given antibiotic, for example if it lacks the drug target or produces drug-deactivating enzymes [59]. In addition to EP-mediated intrinsic resistance, *M. tb* has a characteristic waxy cell wall, rich in mycolic acid, an uncommon long-chain fatty acid, which makes it largely impermeable to antibiotics [60], although some influx of hydrophilic compounds may occur through a limited amount of porins [61].

As opposed to constitutive expression, the up-regulation of EPs can also be transiently induced by the presence of antibiotics. For example, EPs from the ABC, MFS and SMR families up-regulate following exposure to all the drugs in the standard TB regimen [62]. One study documented the up-regulation of three genes in response to INH, (*ini*A, B and C), where *ini*A appeared to be a pump component participating in INH removal. Furthermore, an *M. tb* mutant with an *ini*A deletion showed increased INH susceptibility [63]. In the absence of antibiotics, mycobacterial EPs can also be induced by intracellular residence. In a study by Adams *et al*. [53], *M. tb* and the fish pathogen *Mycobacterium marinum* (*M. m*) cultured inside macrophages were more resistant to RIF in comparison to bacteria grown extracellularly. However, this was no longer the case when *M. tb* strains lacked a functional copy of the EP gene *Rv1258c* [53], which is up-regulated in the presence of RIF [64]. This suggests the involvement of this EP in macrophage-induced resistance [53]. Moreover, resistance to RIF in both *M. tb* and *M. m* was reduced in the presence of the EP inhibitor verapamil. This increase in MIC was non-heritable, implicating phenotypic resistance [53].

In the aforementioned cases, EPs are up-regulated by mechanisms that are independent of genetic change, placing them in the phenotypic resistance category. Despite this, genetic mutations in EP genes or their regulatory elements, such as promoters or transcriptional activators can also lead to EP over-expression [65]. Ultimately, be it by genetic or non-genetic mechanisms, increased EP expression leads to acquired resistance in organisms that should normally be susceptible to a given drug. Importantly, due to the promiscuous nature of some EPs, heightened expression of a single pump can lead to an increase in the MIC of several drugs and, accordingly, a MDR phenotype [65].

In summary, EPs have been used to explain several facets of resistance to drugs. First of all they contribute to intrinsic resistance to antibiotics, together with the mycolic acid cell wall. Secondly, they can contribute to phenotypic resistance by means of their non-genetic up-regulation, which can either be induced by antibiotics or by macrophage residence. Lastly, they can contribute to acquired MDR by means of genetic mutations in regulatory elements or the pumps themselves. However, it is possible to block EPs using EP inhibitors, one example being verapamil. Thioridazine (TZ) is another such EP inhibitor that has been gaining interest as a novel anti-TB drug candidate [53, 66, 67].

1.5 Efflux pump inhibitors

1.5.1 Thioridazine

TZ is a drug that belongs to the phenothiazine group, and has previously been used as a neuroleptic for the treatment of Schizophrenia. It has now been removed from the market in several countries due to its potentially serious cardiotoxic side-effects, such as prolongation of the QT interval [68-70], which is a measurement of the time between ventricular depolarization and repolarization. This can lead to an abnormal heartbeat, or ventricular arrhythmia, and increases the risk of sudden death [71]. Before the introduction of TZ, the first phenothiazine used as a neuroleptic was chlorpromazine (CPZ) [66]. Early on, there were anecdotal reports of the positive effect CPZ had on TB infected patients. However, this was never seriously pursued due to the emergence of the new antibiotics SM and INH during the 1950's, which were more efficient and less toxic than CPZ [72]. Since then, several groups have documented the anti-TB effects of both CPZ and TZ at similar concentrations *in vitro* [72-75]. TZ in particular has been shown to not only inhibit growth of susceptible *M. tb,* but also MDR-strains. In one study, TZ showed 60% inhibition of growth in liquid cultures of *M. tb* at 3 μg/ml and complete inhibition in the range of 12-25 μg/mL [76].

Unfortunately, a mere concentration of 0.5 μg/ml is considered the maximum safe level of TZ in human plasma, which on its own makes it unlikely that this drug can be administered safely at therapeutic concentrations [66]. However, an *in vitro* study from 1992 by Crowle *et al.* [72] showed that approximately 8-fold lower doses of CPZ were needed to inhibit growth of *M. tb* inside macrophages in comparison to extracellular *M. tb.* Although there was no direct evidence for this, Crowle suggested that the effect could be due to an accumulation of CPZ in lysosomes containing the bacteria, implying that lower, less toxic concentrations would be sufficient to reach bactericidal levels *in vivo*. With this in mind, there is some evidence that supports the tendency of phenothiazines to accumulate in eukaryotic cells, by binding to membranes [77], including lysosomal membranes, and concentrating in tissues, especially liver, lung and kidney [78]. More recently, pre-treating macrophages with TZ was found to inhibit intracellular growth of *M. tb* at 0.1 μg/ml regardless of antibiotic susceptibility, when the MIC in culture was found to be as high as 15 μg/ml [74]. This enhanced effect after phagocytosis has also been seen in other intracellular bacteria, such as *Staphylococcus aureus* [79].

TZ and related phenothiazines have been shown to inhibit the action of bacterial EPs by a fluorometric assay in BCG [80]. TZ also inhibits the expression of several EPs, including mmpl7 (associated with INH resistance) and p55 (associated with RIF resistance) [80]. However, it is unclear if EP inhibition is TZ's primary mechanism of action, as they have a variety of targets in both bacterial and eukaryotic cells. Apart from its activity against EPs, TZ has other physiological targets involved in cellular respiration in *M. tb*. For instance, TZ blocks the electron transport chain in mycobacteria by inhibiting type II NADH dehydrogenases [81], succinate dehydrogenase and calcium binding to proteins [82]. TZ has also been implicated in *M. tb* cell envelope damage [83]. Apart from this wide variety of bacterial targets, phenothiazines like TZ also have a hypothesized effect in eukaryotic cells, enhancing the killing effect of macrophages [84]. The fact that TZ has several different mechanisms of action against TB reduces the risk of developing TZ resistance [85].

1.5.2 Combination therapy using antibiotics and efflux pump inhibitors

To combat efflux-mediated tolerance in bacteria, a novel therapy involves a combination of EP inhibitors, such as TZ, with an antibiotic to which the organism has become resistant (**Figure 1.1**). Blocking active drug extrusion by bacterial EPs is expected to restore antibiotic susceptibility and therefore the curative potential of the drug [84, 86]. In the

first studies on CPZ, Crowle *et al.* already found a synergistic treatment effect of this drug with PZA, RIF and INH against bacteria inside macrophages [72]. This *in vitro* synergy was also seen when using TZ with SM and RIF against MDR-strains by Viveiros *et al.* [87].

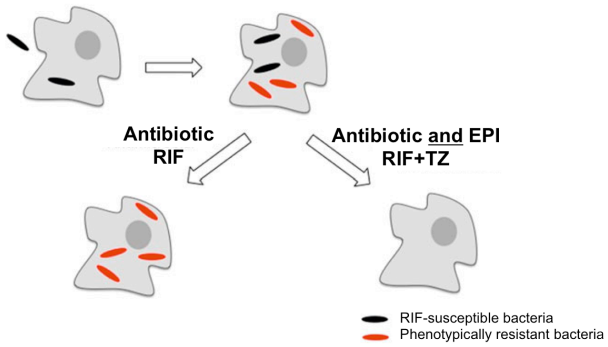

Figure 1.1: Treating with traditional anti-TB drugs such as RIF will not clear intracellular infections with phenotypically resistant bacteria, which among other strategies can reduce RIF efficiency by up-regulating EPs. A novel therapy involves combining RIF with the EP inhibitor (EPI) TZ to clear both susceptible and phenotypically resistant bacteria. Modified from Szumowski *et al.* [88].

As mentioned above, most of the studies done on the antimicrobial effects of TZ and other phenothiazines have been done *in vitro* [74, 75]. However, there have been some *in vivo* studies in the TB mouse model, where bacillary load is quantified from the lungs. These studies show significant reductions in CFUs using both TZ monotherapy and combination treatment with antibiotics, although residual bacteria remained [85, 89, 90]. In one study, Dutta *et al.* [89] did not see any additional treatment effect when using TZ at 10 mg/kg alone or in combination with RIF, although it did improve INH treatment. On the other hand, van Soolingen *et al.* [85] showed that a higher dose of TZ was effective against both drug susceptible and resistant strains *in vivo,* both on its own and in combination with antibiotics. Daily administration of 32 and 70 mg/kg TZ in mice for two months both gave a five-fold decrease in CFUs of susceptible *M. tb* strains. However, due to toxicity concerns with the high dose of TZ, the lower dose of 32 mg/kg was preferred. Additionally, adding 32mg/kg TZ to the standard regimen using RIF, INH and PZA further reduced the bacterial burden in mice [85]. The EP inhibitor verapamil has also been used *in vivo*, where it potentiated the antimicrobial effect of standard TB antibiotics and reduced the rate of relapse [91].

Unlike most of the drugs in the anti-TB regimen, TZ also efficiently kills both actively growing *M. tb* and *M. tb* with hypoxia-induced dormancy [82]. This is a great advantage when it comes to dealing with the non-replicating persisters implicated in *M. tb* relapse and latent infections [85]. TZ's potential against persisters together with its ability to increase the efficiency of the other drugs in our current antimicrobial arsenal makes it an

ideal drug to include in the anti-TB regimen. TZ has actually already been used for compassionate therapy in combination with second-line drugs in a few XDR-TB patients in Argentina and India, with promising results [92, 93]. However, the fact remains that TZ is associated with severe negative side effects, and these studies were therefore carried out under strict monitoring for cardiotoxicity. In this respect, limiting this toxicity is an important and necessary step before TZ can be considered for the standard anti-TB regimen.

1.6 The Zebrafish model of mycobacterial infection

1.6.1 The Zebrafish model of tuberculosis

Several animal models are used to study TB, including rodents, rabbits and non-human primates infected with *M. tb* itself and fish or frogs infected with *Mycobacterium marinum (M. m)* [94]. Among these models, TB in non-human primates most closely resembles the disease in humans [95]. Unfortunately, this model presents several ethical and practical difficulties, in addition to being prohibitively expensive for many studies. In contrast, mouse models using *M. tb* are less problematic and well established [94], but they do not accurately reflect many important aspects of the disease in humans. Importantly, granulomas in mice are not well organized and do not exhibit caseation, necrosis, fibrosis or calcification, which are characteristic traits of a TB granuloma in human patients [96, 97].

The zebrafish (*Danio rerio*), on the other hand, provides a simple yet powerful model for TB research due to its optical transparency and similarities to pathogenesis in human TB. The zebrafish is a small freshwater fish naturally found in India, Pakistan and Bhutan, which has become a common model organism used to study both developmental biology and human disease [98, 99]. Unlike the mouse model of TB, *M. m* infection in the zebrafish model yields caseating, well-organized granulomas, morphologically similar to granulomas in human TB [100, 101].

Both zebrafish embryos and adult fish are susceptible to mycobacterial infection [102, 103]. However, zebrafish embryos initially only rely on their innate immunity, with functional macrophages at 1 day post fertilization (dpf) [104]. Lymphocytes start appearing at 4 dpf, but a mature adaptive immunity is only present after about 4 weeks [105]. Despite this lack of adaptive immunity, early embryonic macrophages can phagocytose the mycobacteria and form tight aggregates. These are histologically similar to granulomas found in adult zebrafish and humans and are accompanied by the up-regulation of granuloma-associated genes [103], although they have fewer lymphocytes [100]. This implies that the innate

immunity is sufficient to launch the granulomatous response, despite the fact that lymphocytes aid in controlling bacterial growth later in infection [100]. In this way, zebrafish have provided new insights into TB pathogenesis, as it was previously believed that adaptive immunity was required for granuloma formation [106].

The TB-like infection produced by *M. m*, often referred to as fish TB, can be treated using the same drugs as in human TB, which all efficiently clear *M. m* infections in zebrafish (except pyrazinamide, to which *M. m* is inherently resistant). Using combinations of the different drugs also significantly improves treatment, closely replicating human data [53]. Importantly, embryos are optically transparent for the first two weeks post fertilization, allowing for real-time imaging of infections and therapy [103]. In addition to this, zebrafish are relatively easy to maintain and breed, with a single female potentially laying up to 200 eggs per week [99]. Zebrafish embryos develop quickly, with most of their important organs in place when they naturally hatch after three days [99]. Furthermore, the genomes of both zebrafish and *M. m* have been fully sequenced [107, 108], and a wealth of transgenic animals exist [100]. The relative ease of keeping zebrafish at high densities and their efficient production of embryos offers potential for high throughput analysis [109].

1.6.2 *Mycobacterium marinum* as a model for *Mycobacterium tuberculosis*

M. m is a naturally occurring pathogen in fish and other ectotherms that causes a systemic granulomatous disease [101, 110]. *M. m* is one of the two closest relatives to *M. tb* outside the *M. tb* complex, the other being *M. ulcerans* [111], making it an obvious model for human TB in the zebrafish model. Unlike *M. tb*, which grows optimally at 37°C, *M. m* grows at 30-32 °C and therefore rarely causes systemic infections in humans but can rather cause superficial lesions known as “swimmer’s granulomas” [97]. *M. m* grows optimally in the dark [112] and has a generation time of four hours during logarithmic growth, compared to the >20 hour generation time needed for *M. tb.* As *M. m* grows relatively fast and is a biosafety level-2 (BSL-2) pathogen, it is easier to maintain and work with in the lab compared to the slow growing *M. tb*, which requires BSL-3 facilities [102]. Like *M. tb, M. m* infects macrophages and replicates intracellularly by arresting phagosome maturation to prevent phago-lysosome fusion, a mechanism that is essential to mycobacterial virulence [97, 101]. *M. m* has orthologs for 80% of all coding sequences in *M. tb*, and these have an average of 85% amino acid identity [108]. The similarity to *M. tb* combined with the relatively short generation time and lower BSL requirements make *M. m* an ideal model for TB in the lab.

1.7 The nanoparticle approach to drug delivery

1.7.1 Drug delivery using polymeric nanoparticles

Conventional drugs administered in their free form face many complications when navigating a complex *in vivo* environment. They need to reach granulomas, which are heterogeneous and difficult to penetrate, making it hard to predict if the drug will be able to accumulate there. An additional level of complexity involves the fact that bacteria can exist both within macrophages in granulomas or in individual cells, or extracellularly in hypoxic caseating granuloma lesions or in liquefied cavities. Some of these bacteria may be dormant and some actively replicating [96]. Granulomas themselves also evolve over the course of an infection, starting out as mainly cellular structures that are easier to penetrate but progressively become less accessible to free drugs due to fibrosis and calcification [33]. Granulomas also differ in their extent of vascularization, which may not only limit the entry of oxygen and nutrients, but can also restrict transport of free drugs to the site of infection [49]. The difficulties of penetrating this complex and dynamic *in vivo* landscape are illustrated by the fact that levels of drugs actually accumulating in a granulomatous lesion are much lower than what is detected in the plasma. The consequence of this is that drugs that have high antimicrobial activity *in vitro* need to be administered for long periods of time, which can lead to non-compliance in patients [33]. This pharmacodynamic information was limited when the standard anti-TB regimen was designed and it is therefore thought that with current dosing standards sub-optimal amounts of RIF actually reach the granuloma. Due to this low efficiency, higher doses of RIF have been suggested for the standard treatment against TB [113].

Polymeric nanoparticles (NPs) are vehicles used for the delivery of drugs or other agents by means of their entrapment or adsorption to a polymer matrix or by chemical bonding to the polymer. Unlike free drug delivery, NP-based drug delivery allows more efficient targeting of drugs to the diseased site. It has been shown that NPs are rapidly phagocytosed by macrophages and brought to the granuloma for local release in zebrafish embryos [114]. The granuloma was previously regarded as a rigid structure but has now been observed to be more dynamic, with highly motile macrophages and the presence of both infected and non-infected macrophages at the necrotic core [27]. Instead of relying on chance penetration of a granuloma by diffusion through tissue or delivery by sporadic vasculature, NPs with RIF and other anti-TB drugs can efficiently be carried to the site of disease inside macrophages traveling to and from the granuloma, eliminating the need to increase drug

doses [114]. This high turnover of macrophages opens for the possibility that new NPs can continuously be brought to the granuloma with repeated administration of encapsulated drugs. However, this would rely on the assumption that the highly dynamic state lasts beyond the initial stages of granuloma formation, into the later stages of fibrosis and calcification, which may not be the case.

Different authors vary somewhat in their ideas of the size range accepted under the definition of NPs, some of which set a range of 10-999 nm, which is the definition used here. The concept of using biodegradable polymers for the sustained release of drugs was first conceived in the 1970s [115]. Since then, nano- and micro-particle formulation using both natural and synthetic polymers have gained significant interest [116]. Unlike conventional free drug delivery, polymeric NPs can be tuned to slowly release drugs in a controlled manner, which contributes to keeping drug concentrations at therapeutically significant levels for longer periods of time. In addition, encapsulation can protect the content- especially in the case of small molecules, DNA or peptides- from degradation and rapid clearance from the body [116].

NP-delivery facilitates local administration, as particles can in theory be targeted passively or actively to exactly where they are needed. Active targeting involves functionalizing the surface with affinity ligands such as antibodies. Passive targeting, on the other hand, does not require any additional ligands as NPs of submicron size are rapidly recognized and taken up by professional phagocytes [114]. Instead of administering high amounts of drug to raise the concentration in the plasma, NPs can be taken up by macrophages and other phagocytes, including neutrophils and monocytes. In this way, less drug can be administered as therapeutic concentrations are achieved locally, sparing healthy tissue from toxic side effects associated with free drug delivery [117].

1.7.2 Nanoparticles for tuberculosis therapy

NP treatment against TB has gained interest due to research by Gopal Khuller and his group, working on murine and guinea pig models of TB. They were able to show that NP delivery improved drug efficiency and reduced the number of doses needed for an improved treatment effect [118-122]. Our group has also shown that NPs localize at the site of infection [114], and RIF encapsulated in NPs is more efficient in clearing mycobacterial infections relative to the corresponding dose of free RIF, both *in vitro* [123] and in the zebrafish model [114]. Using NPs for TB therapy may contribute to shorten the duration of treatment, reduce

frequency of dosing and improve delivery by passive targeting and local release. This new approach to our current anti-TB treatment would be a great advantage in reducing non-compliance and improving treatment efficacy. Passively targeted NPs can be delivered by macrophages to the site of disease, and slow release inside the granuloma, which is normally difficult to penetrate, can help to keep the drugs at therapeutic concentrations and for an adequate amount of time [49, 114].

1.7.3 Encapsulation using the copolymer poly(lactic-co-glycolic) acid

Poly(lactic-co-glycolic) acid (PLGA) is a copolymer commonly used for drug delivery, including the formulation of nano- and microspheres [124]. In the presence of water, the ester linkages in the PLGA polymer are broken down by hydrolysis to yield the monomers lactic acid and glycolic acid. These are byproducts of normal cellular metabolism, and can therefore be broken down to carbon dioxide in the citric acid cycle under physiological conditions [125]. Due to its biocompatible and biodegradable nature, PLGA is not considered toxic and has been FDA-approved for use in human therapy [124, 125].

PLGA copolymers can be synthesized with different ratios of lactic acid to glycolic acid, where a higher proportion of lactic acid makes the polymer more hydrophobic and less biodegradable. PLGA with equal ratios of both monomers (PLGA 50:50) has the fastest rate of degradation and is therefore the most biocompatible [126]. The rate of drug release from the NPs is determined by both polymer degradation and drug diffusion through pores or the remaining polymer matrix. This in turn depends on the nature and size of the drug molecule and polymer. In addition, a drug may be loosely attached to the particle surface or embedded in the particle surface [115]. In order for this drug to be internalized in cells, the NPs need to be taken up by macrophages phagocytosis. Both uptake and bio-distribution of NPs is, therefore, dependent on the physical properties of NPs, including size, surface charge, hydrophobicity and immunogenicity [116].

2 Aim

This master's thesis aims to (1) develop a protocol for the encapsulation of TZ in polymeric PLGA NPs, (2) compare the toxicity of free TZ with that of encapsulated PLGA-TZ and (3) use PLGA-TZ NPs together with PLGA-RIF NPs to explore the ability of EP inhibitors to potentiate antibiotic therapy. These aims will be investigated using an *in vitro* model of murine macrophages infected with *Mycobacterium bovis* BCG and *in vivo* using the zebrafish model infected with *M. m*.

3 Materials and methods

3.1 PLGA nanoparticle preparation

3.1.1 Single emulsion

This protocol was adapted from Kalluru *et al.* 2013 [123]. Making NPs by single emulsion (oil-in water emulsion), requires the preparation of two non-miscible phases, one of which is organic and the other aqueous [116]. Depending on the application of the resulting NPs, this method can be used for the encapsulation of hydrophobic dyes (such as coumarin-6) to facilitate imaging, or hydrophobic drugs (such as RIF or TZ) to use in treatment experiments. Regardless, the compound to be encapsulated is dissolved in an organic solvent together with the PLGA polymer to make the organic phase. The aqueous phase consists of polyvinyl alcohol (PVA), which acts like an emulsifier that stabilizes the particles and makes them water-soluble. The size of NPs depends on many factors, including polymer concentration, amount of emulsifier added, drug loading, miscibility of phases, the ratio of water to solvent and the amount of energy applied during NP preparation [127].

The following compounds were encapsulated:

- RIF (Sigma-Aldrich, St. Louis, MO, USA)
- TZ base (Sigma-Aldrich, St. Louis, MO, USA), made by our collaborators in Bo Nystrøm's group at the University of Oslo by removing the hydrochloride group from TZ-hydrochloride to yield hydrophobic, free base form, as described in US patent 4722948 [128].
- Coumarin-6 dye with green fluorescence (Sigma-Aldrich, St. Louis, MO, USA),

The following copolymers were used for encapsulation:

- PLGA (50:50) Resomer® RG 502 (Evonik Röhm GmbH, Darmstadt, Germany) containing equal ratios of both monomers lactic acid and glycolic acid.
- PLGA (75:25) Resomer® RG 752 S (Evonik Röhm GmbH, Darmstadt, Germany) containing 75% lactic acid and 25% glycolic acid.
- PLA Resomer® RG 202 S (Evonik Röhm GmbH, Darmstadt, Germany) containing 100% polylactic acid.

To prepare the organic phase, 100 mg of polymer, and 100 mg of the drug or dye to be encapsulated were dissolved in 10 ml dichloromethane (DCM; Sigma-Aldrich, St. Louis, MO, USA) in a small Erlenmeyer flask sealed tight with parafilm and left stirring over night to allow the solutes to completely dissolve. For the aqueous phase, 1% or 4% PVA (average molecular weight 57-66 kDa; Alfa Aesar, Ward Hill, MA, USA) was dissolved in 20 ml distilled water under heated stirring at 80°C in a sealed glass bottle for 1 hour. Once there were no visible PVA crystals, the heat was turned off and the solution was left stirring overnight to ensure complete dissolution. To form the emulsion, the aqueous phase was filtered using a 0.22 μm filter into a small beaker, before the organic phase was mixed in. The solution was consequently sonicated using a tip sonicator (Power 750 Watt, Sonics & Materials Inc., Church Hill Road, Newtown, USA) for 3 minutes at 450 Watt (60% of the maximum power output). To evaporate the unwanted organic solvent (DCM), the emulsion was divided into two small Erlenmeyer flasks and left stirring overnight. Importantly, the flasks were covered with aluminum foil with a 2 mm hole to facilitate slow, gradual evaporation of the DCM. This prevents disruption of the NP polymeric matrix, which can cause premature drug release.

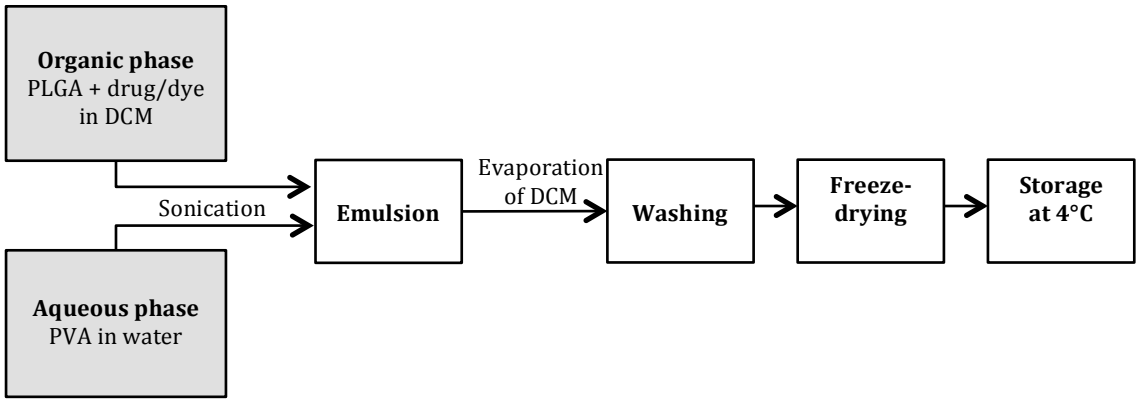

Figure 3.1: Schematic overview of PLGA NP preparation by single (oil-in water) emulsion

Following DCM evaporation, the solidified NPs remain in aqueous suspension. This suspension was transferred to ultracentrifugation tubes and weighed to confirm the evaporation of the organic solvent. The particles were consequently washed twice by ultracentrifugation at 10,000 rpm (17,000 × g) using a SW32 Ti rotor (Beckman Coulter, Fullerton, CA, USA) for 15 minutes using sterilized milliQ water to remove excess PVA. The resulting pellet was then re-suspended in 2 ml 2.5% trehalose (Sigma-Aldrich, St. Louis, MO, USA), a cryo-protectant for the subsequent lyophilization. Lastly, this suspension was

transferred to a cylindrical glass flask and slowly rotated at an angle in a liquid nitrogen bath to allow it to freeze in a thin layer. The frozen flask was then attached to a freeze dryer (Freezone 2.5, Labconco, Kansas City, MO, USA) and left for 24 hours, enough to allow complete sublimation of the water in the suspension. The resulting dried NPs were then scraped out using a spatula and stored at 4°C. The procedure is summarized in **Figure 3.1**.

3.1.2 Nano-precipitation

Nano-precipitation is another method used to make polymeric NPs. Compared to single emulsion, this is a simpler and milder technique in that it does not require sonication. It can therefore be suitable for encapsulating more sensitive compounds such as DNA. However, single emulsion usually leads to a higher encapsulation efficiency and final drug loading than nano-precipitation [116]. Like single emulsion, this method combines an aqueous phase with an organic phase; however, with this technique a water-miscible solvent is used to dissolve the drug/dye and the PLGA polymer. Although this method can be used for the encapsulation of hydrophilic compounds, it is more suited for hydrophobic compounds due to the propensity of hydrophilic substances to escape the organic phase and stay in the water phase [116]. To make the aqueous phase, a 1% weight/volume (w/v) PVA solution was prepared as described in section 3.1.1. To make the organic phase, 20 mg of PLGA (50:50) and 20 mg of drug, in this case TZ, were dissolved in 1 ml dimethyl sulfoxide (DMSO; Sigma-Aldrich, St. Louis, MO, USA). Both solutions were left stirring overnight to allow complete dissolution. The following day, 5 ml of the 1% PVA was filtered using a 0.22 μm filter into a beaker. Under magnetic stirring, the organic phase was added drop-wise to the aqueous phase using a 22 gauge needle and 1 ml syringe at a rate of approximately 0.5 ml/min. The solution was left stirring for 5 hours before the NPs were washed by centrifugation and freeze dried as described in section 3.1.1.

3.2 Nanoparticle characterization

3.2.1 Measurement of nanoparticle drug loading

The amount of drug encapsulated in PLGA-RIF and PLGA-TZ NPs was quantified by means of High Pressure Liquid Chromatography with UV detection (HPLC-UV) in Steven Wilson's analytical chemistry lab at the University of Oslo [123]. Standard curves were made using free drug. For both particle types, 1 mg/ml solutions were made in acetonitrile (ACN; HiPerSolv Chromanorm, VWR, Radnor, PE, US) and sonicated for 15 minutes to dissolve

the NP and release the encapsulated drug. The samples were centrifuged to pellet the NP debris (13,000 × g, 1 minute), and the supernatant containing free drugs was analyzed by HPLC. When necessary, the samples were diluted 10 times before injection. The samples were injected by an Agilent 1200 series GL1377A micro WPS auto sampler (Agilent technologies, Palo Alto, CA, USA). RIF was separated with an ACE3 C18 column, and TZ was separated with an ACE3 C8 column (both with 4.6 mm x 150 mm inner diameter; Advanced Chromatography Technologies, Aberdeen, UK). An Agilent 1100 series GL1378 pump was used to deliver a mobile phase at a flow rate of 1 µl/min. In the case of RIF, the mobile phase consisted of 70% ACN and 0.1% formic acid in water. In the case of TZ, the mobile phase consisted of 50% ACN and 0.1% formic acid in 10mM ammonium formate (pH 6.3). The analytes were detected using an Agilent 1200 series GL1365D MWD detector set to 480 nm for RIF and 254 nm for TZ. Each measurement was based on three independent samples.

3.2.2 Transmission electron microscopy

To visualize and estimate the size range of the manufactured NPs we used transmission electron microscopy (EM). Dry NPs were re-suspended in milliQ water at 0.5 mg/ml. A drop of this suspension was placed on a sheet of parafilm. Using forceps, a clean hexagonal formvar grid was floated on the drop for 1 minute to allow the NPs to attach. Subsequently, the grid was floated on four drops of water, one after another, to remove any unattached NPs. Then the sample was treated with negative stain by floating the grid on a drop of 3% uranyl acetate solution for 30 seconds. This is done to achieve the contrast necessary for visualization against the grid background [129]. Excess uranyl acetate was removed by gently touching a filter paper. The grid was allowed to air dry at room temperature (RT) before loading it on the EM sample holder. The imaging was performed with a Phillips transmission EM (CM100; Philips, Eindhoven, The Netherlands). Using a focused electron beam, the sample was visualized as it interacts with and scatters electrons. The images were recorded digitally with a Quemsa TEM CCD camera and iTEM software (Olympus Soft Imaging Solutions, Germany).

3.2.3 Measurement of nanoparticle surface charge and size

The Malvern Zetasizer Nano ZS (Malvern Instruments Ltd., Worcestershire, UK) is an instrument used to measure NP hydrodynamic diameter by dynamic light scattering at one

angle (backscatter at 173°) [130]. In addition to diameter, the variation in size of the particles was quantified in terms of the polydispersity index (PDI). Surface charge was also determined by means of the electrophoretic mobility, or movement of NPs in an applied electric field, which is expressed as the zeta-potential. These measurements revealed important physical characteristics of the NPs that can affect their uptake and circulation time. PLGA-RIF and PLGA-TZ were re-suspended at 1 mg/ml in distilled water prior to measurement of diameter, PDI and zeta-potential at 25°C. The samples were added to 12-mm glass cell PCS1115 capped cuvettes fitted with dip-cell palladium electrodes with 2 mm spacing, and placed inside the Zetasizer for measurement.

3.3 *In vitro* infection and treatment

3.3.1 Isolation and differentiation of primary murine macrophages

Primary bone marrow derived macrophage cells were isolated from mouse bones using an adapted protocol from Kalluru *et al.* [123]. Four to twelve week old C57BL/6 mice (male and female) were sacrificed by cervical dislocation and soaked in 70% ethanol. Using sterile equipment, the femur and tibia were dissected out and soaked in PBS (Sigma-Aldrich, St. Louis, MO, USA) for 5 minutes to soften any remaining tissue. Using autoclaved tissues, the bones were thoroughly rubbed to remove the softened tissue. The clean bones were consequently placed in 70% ethanol and quickly transported to a sterile hood. Once in the hood, the bones were immediately washed three times with PBS to remove any residual ethanol. Clean bones were kept in PBS to prevent them from drying out. Using sterile scissors, the ends of the bones were carefully cut off to reveal the bone marrow inside. The marrow was harvested from both ends by injecting RPMI 1640 cell culture media (Lonza, Basel, Switzerland) through the central cavity in the bones using a 5 ml syringe fitted with a 25 gauge needle. The marrow was collected in a non-treated culture dish and re-suspended in cell media. This suspension was then collected in a 50 ml falcon tube and centrifuged at 400 ×g for 5 minutes, yielding a red pellet containing both red blood cells and mononuclear cells. To selectively remove the red blood cells, the pellet was re-suspended in red blood cell lysis buffer (Sigma-Aldrich, St. Louis, MO, USA) and incubated until the media turned yellow, indicating that the lysis is complete approximately after 3-5 minutes. To stop the lysis, fresh cell media was added and the cells were again spun down at 400×g for 5 minutes. One can verify that the lysis has been successful because the removal of red blood cells makes the pellet appear yellow. The supernatant was again discarded and replaced with full RPMI

primary macrophage media, supplemented with 10% fetal calf serum (FCS; Sigma-Aldrich, St. Louis, MO, USA), 1% Penicillin-Streptomycin (PS; corresponds to 50 U/ml of each antibiotic; Sigma-Aldrich, St. Louis, MO, USA) and 50 μM β-mercaptoethanol (Sigma-Aldrich, St. Louis, MO, USA). To differentiate the monocytes into macrophages, 40 ng/ml recombinant murine macrophage colony-stimulating factor (M-CSF; ImmunoTools, Friesoythe, Germany) was added to the cell media. Alternatively, 20% L929 conditioned media was used as a source of M-CSF. Conditioned media was made by collecting media used for culturing L929 murine fibroblasts, which secrete M-CSF. Finally the cell suspension was filtered into a new 50 ml falcon tube using a 70 μm cell strainer (BD Biosciences, Franklin Lakes, NJ, USA) in order to remove any residual bone and tissue. The cells were plated in non-treated culture dishes at a density of approximately 8×10^6 cells per dish and allowed to differentiate for 6-7 days, changing the media every other day. Allowing the isolated cells to differentiate on non-treated culture dishes selects for mononuclear cells, as these have a relatively higher binding affinity than other cell types present in the bone marrow [131]. After differentiation, the cells can be scraped and either be used immediately or frozen at - 80°C in FCS with 10% DMSO for future use.

3.3.2 Macrophage characterization by CD14 immunolabeling

Macrophages were characterized by preforming CD14 immunolabeling. CD14 is considered a specific marker for monocytes, normally expressed late in monocyte differentiation [132] Treated cells were imaged using a upright confocal laser scanning microscope, (FluoView 1000 BX61W1, Olympus, Tokyo, Japan). For the CD14 immunolabeling, frozen primary macrophages were thawed and plated at a density of 4.8×105 cells per well on 14 mm glass coverslips coated with poly-L-lysine (see appendix, supplementary methods). To maintain the differentiated state, 20% L929-conditioned media was used. RAW macrophage cells were also seeded as a positive control. After allowing one day for recovery, cells were washed with PBS and then fixed for 15 min using 4% paraformaldehyde (Sigma-Aldrich, St. Louis, MO, USA) in PBS. Cells were then incubated for 1 hour at RT in 1% (w/v) BSA in PBS with 0.1% tween prior to addition of primary antibody solutions (Rat anti-mouse CD14; BD biosciences, Franklin Lakes, NJ, USA) at two concentrations, 1:100 and 1:500 in all wells except negative controls. Cells were left in primary antibody solutions overnight at 4°C. The following morning a PBS wash was done before adding a secondary antibody, conjugated to a red fluorescent marker (cy3 anti-rat;

Jackson ImmunoResearch, West Grove, PA, USA) at a concentration of 1:500 for 1 hour at RT. Lastly, cells were washed again and nuclei were stained with Hoechst (Sigma-Aldrich, St. Louis, MO, USA) 1:1000 in PBS. The coverslips were given a final wash before they were mounted on microscope slides and fixed in place using mowiol (Sigma-Aldrich, St. Louis, MO, USA) as an adhesive. These slides were imaged in the confocal microscope.

3.3.3 RAW cell culture

RAW macrophages were kept in DMEM cell media (Sigma-Aldrich, St. Louis, MO, USA) supplemented with 1% PS and 10% FCS. Cells were passaged 1:4 every second day and seeded on treated culture dishes or poly-L-lysine treated glass coverslips for confocal imaging. Cells were used for a maximum of 20 passages.

3.3.4 Macrophage uptake of fluorescent nanoparticles

To confirm macrophage phagocytosis, freshly isolated primary murine macrophages were treated with NPs loaded with the dye Coumarin-6, which exhibits green fluorescence. Cells were seeded at a density of 3.8×10^5 cells/well on poly-L-lysine coated glass coverslips. NPs were re-suspended in full primary macrophage media and sonicated for 3 minutes. The NP solution at a concentration of either 25 μg/ml or 50 μg/ml was then added to the cells and left to incubate at 37°C to allow macrophage uptake. After 3 hours, cells were washed three times with PBS and fixed with 4% paraformaldehyde for 10 minutes. The fixed cells were washed again in PBS and mounted on microscope slides using mowiol as an adhesive. These slides were imaged in the confocal microscope.

3.3.5 CCK-8 viability assay

The Cell Counting Kit 8 (CCK-8; Sigma-Aldrich, St. Louis, MO, USA) was used to determine the toxicity of free and encapsulated TZ in primary macrophage culture. This assay was also used to test the effect of M-CSF on cell viability. CCK-8 is a colorimetric assay that uses the tetrazolium based salt WST-8, which is reduced by dehydrogenases in the cell, producing a brown color that is proportional to the amount of viable cells in the sample [133].

Primary murine macrophages were seeded at a density of 4×10^4 cells per well in transparent 96-well cell culture plates. To maintain the macrophages in a differentiated state, 40 ng/ml M-CSF was added fresh at each media change. After seeding, the cells were left overnight to allow them to settle in a monolayer. The next day they were treated with either

free TZ or the corresponding concentrations of TZ encapsulated in PLGA NPs. While the NP suspension was only left on the cells for three hours, the free drug was added continuously throughout the experiment. After three hours, all the cells (free drug and NP treated) were washed with 37°C PBS, and replaced with fresh media supplemented with free TZ where appropriate. To prepare the treatment conditions, the TZ (free and encapsulated) used for treatment was first dissolved in RPMI cell media (with 1% PS and 10 % FCS) at a concentration of 1 mg/ml. These stock solutions were then diluted in full RPMI (with 1 % PS, 10% FCS and 40 ng/ml M-CSF) to achieve a final concentration corresponding to 2.5 μg/ml, 5 μg/ml or 7.5 μg/ml of free TZ. Cells were also treated with empty PLGA NPs and a combination treatment with particles equivalent to 5 μg/ml TZ and 8 μg/ml RIF.

Measurements using the CCK-8 reagent were done at 3, 6 and 9 days, with three replicates per condition. The media was removed and the cells were washed once using 37°C PBS. Clear RPMI (without phenol red) was mixed with 5% (v/v) CCK-8 reagent and added to each well, prior to a 40 minute incubation at 37°C. The reagent was also added to wells with no cells to measure background absorbance. After the incubation, 100 μl of the reagent was sampled from each well and placed in a new transparent 96 well plate. This was then brought to a plate reader (Victor2, PerkinElmer, Waltham, MA, USA), and absorbance was read at 450 nm for 0.1 seconds.

3.3.6 Culturing BCG

BCG transformed with a plasmid coding for the red fluorescent dsRed protein and hygromycin resistance (BCG dsRed, gift from Nathalie Winter and Brigitte Gicquel from the Pasteur Institute, Paris) were kept in liquid culture at 37°C. Liquid culture medium was prepared using Difco Middlebrook 7H9 broth supplemented with 0.02% glycerol (Merck KGaA, Darmstadt, Germany), 10% OADC (oleic acid (Sigma-Aldrich, St. Louis, MO, USA), albumin (Sigma-Aldrich, St. Louis, MO, USA) dextrose/glucose (Merck KGaA, Darmstadt, Germany) and 0.025% Tween 80 (Sigma-Aldrich, St. Louis, MO, USA). Hygromycin (Sigma-Aldrich, St. Louis, MO, USA) was added at 50 μg/ml to select for fluorescent BCG.

To start new liquid culture, either a single colony grown on solid media was picked, or frozen stock was added to full 7H9 media. Bacteria were grown on solid media at 37°C on Difco Middlebrook 7H10 agar plates (see appendix, supplementary recipes) with OADC and 50 μg/ml hygromycin. Plates were sealed in plastic bags to prevent them from drying out.

3.3.7 Primary macrophage infection and time-kill assay

Freshly isolated primary murine macrophages were seeded in cell-culture treated 12 well plates at a density of 5×10^5 cells per well and left to settle overnight. The next day, infection media was prepared by harvesting log phase (OD_{600} 0.4-0.9) dsRed-BCG at 3000×g for 10 minutes. The BCG were washed twice using PBS, re-suspended in RPMI cell media and sonicated for 10 minutes in a bath sonicator to ensure a homogenous suspension. The BCG suspension was diluted to an OD of 0.035 (3.5 $5x10^6$ CFU/ml) in RPMI cell media, and added to the plated cells for infection for 3 hours. To calculate multiplicity of infection (MOI), the number of bacteria are divided by the number of macrophages in the well. In this case, the MOI was 7. After infection, cells were washed twice with warm PBS in order to remove any extracellular bacteria. Fresh full RPMI was added to all wells for 1 hour to allow the cells to recover from infection. During this time, treatment solutions containing PLGA-RIF, PLGA-TZ or free RIF and free TZ were prepared for all conditions, using the concentrations summarized in **Table 3.1**. The seven combinations tested are listed in **Table 3.2**. Each condition was prepared in triplicate for each time-point, and treatments were added to the cells for 3 hours.

Table 3.1: Concentrations of RIF and TZ used for the CFU time-kill assay expressed as free drug weight and corresponding weight of PLGA NPs.

	NP loading	Free drug	Encapsulated drug
PLGA-RIF NP	31.8%	8.0 µg/ml	25 µg/ml
PLGA-TZ NP low	26.5%	2.5 µg/ml	9.4 µg/ml
PLGA-TZ NP high	26.5%	5.0 µg/ml	18.8 µg/ml

Table 3.2: Summary of treatment conditions used for the time-kill assay.

Condition	RIF added	TZ added	
	8.0 µg/ml	2.5 µg/ml	5.0 µg/ml
1 BCG control	-	-	-
2 PLGA-RIF NP	+	-	-
3 PLGA-TZ NP low	-	+	-
4 PLGA-TZ NP high	-	-	+
5 Combination NP low	+	+	-
6 Combination NP high	+	-	+
7 Combination free	+	-	+

Concentrations represent actual drug weight, not NP weight

In order to compare sustained release of the NPs with free drugs, a combination treatment using 5.0 µg/ml of TZ and 8.0 µg/ml RIF was included. Treatment with free drug had the same duration as the NP treatments. Following treatment, cells were again washed twice with warm PBS. Fresh full RPMI cell media supplemented with cytokine was then added to all wells. Cell lysis was carried out after 3 hours, 3 days, 6 days and 9 days of treatment. To do this, cell media was aspirated and 1 ml of RT 0.005% SDS (Sigma-Aldrich, St. Louis, MO, USA) in sterile milliQ water was added to each well. After 5 minutes, the contents of each well was pipetted up and down five times in order to aid cell lysis. The lysate was subsequently collected in an eppendorf tube. A dilution series was made for each sample in warm PBS, and these were plated on pre-warmed 7H10 agar plates supplemented with OADC and 50µg/ml hygromycin. Plates were incubated at 37°C in sealed plastic bags for 16 days, just enough to allow visible colonies to form for CFU enumeration.

3.4 BCG luciferase assay

3.4.1 Isolation of Luciferase plasmid

Luciferase is an enzyme found in fireflies with a half-life of three hours in cells. Upon the addition of adenosine triphosphate (ATP), magnesium and the luciferase substrate, luciferin, the enzyme will produce a bioluminescent signal, as shown in **Figure 3.2**. The *luc* gene, which produces the luciferase enzyme can be introduced to bacterial cells by transformation and serve as a reporter for the amount of viable bacteria in a sample

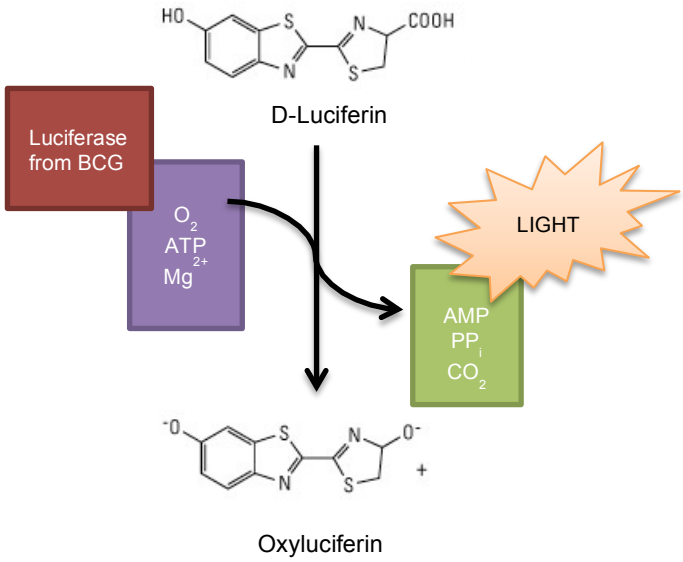

Figure 3.2: Schematic showing the luciferase reaction that forms the basis of the luciferase assay. The *luc* gene coding for the luciferase enzyme can be transformed into bacteria. The bacteria can then be lysed, releasing the enzyme that, when exposed to its substrate D-luciferin, produces a bioluminescent signal and necessary cofactors ATP, oxygen and magnesium.

E. coli DH5α transfected with the plasmid pMH109-luc coding for firefly luciferase (and hygromycin resistance) was kindly sent to us by Trude Flo (NTNU, Trondheim, Norway), who in turn received it from David Sherman (University of Washington, Seattle, WA, USA) [134]. In addition to hygromycin resistance, the plasmid encodes features of the mycobacteriophage L5, including an attP site that efficiently targets the plasmid to the attB site in mycobacterial chromosomes, and an integrase that promotes this incorporation process [135]. Inside mycobacteria, pMH109-luc is constitutively expressed under a mycobacterial optimal promoter (MOP) on the plasmid.

The DH5α cells were cultured overnight in LB Media with 150µg/ml hygromycin. The next day the overnight culture was streaked out on LB-agar plates with 150µg/ml hygromycin. These colonies were used to make new liquid culture utilized for plasmid isolation and glycerol stocks. The plasmid was isolated using a maxi prep kit from Nucleobond (Macherey-Nagel GmbH & Co. KG, Düren, Germany). Plasmid purity was checked using NanoDrop™ (Thermo Scientific, Wilmington, DE, USA), which revealed that the 260/280 value was 1.88.

3.4.2 Electroporation of wild type BCG with luciferase plasmid

The following was adapted from Goude *et al.* 2008 [136]. Wild type BCG were given to us by Tone Tønjum (Rikshospitalet, Oslo, Norway). These were grown until exponential phase, in this case an OD_{600} of approximately 0.5. Cultures were kept on ice for 1 hour, and then harvested by centrifugation at 3000×g for 10 minutes. This was followed by three washes using ice-cold 10% (v/v) glycerol in milliQ water. The volume of 10% glycerol used was reduced with each wash from 30ml to 5 ml and lastly 1 ml. The isolated plasmid and BCG were kept on ice. Three eppendorf tubes were prepared with 200µl ice-cold BCG culture. DNA was added to two of the tubes at 1 µg and 2µg. The last tube remained as a negative control with no DNA added. The samples were incubated for 10 minutes on ice, and then transferred to 2 mm re-usable electroporation cuvettes (BTX, Harvard Apparatus, Holliston, MA, USA). This was done carefully, avoiding bubbles in order to minimize the chance of arcing, an electric discharge that can kill the bacteria in the sample.

The cuvettes were placed in the slot of an electroporator (Bio-Rad, Hercules, CA, USA) set to -2.5 kV, 25 µF and 600 Ohm. Immediately after electroporation, 1 ml warm 7H9 was added to the cuvette, and the contents were transferred to a new eppendorf tube. The transformed bacteria were allowed to recover at 37°C for 4 hours. To select for transformed

individuals the bacteria were plated out on 7H10 plates with OADC supplement and 50µg/ml hygromycin. Once colonies had grown, after approximately 3 weeks, BCG transformed with luciferase (BCG-lux) were cultured in the same way as dsRed BCG.

3.4.3 Correlation of CFU with luciferase quantification

Frozen primary murine macrophages were plated out in non-treated cell culture dishes and left to recover for 3 days at 37 °C. Cells were then scraped and seeded at a density of 500,000 cells/well on two 12-well plates and allowed to settle in a monolayer. The following morning, BCG lux cultures were processed for macrophage infection as described in section 3.3.7. Infection media was added to cells in duplicates at the following OD_{600}: 0.05, 0.01, 0.005, 0.001 and 0.0005. This range corresponds to $5x10^6$-$5x10^4$ bacteria, or an MOI of 10-0.1. Duplicate wells were mock infected for luciferase controls. The day after infection, macrophages were lysed by incubating them for 5 minutes in 0.005% SDS in milliQ water as before. This causes the release of intracellular bacteria which can either be plated out or lysed and processed for luciferase quantification.

Samples to be quantified by CFU were subjected to serial dilutions and plated out on warm 7H10 plates with OADC and 50 µg/ml hygromycin. Plates were sealed in plastic bags and left at 37°C. Colonies were counted after 3 weeks.

Samples to be quantified by luciferase assay were spun down at 5000 rpm (2400×g) for 3 minutes to collect the bacteria, and the supernatant was removed. Samples were spun down a second time to ensure all residual supernatant was removed, and finally re-suspended in 20µl 1x passive lysis buffer (from the dual luciferase assay kit; Promega, Madison, WI, USA), thoroughly vortexed and briefly sonicated to mix. Samples were then left on ice for 10 minutes, followed by a second vortex and sonication to ensure complete lysis of the bacteria. This caused the release of the luciferase enzyme produced by viable bacteria. The reconstituted luciferase substrate is kept at -80°C as instructed by the manufacturer. This substrate contains ATP, luciferin, and magnesium required for the bioluminescent reaction. The substrate was prepared by thawing it in a 24 °C water bath for 30 minutes to ensure that the solution was at RT. If the substrate is too cold, it can reduce the signal produced by the reaction. For luciferase quantification, the 20µl bacterial samples were added four at a time to a white, opaque 96-well plate (Corning Inc., Corning, NY, USA). With strict attention to timing, 100µl of the luciferase substrate was added to each of these wells, with 2 seconds between each addition. After 25 seconds had passed from the addition of substrate to the first

well of the series, the plate was placed inside a Victor^2 plate reader (PerkinElmer, Waltham, MA, USA) set to luciferase detection for 1 second per sample and a delay of 2 seconds between each reading. For graphical representation, the values were normalized to the highest value obtained and expressed as relative light units (RLUs).

3.5 In vivo infection and treatment

3.5.1 Zebrafish care and husbandry

Zebrafish were kept in our facility at the University of Oslo. Aquaria were kept at 28°C, with continuous circulation of tank water containing Instant Ocean ® sea salt (United Pet Group, Blacksburg, VA, USA), calcium chloride, and sodium bicarbonate. Approximately 10% of the total system volume was exchanged daily, and the light cycle was kept at 12:12 hours. Fish were fed three times daily, twice with brine shrimp and once with dry feed. For maximum output, fish were allowed to rest for two weeks between each breeding. The night before fish were bred, a small plastic box filled with two layers of glass marbles was placed in a tank with a male/female ratio of 3:2. The fish start breeding at dawn, or just after the light comes on in the morning and lay their eggs between the marbles where the other fish in the tank cannot reach and eat them. After allowing 3 hours of breeding, the box with marbles was carefully removed from the tank and the eggs harvested using a sieve. Fertilized eggs were washed carefully several times using embryo water (see appendix, supplementary recipes), and any abnormal-looking eggs (unfertilized or dead) were removed. Clean eggs were kept in fresh embryo water in petri dishes with no more than 100 eggs per dish in an incubator set to 28°C. After about 30 hours (1 dpf), eggs were manually dechorionated using forceps. Embryo water was changed daily prior to and for the duration of all experiments. Dechorionated embryos were ready for injections at 2 dpf. The strains used for survival and toxicity studies were “Casper” (roy$^{-/-}$; nacre$^{-/-}$; a gift from Darren Gilmour, EMBL, Heidelberg, Germany) which maintain optical transparency throughout embryo and adult life [137]. This lack of pigment makes it easier to preform experiments and is useful for imaging at later time- points.

In the experiments that exceeded 6 dpf and zebrafish initiated feeding, we fed the larvae with rotifers. Ethical permission was obtained for animal experimentation from the Norwegian national animal research authority (FOTS permission ID 5214).

3.5.2 Toxic indicators in zebrafish

Equal concentrations of free or encapsulated TZ in 2% (w/v) polyvinyl pyrrolidone in PBS (2% PVP, molecular weight 10 kDa; Merck KGaA, Darmstadt, Germany) were injected in zebrafish embryos at 3 dpf. Mock injections consisted of 2% PVP only. Embryo water was changed daily, and feeding with rotifers (see appendix, supplementary methods) was initiated at 6 dpf. Embryos were monitored daily to record mortality, swim bladder inflation (see **Figure 3.3**), yolk discoloration and pericardial edemas [138-140]. To quantify this, a disease score was calculated based on the toxic indicators. Each indicator was given a score of either 0,1 or 2, where 0 is the absence of the trait and 1 or 2 indicates two levels of severity, as summarized in **Table 3.3**. Examples of the different degrees of edema severity are shown in **Figure 3.4**.

Table 3.3: Scores assigned to morphological toxic indicators in order to quantify the effect of injecting free and encapsulated TZ at 32 mg/kg. Adding the scores outlined in this table together gave the value reported as disease score.

Trait	Score		
	0	1	2
Edema	No edema	Small edema	Severe edema
Swim bladder inflation	Yes	No	-
Yolk sac discoloration (necrotic spots)	Yes	No	-
Heart-rate	Normal	Abnormal	-

For heart rate quantification, un-sedated embryos were transferred to a 2% agar injection plate in a drop of water. Using a Leica M205 FA stereomicroscope (Leica microsystems, Wetzlar, Germany), the heart was brought into focus, and a 10-second video was recorded for each fish. The image sequence was imported into the image processing software Fiji [141] and heartbeat was quantified using a counter. These values were multiplied by 6 to obtain beats per minute (bpm).

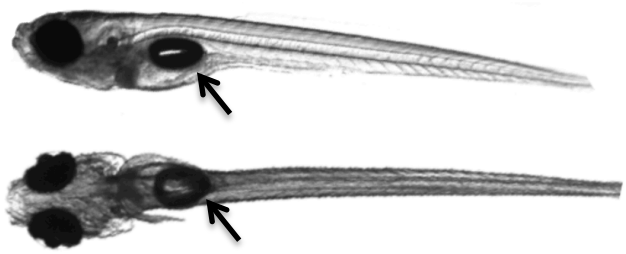

Figure 3.3: A representative "Casper" embryo with inflated swim bladder (highlighted by arrow) at 7dpf in lateral (top) and dorsal (bottom) projections.

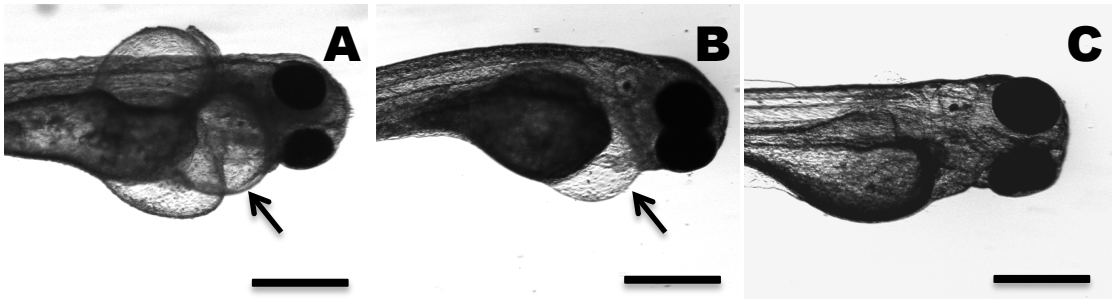

Figure 3.4: Zebrafish larvae at 1dpt or 2dpt, displaying pericardial edemas with various degrees of severity. The larvae shown in panel A is classified as severe edema and therefore assigned 2 points in the disease score system. The larvae shown in panel B has a moderate edema and therefore scores 1 point. The larvae shown in panel C has not developed pericardial edema, and is therefore assigned 0 points. Scale bar represents 0.5 mm.

3.5.3 Culturing *Mycobacterium marinum*

M. m was cultured and prepared for infection of zebrafish larvae as outlined in [102, 112]. *M. m* transformed with a plasmid coding for the red fluorescent protein dsRed and kanamycin resistance (msp 12::dsRed2, gift from Lalita Ramakrishnan, University of Washington, Seattle, WA, USA) was kept at 30-32 °C in a dark room in an incubator with a shaking stage. Liquid culture medium was prepared using Difco Middlebrook 7H9 broth supplemented with 0.02% glycerol, 10% ADC (albumin, dextrose, catalase) and 0.05% Tween 80. Kanamycin (Sigma-Aldrich, St. Louis, MO, USA) was added at 50 µg/ml to select for fluorescent *M. m*. To start new liquid culture, either a single colony picked from an agar plate or an aliquot taken from frozen stock was added to full 7H9 media as described for BCG in section 3.3.6. Bacterial properties change during freezing and thawing [112], therefore using bacteria directly from frozen stock was avoided. Stocks were instead allowed to recover for a few days and were sub-cultured once before use.

3.5.4 Processing *Mycobacterium marinum* for microinjection

On the day of the infection, bacteria were harvested in the exponential phase, OD_{600} of 0.5-0.9. Prior to OD_{600} measurement the culture was re-suspended twice using a 22-gauge needle and 20ml syringe to disrupt any bacterial aggregates. A 1.5ml sample of the exponential culture was centrifuged at 5000 rpm (2400×g) and the bacterial medium was removed. In order to minimize clogging of the bacteria in the microinjection needle, the culture was re-suspended in 2% PVP and passaged through a 27-gauge needle 10 times. After re-suspension the OD_{600} was measured again to ensure a final OD_{600} of 0.9, which corresponds to 5.09×10^7 CFU/ml. When injecting 2 nl, this gives approximately 50 bacteria, which establishes a moderate infection, suitable for survival studies. In 500µl bacterial

solution, 50µl 2% (w/v) phenol red (Sigma-Aldrich, St. Louis, MO, USA) was added to visualize the inoculation and easily identify unsuccessful injections.

3.5.5 Preparation of treatment solution for *in vivo* survival studies

Freeze dried PLGA-TZ NPs were stored at 4°C until needed. On the day of the injection, NPs were re-suspended in 2% PVP to a final concentration of 15 mg/ml. In order to make a homogenous NP solution, this suspension was sonicated 2-5 minutes in a bath sonicator and checked periodically in a light microscope to ensure the absence of large visible aggregates. The PLGA-TZ NPs have 26.54% loading, so a solution containing the corresponding amount of free TZ was also made, with 3.981 mg/ml of the water soluble TZ-hydrochloride in 2% PVP. Thus the same volume was injected for both free and encapsulated PLGA-TZ. For the mock injections 2% PVP alone was used. Phenol red was not added to these solutions for visualization of the injection, because this caused the TZ to precipitate and clog the microinjection needle.

3.5.6 Zebrafish microinjection

The following procedure was adapted from Cosma *et al.* [102]. On 2 dpf the embryos are sufficiently developed to allow injection with either *M. m* or NPs re-suspended in 2% PVP. Prior to injections, embryos were kept in sterile embryo water and stored at 28°C. At 1 dpf, embryos were either dechorionated manually and washed thoroughly and screened to ensure that they were properly developed and healthy.

Microinjection needles were made using borosilicate capillaries (outer diameter 1.0 mm, inner diameter 0.78 mm, length 100 mm, Harvard Apparatus, Holliston, MA, USA) in a Flaming/Brown P-97 micropipette-puller (Sutter, Novato, CA, USA) with the settings: delay 110, heat 610, pull 40, velocity 50 and pressure 500. Using a micro-loader pipette tip, a microinjection needle was loaded with dsRed *M. m* or treatment solution and mounted on a micromanipulator (Narishige, Tokyo, Japan). The needle is attached to a pressure controller (Femtojet; Eppendorf AG, Hamburg, Germany), which produces a defined pulse of nitrogen leading to a precise injection volume. To calibrate the ejected volume, the needle opening size as well as the pressure and duration of the injection were adjusted until the desired volume of injection was reached. To do this, the tip of the needle was carefully broken off using fine jewelers forceps (Dumont No. 5) before injecting into mineral oil (Sigma-Aldrich, St. Louis, MO, USA) and measuring the diameter of the resulting droplet at 59.9× using an

arbitrary scale printed on the inside of the ocular. We have previously measured the size of the droplet using a 1 cm ruler at this magnification, as shown in **Figure 3.5**, and can therefore use this to determine the volume injected by the diameter of the drop produced.

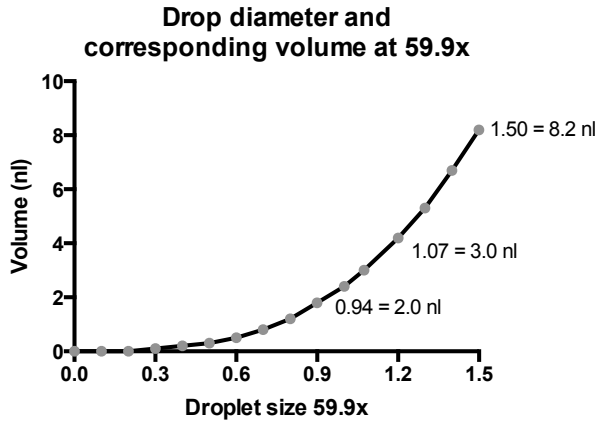

Figure 3.5: Relationship between drop diameter and volume at 59.9x magnification. Labels on the curve represent volume in nl.

The embryos were sedated by immersion in 230µg/ml tricaine stock solution (see appendix, supplementary recipes) in embryo water for 2 minutes. The sedated embryos were positioned on a 2% (w/v) agarose (Sigma-Aldrich, St. Louis, MO, USA) injection plate using a transfer pipette, and excess water was removed to immobilize the larvae during injection. Both bacteria and NPs were administered by injecting into the posterior cardinal vein or at the yolk circulation valley, as shown in **Figure 3.6**. The injected embryos were immediately placed in fresh embryo water to recover from sedation.

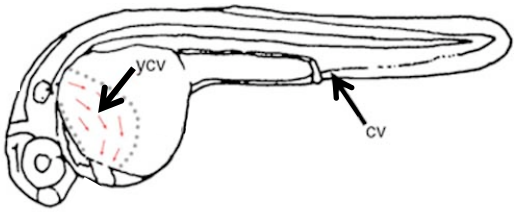

Figure 3.6: Injection sites in the zebrafish. Figure adapted from Cosma *et al.* [102]. CV= caudal vein. YCV= yolk circulation valley.

3.5.7 Embryo survival experiments

Zebrafish embryos were prepared for infection with dsRed *M. m* on 2 dpf as described above. Control embryos were injected with 2% PVP mock treatment instead of bacterial suspension. The injected embryos were allowed to recover over night in fresh embryo water. The next day, at 3 dpf, embryos were again injected with PLGA-TZ NPs, empty PLGA NPs

or mock injections. The different groups were separated in a 6-well plate. For the drug baths, a stock solution of 10 mg/ml RIF was made. To completely dissolve RIF in the embryo water, it was first dissolved in 20% DMSO, such that the final concentration of DMSO in the embryo water was 0.004% by volume. The groups that were not given the RIF bath treatment were kept in embryo water with 0.004% DMSO only. All embryo water was changed daily for the duration of the experiment. At 6 dpf, when the larvae initiate feeding, rotifers were given to all groups.

PLGA-TZ NPs were prepared as described above. In the first experiment 3 nl of the 15 mg/ml stock solution was injected, corresponding to 12 ng TZ by drug weight. Larvae typically weigh around 1 mg, so this corresponds to about 12 mg/kg. However, this dose did not have much of an effect and was therefore increased to 32.6 ng of TZ, approximately a dose of 32 mg/kg, which corresponds to the amount used by Van Soolingen *et al.* [85] to significantly reduce CFUs and show a synergistic effect with RIF in a TB mouse model. Therefore, in the second experiment, 8.2 nl of stock solution was injected (summarized in **Table 3.4**). To inject these amounts, the drop-size was calibrated to 0.9 and 1.5 at 59.9×, in accordance with **Figure 3.5**.

Table 3.4: Therapeutic doses of PLGA-TZ injected in zebrafish larvae in the first and second survival experiments

Experiment	Volume injected 15 mg/ml stock	Size of drop at 59.9×	Amount of PLGA-TZ	Amount of free TZ
1	3.0 nl	0.9	45 ng	12.0 ng
2	8.2 nl	1.5	123 ng	32.6 ng

3.6 Statistics

All statistical analysis was preformed in GraphPad Prism 6 software (GraphPad Software, La Jolla, CA, USA). In all cases, post-hoc tests for multiple comparisons were only run only after confirming overall significance of the test in question. Results obtained in the CCK assay, the disease-score and heart-rate analysis were analyzed by an unmatched one-way analysis of variance (ANOVA), with Turkey's post-hoc test for multiple comparisons, comparing individual time-points separately. The CFU time-kill assay was analyzed using an unmatched two-way ANOVA with Turkey's post-hoc test for multiple comparisons, comparing individual time-points separately. As opposed to the one-way ANOVA, this tests the influence of two independent factors on the CFU value, in this case treatment over time.

In the overall analysis, significance in each of these factors is assessed, as well as the ”interaction” between them. If this interaction is not significant ($P>0.05$), the two factors tested influence the measured variable independently of each other. On the other hand, if there is a significant interaction ($P<0.05$), this means that the various treatment groups change differently over time, and that the two factors influence each other. Correlation between CFU and luciferase assays was done using a parametric two-tailed Pearson correlation analysis. Survival studies were analyzed using a Kaplan-Meier representation and Log-rank (Mantel-cox) test with a Bonferroni correction (for $n=3$, $p<0.0170$ for statistical significance) for the comparison of pairwise curves. This procedure compares entire curves, not individual time points as ANOVA does.

4 Results

4.1 Synthesis and characterization of nanoparticles

4.1.1 Encapsulation of coumarin-6 and rifampicin

Our group has previously established a protocol for the preparation of fluorescent NPs and RIF-loaded NPs by single emulsion using the PLGA polymer [114, 123]. For the purposes of this thesis, new batches of RIF NPs and fluorescent green coumarin-6 NPs were made according to this protocol, as summarized in **Table 4.1**.

Table 4.1: Summary of preparation method and components of NPs made either with the green fluorescent dye coumarin-6 or the standard anti-TB drug RIF. Drug-loading was determined by HPLC, n=3. The amount of PVA used in each case is given as percent weight/volume (% w/v).

Method	Polymer	PVA (% w/v)	Dye/drug	Drug loading (%)
Single emulsion	PLGA (50:50)	1	Coumarin-6 (green)	-
Single emulsion	PLGA (50:50)	1	Rifampicin	31.8

4.1.2 Encapsulation of thioridazine

Although a former PhD student in the lab had previously made PLGA-TZ NPs, the loading achieved was relatively low, at 16%, necessitating large quantities of NP to achieve therapeutic dosing. In an attempt to increase the loading, different parameters were tested, including method of preparation, polymer type and amount of PVA. Due to its biodegradability, we have previously used mostly PLGA (50:50) to make both RIF and TZ NPs. However, as TZ is more hydrophobic than RIF, polymers with higher ratios of lactic acid to glycolic acid, PLGA (75:25) and PLA only, were tested. The amount of PVA was also varied. Drug loading was determined by HPLC (**Table 4.2**).

Table 4.2: Summary of preparation methods and NP components tested for optimal encapsulation of TZ. Drug loading was determined by HPLC, n=3. The amount of PVA used in each case is given as percent weight/volume (% w/v).

Method	Polymer	PVA (% w/v)	Drug loading (%)
Single emulsion	PLGA (50:50)	1	25.9
Single emulsion	PLGA (50:50)	4	26.5
Single emulsion	PLGA (75:25)	1	39.7
Single emulsion	PLA	1	27.1
Nano-precipitation	PLGA (50:50)	1	25.3

The NPs with the highest drug loading were prepared with the more hydrophobic PLGA (75:25) polymer, with 39.7% encapsulated TZ. However, these NPs were impossible to re-suspend in water, so they were not suitable for *in vitro* cell work or *in vivo* injections. This was also the case for the PLA NPs and the NPs prepared by nano-precipitation. The standard method of single emulsion, using the same PLGA (50:50) polymer as before, produced the best NPs for experimental use. Ultimately, with the exception of the choice of polymer, none of the parameters tested greatly affected the encapsulation of TZ. Most of the NPs had a loading of approximately 25-27%. As might be expected, the TZ NPs with 4% PVA were the easiest to re-suspend, and were therefore chosen for subsequent experiments.

4.1.3 Nanoparticle characterization and imaging

The PLGA-RIF and PLGA-TZ NPs that were to be used for toxicity and treatment experiments were re-suspended in water and characterized using a Zetasizer to measure their average diameter and surface charge. The results are shown in **Table 4.3**.

Table 4.3: Characterization of PLGA-RIF and PLGA-TZ NPs as measured by the Zetasizer, including size and size variation (PDI), surface charge and drug loading. NPs were re-suspended in distilled water prior to measurement. PDI= polydispersity index. Sizes are expressed as mean ± standard deviation (SD), n=3.

	NP components	Zeta potential ± SD (mv)	Diameter ± SD (nm)	PDI	Drug loading (%)
PLGA-RIF NP	PLGA 50:50, 1%PVA	-20.7 ± 0.7	488 ± 85	0.2	31.8
PLGA-TZ NP	PLGA 50:50, 4%PVA	-14.2±0.8	550 ± 72	0.3	26.5

The PDI is a dimensionless quantification of the particle size distribution. A greater tendency to aggregate can make NPs appear more poly-dispersed, and a high PDI therefore indicates that NPs are more unstable in solution. Typically, the PDI should not exceed 0.7 for PLGA NPs, as this can indicate the presence of dust, contamination or aggregation of particles [130]. The NPs characterized here have a low PDI. In addition, they have a relatively high negative charge, which also means they will have a lower tendency of aggregating. They are also within the favorable size-range for macrophage phagocytosis (100 nm-3μm) [116, 142]. To further characterize NPs, the coumarin-6 NPs were imaged by fluorescence microscopy to confirm the encapsulation of green dye, as shown in **Figure 4.1A**. Imaging in the transmission EM was also carried out to visualize the NPs in the sample and to give a more qualitative evaluation based on size, shape, degree of aggregation and extent of polydispersity. The coumarin NPs were green fluorescent, and upon closer

inspection in the EM, they were round, relatively mono-disperse and displayed no aggregation, as shown in **Figure 4.1B**.

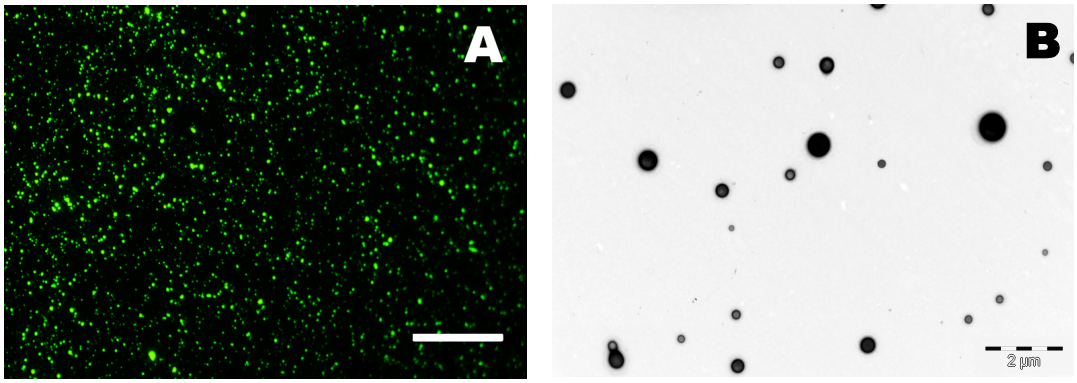

Figure 4.1: Coumarin-6 NPs imaged in the fluorescence microscope (A) and the transmission EM (B). Scale bars for fluorescence image and EM represent 100 µm and 2 µm, respectively.

The remaining TZ NPs that could be re-suspended in water were also imaged in the EM. There was no visible difference between batches (**Figure 4.2**), but we can say that these particles were also round, relatively mono-dispersed and displayed no visible aggregation. Relative NP size can also be measured by looking at the EM images, and this was done for some of the particles (**Table 4.4**). The mean size estimated by EM was less than half of the mean size established by the Zetasizer.

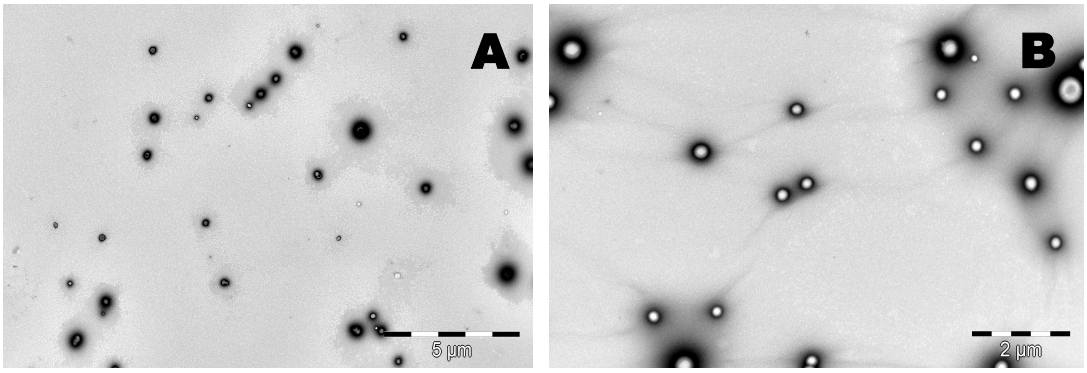

Figure 4.2: Transmission EM images of PLGA-TZ NPs prepared by nano-precipitation with 1% PVA (A) and PLA-TZ NPs prepared by single emulsion with 1 % PVA (B). Scale bars in A and B represent 5 µm and 2 µm, respectively.

Table 4.4: Size estimation by EM of PLGA-coumarin-6 and PLGA-TZ NPs. Sizes are expressed as mean diameter ± standard deviation (SD). N= number of individual measurements.

	NP components	Diameter ± SD	N
PLGA-coumarin-6 NP	PLGA (50:50), 1% PVA	299.03±214.18	20
PLGA-TZ NP	PLGA (50:50), 4% PVA	220.45±107.46	12

4.2 Optimization of primary cell culture

In pilot experiments with primary murine macrophages, the cell morphology was unexpectedly elongated and fibroblast-like. This led us to question whether the macrophages were properly differentiated, and so we tried changing the concentration of M-CSF and testing for macrophage characteristics. In order to evaluate how different levels of the recombinant M-CSF cytokine affected cell viability, cells were incubated in media supplemented with 0-40 ng/ml M-CSF, and measurements using the CCK-8 assay were taken at 1, 3 and 6 days (**Figure 4.3**). After 1 day of incubation, the cells with no M-CSF were significantly more viable than those in all other groups. This trend was reversed at 3 and 6 days, showing instead a dose-dependent increase in viability. However, the cells treated with 5 ng/ml M-CSF did not show any significant difference from untreated cells at 3 or 6 days.

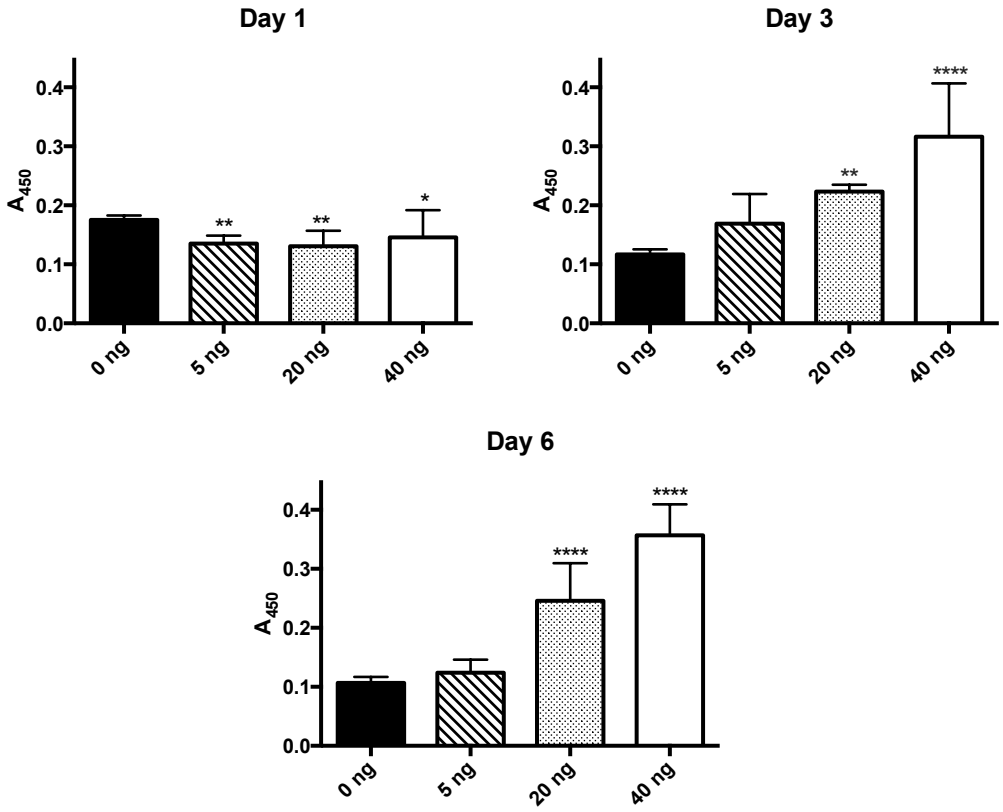

Figure 4.3: Cell viability in primary murine macrophages incubated in different concentrations of recombinant M-CSF, measured by the CCK-8 assay (n=3). A_{450} values are expressed as mean ± 95% confidence interval. Asterisks represent significant difference from untreated cells, as determined by one-way ANOVA in GraphPad Prism 6, * $P < 0.05$, ** $P < 0.01$ and **** $p < 0.0001$.

Cells treated with different amounts of M-CSF also changed morphology after 3 days of incubation. Wells without M-CSF had more detached cells, and the attached cells looked

more rounded, indicating decreased viability. As the concentrations of cytokine were increased, the cells looked healthier but also more elongated and fibroblast-like. This was especially prominent at the highest concentration, 40 ng/ml M-CSF, which is the concentration that had been previously used in our group, and which we have used for subsequent studies in this thesis.

Another factor which affected macrophage morphology was the surface treatment of the culture dishes. Surface treatment makes the dish hydrophilic and negatively charged when in contact with cell media [131]. This makes it easy for adherent cells to attach and grow. Monocytes have a relatively high binding affinity, and therefore do not neccesarily require this kind of treatment in order to grow. Treated dishes yielded cells with elongated morphology, whereas untreated dishes gave more rounded cells. The same phenotype was seen regardless of the source of M-CSF used for differentiation, recombinant M-CSF or 20% L929 conditioned media **(Figure 4.4**).

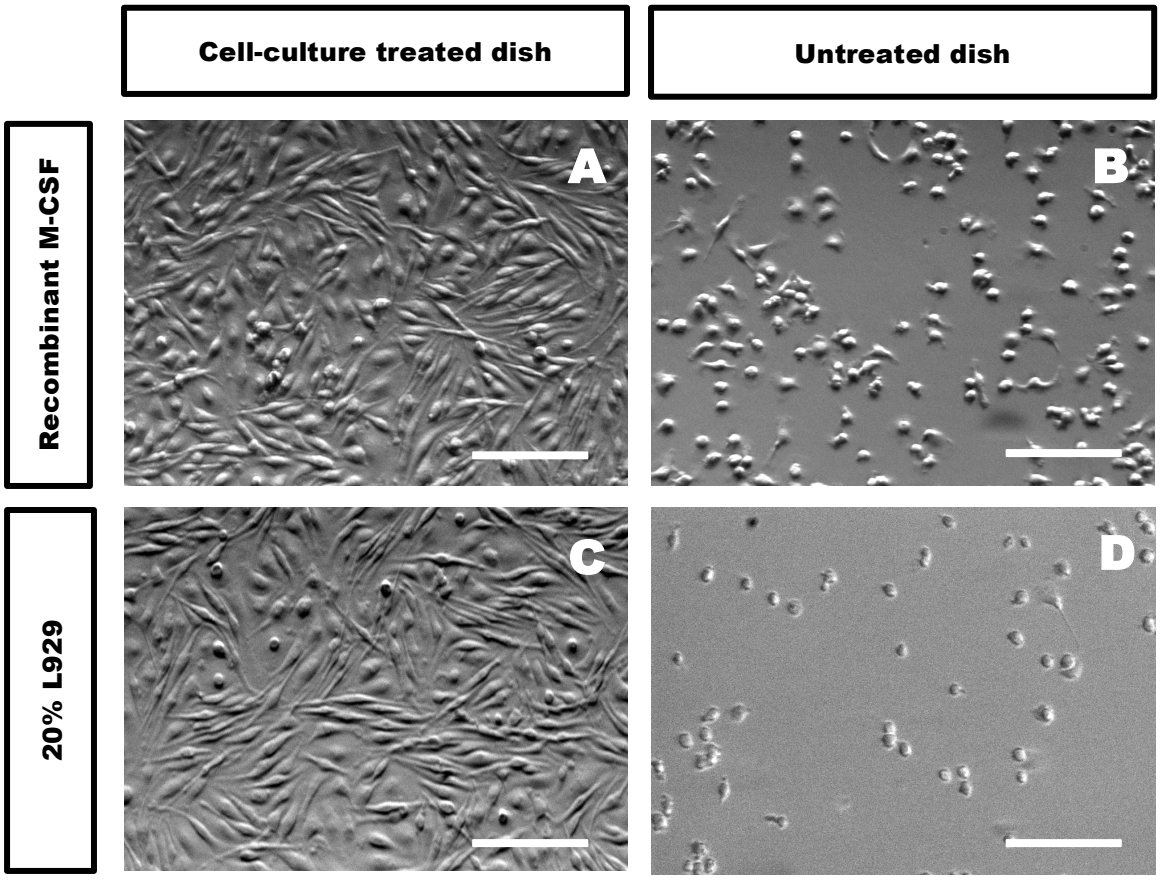

Figure 4.4: Stereomicroscope images of 2-week old primary murine macrophages differentiated by incubation in 40 ng/ml of the recombinant M-CSF (rmM-CSF) cytokine (A and B) or 20% L929 (C and D) on a cell culture treated dish (A and C) and an untreated bacterial dish (B and D). Scale bar represents 200 μm.

To further evaluate if the macrophages were properly differentiated, we tried to evaluate typical macrophage traits including testing for the macrophage surface marker CD14, and testing their phagocytotic ability. First of all, CD14 expression was tested by immunolabeling and confocal imaging. The primary murine macrophages were positive for CD14 (red fluorescence) in 96-100% of the cells (**Figure 4.5A**). As a positive control, we also labeled the mouse RAW macrophage cell line, which also had the CD14 signal (**Figure 4.5B**). The negative control (no primary antibody) did not show any specific labeling (**Figure 4.5C**).

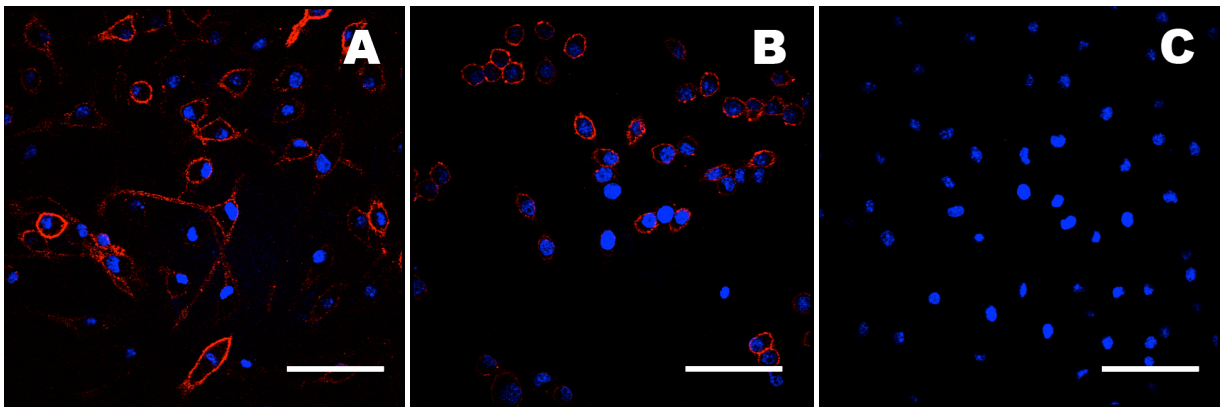

Figure 4.5: Macrophage characterization by CD14 staining. Primary murine macrophages (A) stained with CD14 (red) and Hoechst to visualize nuclei (blue). RAW cells used as positive control (B) and negative control in absence of primary CD14 antibody (C). Scale bar represents 50 µm.

A defining characteristic of macrophages is their strong phagocytic activity. We therefore tested macrophages for their ability to take up NPs by incubating them with green fluorescent PLGA-coumarin-6 NPs. Fluorescence confocal microscopic analysis showed intracellular NPs in all cells **(Figure 4.6)**.

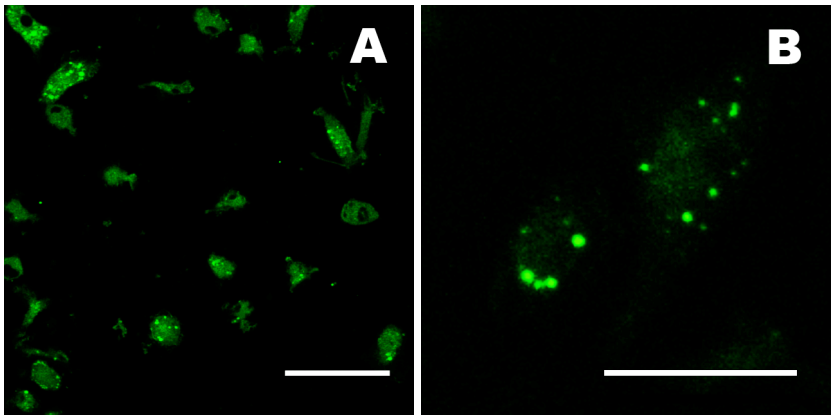

Figure 4.6: Test of macrophage phagocytic activity by means of fluorescent NP uptake. Cells were imaged in the confocal microscope. Scale bars represent 50 µm.

4.3 *In vitro* CCK toxicity assay

Cell viability was quantified following treatment of primary murine macrophages with equal concentrations of free and encapsulated PLGA-TZ (2.5, 5.0 and 7.5 μg/ml) for a total of 9 days, with measurements at day 3, 6 and 9. Already from day 3, the cells in conditions with higher concentrations of free TZ were visibly changed to a more rounded morphology and many were detached. However, the encapsulated form of the drug did not affect the cells in this way at the same concentrations of drug. Results are summarized in **Figure 4.7**.

The two highest concentrations of encapsulated TZ (5 and 7.5 μg/ml) were significantly less toxic than their free dose counterparts at both day 6 and day 9 (both $p < 0.0001$). The lowest concentration of free drug used, 2.5 μg/ml TZ did not show any significant *in vitro* toxicity compared to untreated cells for the duration of the CCK8 assay. The viability of cells treated with free TZ at 5 μg/ml, on the other hand, was significantly reduced to only 60% that of controls after 3 days ($p < 0.05$), and 7% after 6 days ($p < 0.0001$), with no viable cells left at the last time-point. Cell viability after treatment with free TZ at 7.5 μg/ml was also significantly reduced to 12% after just 3 days ($p < 0.0001$), with no viable cells left already after six days. In striking contrast, throughout the 9 days of treatment at the corresponding concentrations of TZ, the viability of all the PLGA-TZ-treated groups was not significantly different from untreated cells. This was also the case for treatment with empty PLGA NPs and even the combination treatment group, which had a total of 43.8 μg/ml NPs (by NP weight), corresponding to 8 μg/ml RIF and 5 μg/ml TZ.

The low dose of 2.5 μg/ml free TZ caused viability to increase above that of controls at day 6 and 9. This is possibly because low levels of toxic substances often stimulate metabolic activity in cells. When the concentration of TZ was increased, there followed a dose dependent increase in toxicity already at 3 days. However, this toxicity was reduced when using the encapsulated form of TZ, indicating that the PLGA NPs were able to shield the cells from TZ's toxic effects. This is most likely due to slow release of the drug.

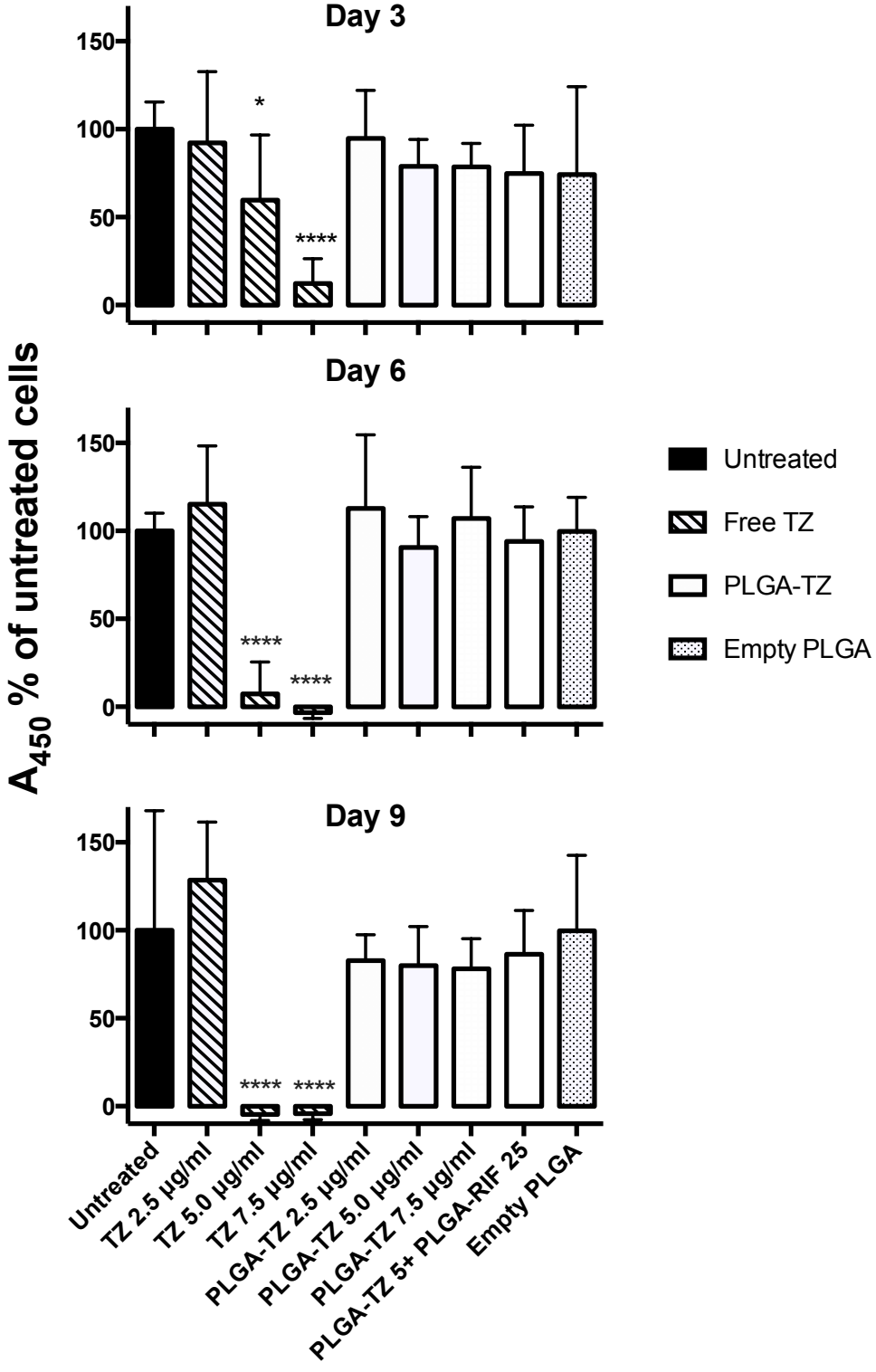

Figure 4.7: Viability of cells in response to TZ as measured by absorbance at 450 nm (A_{450}) using CCK-8 assay (n=3). TZ was added to cells at 2.5, 5.0 and 7.5 µg/ml in free form and at corresponding concentrations of the encapsulated form (PLGA-TZ). A_{450} values are expressed as mean ± 95% confidence interval, normalized to untreated cells for each time-point. Asterisks represent significant difference from untreated cells, as determined by one-way ANOVA in GraphPad Prism 6, * $P < 0.05$ and **** $p < 0.0001$.

4.4 *In vitro* treatment effect

4.4.1 Colony forming unit time-kill assay

The CFU time-kill assay is considered a standard microbiological technique for the quantification of bacterial load. This method was used to determine the therapeutic effect of our newly synthesized TZ and RIF NPs. PLGA-RIF (at 8 μg/ml by drug weight) and PLGA-TZ NPs (at 2.5 and 5 μg/ml by drug weight) were tested alone and in combination with each other, in primary murine macrophages infected with BCG. One treatment condition used a combination of free TZ and free RIF (5 and 8 μg/ml, respectively). In both cases, treatment lasted for 3 hours, and no notable toxic effects with respect to morphology and cell attachment were seen in any of the treatment conditions, including free drug-treated wells.

Results of the CFU analysis are shown in **Figure 4.8**, and only statistical significance at the last time-point is shown, to emphasize the overall treatment effect. A two-way ANOVA analysis revealed that there was a significant interaction ($p < 0.0001$) between the two variables, indicating that the treatments change differently relative to each other over time.

Unlike previous CFU experiments in our group, which show a steady decrease in bacterial load in untreated controls and all treatment groups [123], all groups in the experiment presented here showed net growth of bacteria at the final time-point. The different conditions seem to be separated into two distinct populations: those that were RIF-treated and those that were not. All conditions treated with RIF, whether free or encapsulated, had an initial drop in CFUs not seen in conditions lacking RIF. However, this initial drop did not last beyond 3 days, and in all samples the BCG started growing again after day 3 and continued to grow until the end of the assay. Treatment using PLGA-TZ NPs alone, at both high and low doses, had a significantly reduced BCG load at the final time-point. Furthermore, the combination treatment using 8 μg/ml PLGA-RIF and 5 μg/ml PLGA-TZ was significantly more effective at killing BCG than the PLGA-RIF treatment alone at day 3. At day 9, both the combination treatments using RIF NPs and 2.5 or 5 μg/ml of TZ NPs were significantly better (giving a 2-fold greater reduction of CFUs) than the PLGA-RIF alone.

The free RIF- free TZ combination treatment was also much more efficient than expected. Free drugs were added only once for 3 hours, before cells were washed twice with PBS and given fresh media. Despite this, the free drug combination treatment was comparable in efficiency to the NP combination treatments. At day 3, free drug treatment even appeared to be more effective at lowering CFUs than the corresponding concentration of

encapsulated drugs, although this difference was not significant. However, at day 9, free drugs did give slightly higher CFUs than their NP counterparts, although this was not considered significantly different.

This experiment was also adapted for enumerating bacterial load using the *M. tb* strain H37Rv in human macrophages by our collaborator David Pires in Elsa Anes's group (University of Lisbon, Lisbon, Portugal). Data from this experiment is shown in **Figure 8.1** in the appendix, under supplementary results.

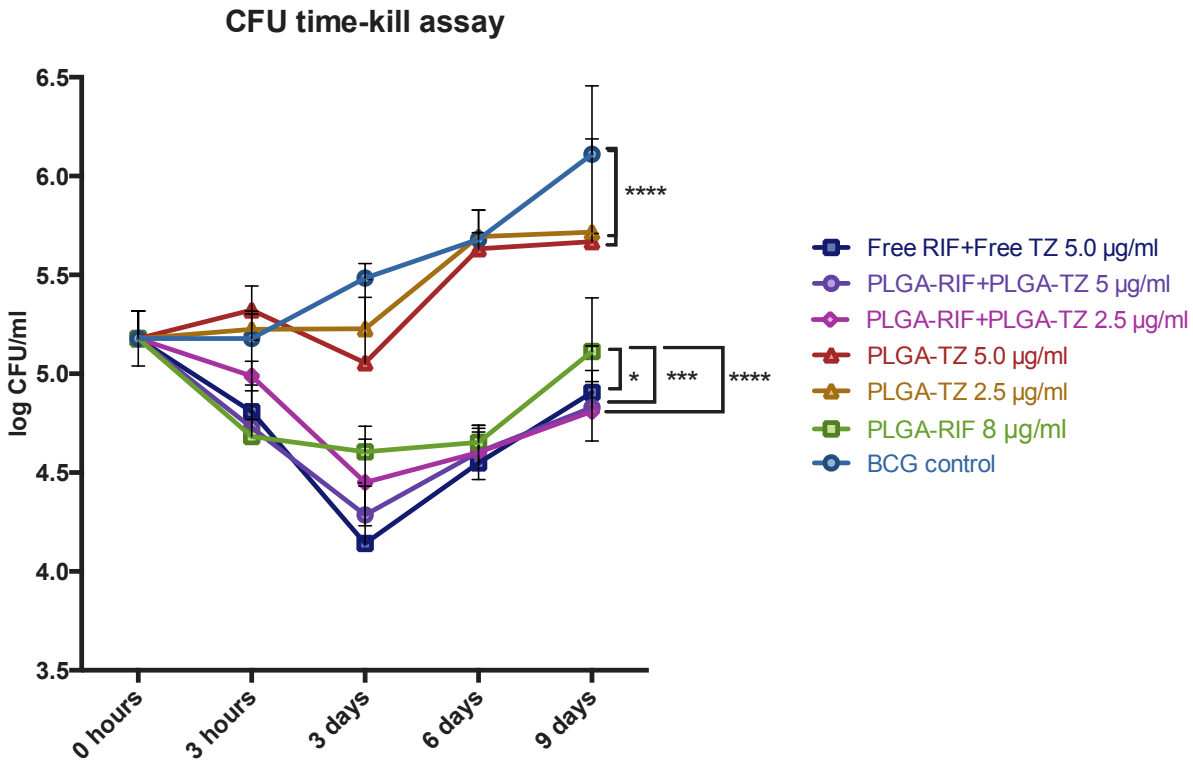

Figure 4.8: Colony forming unit assay using encapsulated PLGA-TZ NPs (at 2.5 or 5 µg/ml in drug weight) and PLGA-RIF NPs (at 8 µg/ml in drug weight) or free TZ and RIF (at 5 and 8 µg/ml in drug weight respectively). Treatment duration was 3 hours for both NP and free treated conditions (n=3). Values are given as mean log CFU/ml ± 95% confidence interval. Asterisks represent statistical significance, as determined by two-way ANOVA in GraphPad Prism 6, * $p < 0.05$, ** $p < 0.001$, **** $p < 0.0001$.

4.4.2 Developing a BCG luciferase time-kill assay

To ensure correlation of the traditional CFU time-kill assay with the luciferase time-kill assay, the two methods were carried out in parallel to quantify bacterial load of primary cells infected with BCG-lux at a range of concentrations (OD_{600} 0.05-0.0005). Values were normalized to the reading obtained from the highest MOI (**Figure 4.9**). A Pearson correlation analysis was carried out, which determines the linear correlation coefficient (r). The r-value measures the strength and direction of a linear correlation such that an r of 1.0 is a perfect positive correlation, and the closer r is to 1.0, the more correlated the two methods are. The

coefficient of determination (r^2) can also be computed, where r^2 represents the proportion of the data whose variation can be explained by the linear relationship between x and y. The analysis gave an r of 0.999 (P= 0.00004) for both pairs, and thus an r^2 of 0.998 (99.8%), indicating a high degree of correlation (**Figure 4.10**).

An initial infection OD_{600} of 0.05 corresponds to $5x10^6$ BCG to which the macrophages were exposed for 3 hours. However, the number of CFUs extracted 24 hours later was 7.6-fold lower than initial number of CFUs used for infection, likely due to the loss of bacteria during infection or the lysis procedure. Lysis of the macrophages infected with the lowest infection OD_{600} of 0.0005 only yielded approximately 1300 bacteria after 24 hours, which is more than 38-fold less than the initial level of infection.

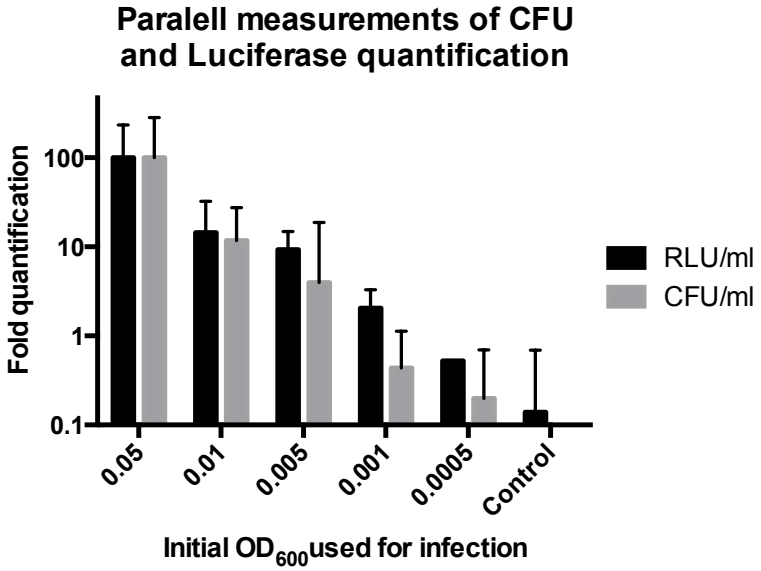

Figure 4.9: Bacterial quantification of BCG-lux by parallel experiments using two different methods: traditional CFU enumeration and the luciferase assay. Values are expressed as mean ± 95% confidence interval.

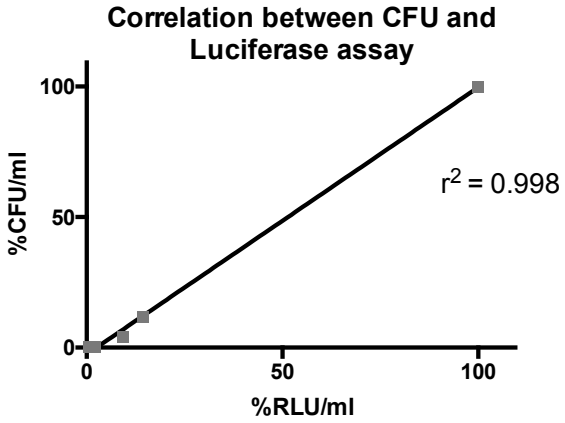

Figure 4.10: Graphical representation (linear regression) of the coefficient of determination (r^2) between the CFU and luciferase quantification methods, which represents the strength of their correlation.

4.5 *In vivo* toxicity analysis

4.5.1 Toxicity indicators in zebrafish larvae

To determine TZ's toxicity *in vivo*, free TZ and encapsulated PLGA-TZ NPs was injected into zebrafish larvae at 3 dpf at the dose used for survival studies, 32 mg/kg. Strikingly, free TZ in larvae immediately caused the heart to stop beating, and in some cases, it did not start beating again for more than 60 seconds, while in others it did not start beating again at all. In fact, one fourth of the larvae injected with free TZ did not survive the treatment on the first day, while all the fish in the NP-injected or mock-injected groups survived for at least the first 4 days after treatment. In fact, the overall survival of the NP-treated larvae was not considered significantly different from the mock-treated larvae ($p=0.1410$) but was significantly different from the survival of larvae treated with free TZ ($p< 0.0001$) as shown in **Figure 4.11**. Of the fish treated with free TZ that did survive, by 4 days post treatment (dpt) 5 out of 6 had severe edemas (see edemas in **Figure 4.14**), all 6 lacked swim bladders and 3 out of 6 had yolk sac discoloration (see summary of morphological indicators in **Table 8.1** in appendix, supplementary results). By these morphological indicators, the NP-treated larvae were not particularly different from mock-treated larvae, as seen in **Figure 4.14**. To quantify this, a disease score was calculated. The mean scores assigned to each group were plotted in a scatter plot, shown **Figure 4.12**. In terms of disease score, the mock-treated fish were not considered significantly different from the PLGA-TZ treated group, but the free TZ-treated group scored significantly higher than the mock and PLGA-TZ treated groups ($p< 0.0001$ and ($p< 0.001$ respectively).

In addition, the heart-rate in larvae injected with free TZ was also slowed to almost half of the mock-treated group, while the heart-rate of PLGA-TZ-injected group was not significantly different from the mock-treated group (**Figure 4.13**). For simplicity, only significance at 1 dpt is shown in **Figure 4.13**. However, at 3 dpt the heart-rates of mock-treated and PLGA-TZ-treated groups were still not significantly different, whereas the heart-rate of the free TZ-treated group was significantly different to both mock-treated ($P<0.01$) and to PLGA-TZ-treated larvae ($P<0.05$). Judging from these results and results in **Figures 4.11-4.14** the overall health of the PLGA-TZ-treated group was comparable to that of the mock-treated group.

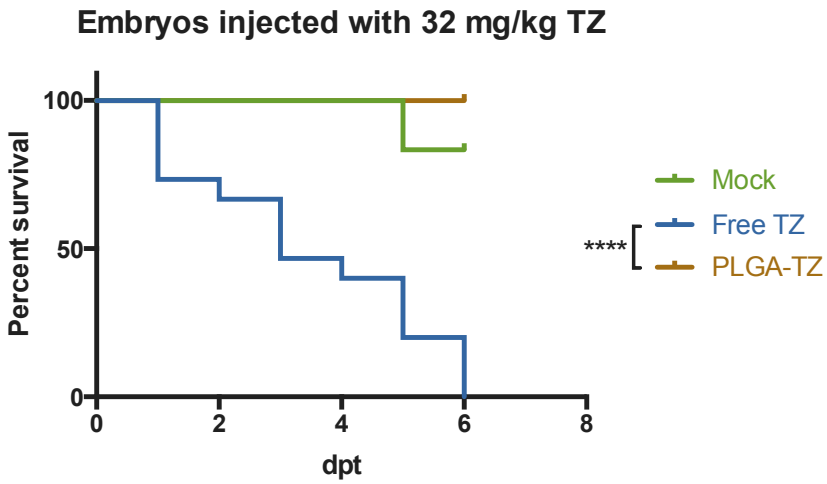

Figure 4.11: Survival of zebrafish larvae injected with 32 mg/kg free TZ or corresponding amounts of PLGA-TZ in 2% PVP. Mock-injected larvae were injected with the same volume of 2% PVP only. Survival curves representing mock-injected and PLGA-TZ injected larvae were not significantly different (p=0.1410). Asterisks represent statistical significance, as determined by survival analysis in GraphPad Prism 6, **** $p < 0.0001$. (Initial n= 15, 13 and 6 for free, NP and mock respectively)

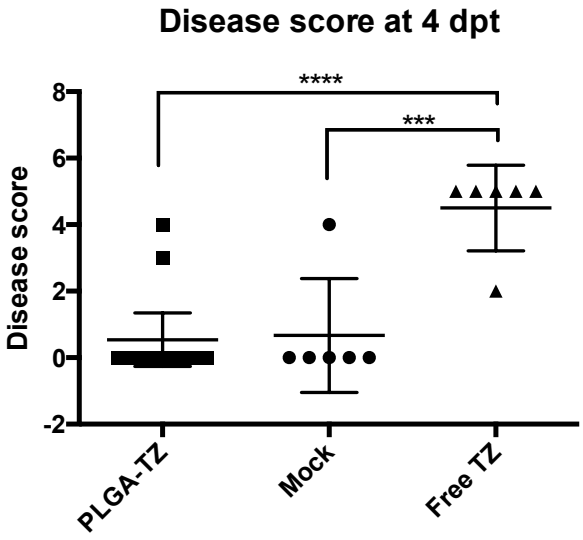

Figure 4.12: Scatter plot representing disease score at 4 dpt of zebrafish larvae injected with free TZ or PLGA-TZ at 32 mg/kg in 2% PVP. Mock-injected larvae were injected with the same volume of 2% PVP only. The disease score was calculated by assigning values to morphological toxic indicators as outlined in **Table 3.3**. Each symbol represents the score of individual larvae, and the horizontal line represents the mean. Error bars denote the 95% confidence interval. Asterisks represent statistical significance, as determined by one-way ANOVA analysis in GraphPad Prism 6, *** $p < 0.001$, **** $p < 0.0001$. (n= 6, 13 and 6 for free, NP and mock respectively)

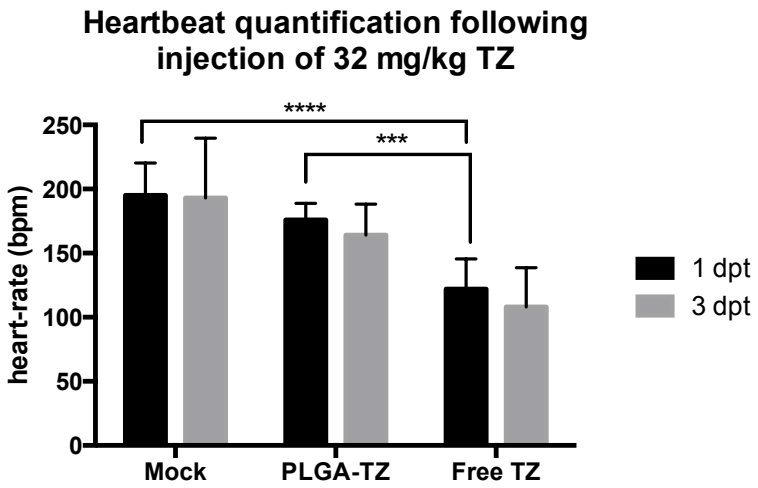

Figure 4.13: Heart-rate quantification in zebrafish larvae injected with 32 mg/kg free TZ or corresponding amounts of PLGA-TZ in 2% PVP. Mock-injected larvae were injected with the same volume of 2% PVP only Heart-rate is given in mean beats per minute (bpm) ± 95% confidence interval. Heart rates of mock-injected larvae were not considered significantly different from PLGA-TZ injected larvae. Asterisks represent statistical significance, as determined by one-way ANOVA analysis in GraphPad Prism 6, *** $p < 0.001$, **** $p < 0.0001$. For simplicity only significance at 1 dpt is shown (n= 11, 13 and 6 for free, NP and mock respectively at 1 dpt and n=7, 13 and 6 for free, NP and mock respectively at 3 dpt).

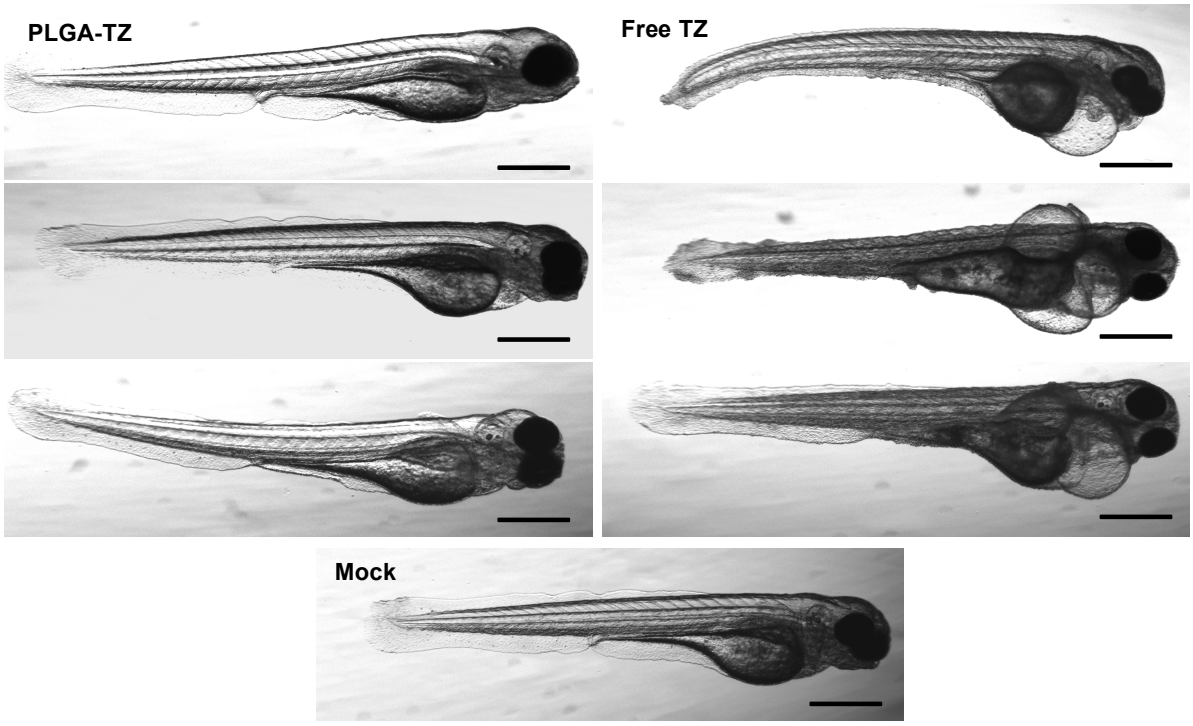

Figure 4.14: Morphological comparison of larvae at 2 dpt (4 dpf) after injection of free TZ, encapsulated PLGA-TZ, or mock treatment. Following treatment, free TZ-injected larvae developed pericardial edemas and necrotic spots not seen in PLGA-TZ-injected fish at the same dose of TZ (32 mg/kg). Scale bar represents 0.5 mm.

4.6 *In vivo* combination therapy

4.6.1 Treatment using injected PLGA-TZ NP at 12 mg/kg and RIF bath

In addition to reducing toxicity, NP treatment may make drug delivery more efficient. However, the toxic nature of TZ at the concentrations used for treatment makes it difficult to directly compare free and encapsulated forms of the drug. Therefore, PLGA-TZ NPs were used in all *in vivo* treatment experiments.

TZ therapy was tested *in vivo* in zebrafish infected with *M. m* at 2 dpf and injected with PLGA-TZ NPs or mock-injections at 3 dpf. Free TZ was not used due to the high toxicity of the treatment dose. Combination treatment was tested by adding free RIF to the embryo water at 200 µg/ml (instead of injecting RIF), to avoid potential harmful effects from multiple injections. In the first survival experiment, 3 nl of PLGA-TZ NPs solution was injected in larvae, corresponding to a treatment dose of 12 mg/kg. Survival was recorded daily and results are shown in **Figure 4.15**. Unlike the synergistic tendency seen in the *in vitro* data, the PLGA-TZ/RIF combination treatment was not significantly different from RIF treatment alone (p=0.8622). Furthermore, PLGA-TZ treatment alone was not significantly different compared to the mock treated larvae (p=0.4478). Unsurprisingly, treatment with RIF bath alone significantly improved survival compared to mock treated larvae (p=0.0015).

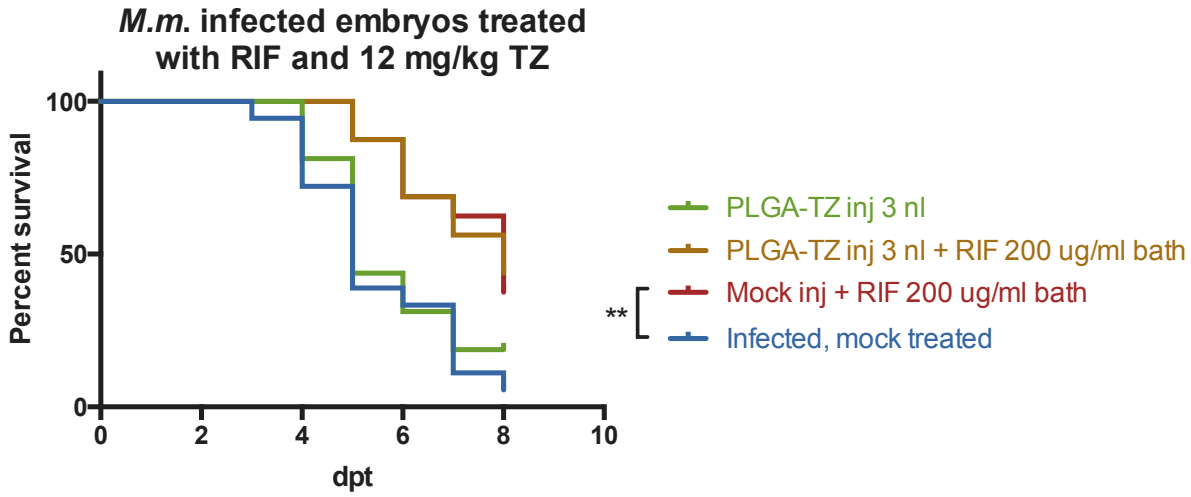

Figure 4.15: Survival of zebrafish larvae (n=16-18) injected with 12 mg/kg PLGA-TZ in 2% PVP or mock injected with 2% PVP only, and treated with 200 µg/ml RIF bath or embryo water only. Survival curves representing the PLGA-TZ/RIF combination treatment were not significantly different from RIF bath treatment only (p=0.8622). PLGA-TZ treatment alone was also not significant compared to mock treated larvae (p=0.4478). Asterisks represent statistical significance, as determined by survival analysis in GraphPad Prism 6, ** $p < 0.01$

4.6.2 Treatment using injected PLGA-TZ at 32 mg/kg and RIF bath

The experiment outlined in the section above was repeated, but this time the dose of TZ was increased to 32 mg/kg, which has previously been shown to potentiate therapy in a mouse model of TB [85]. The results are shown **in Figure 4.16**. In this experiment, the increased dose of PLGA-TZ combined with the RIF bath significantly increased the survival of the larvae compared to RIF bath treatment alone (p=0.0027). However, the PLGA-TZ treatment alone did not significantly increase larvae survival, unlike the *in vitro* results.

The last surviving larvae from the PLGA-TZ/RIF bath combination group and the RIF-bath treated only group were also imaged in the fluorescence microscope at 11 dpt to estimate the relative bacterial burden (**Figure 4.17**). The larvae that received PLGA-TZ/RIF bath combination treatment had reduced visible fluorescent bacterial load relative to larvae treated with RIF bath only, suggesting that the combination treatment was more efficient. In fact, one individual receiving combination treatment showed almost complete clearance of the fluorescent bacteria.

The experiment was repeated a second time using the same dose of PLGA-TZ NPs (32 mg/kg) and RIF bath treatment. In order to see what contribution the PLGA component of the NPs had on therapy, a combination treatment using injection of empty (drug-free) PLGA NPs with RIF bath was also included (**Figure 4.18**). Again, the PLGA-TZ/RIF bath combination treatment significantly improved survival relative to treatment with RIF bath alone (p=0.0146), while PLGA-TZ therapy alone was not significantly different from mock treated larvae (p=0.8043). Interestingly, combination treatment with injected drug-free PLGA NPs and a RIF bath was not significantly different from either PLGA-TZ/RIF bath combination treatment (p=0.1452) or RIF bath alone (p=0.2386).

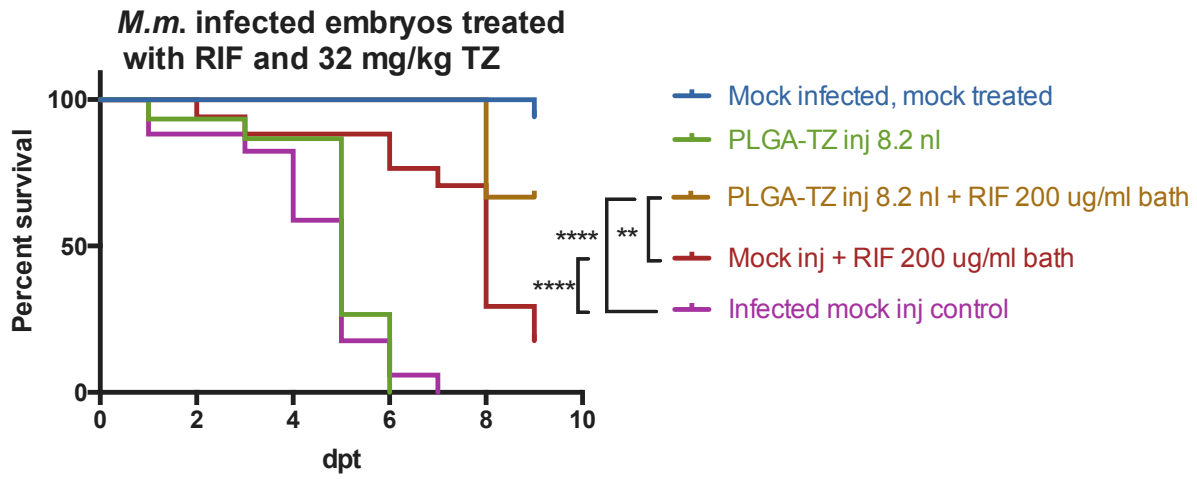

Figure 4.16: Survival of zebrafish larvae (n=15-17) injected with 32 mg/kg PLGA-TZ in 2% PVP or mock injected with 2% PVP only, and treated with 200 µg/ml RIF bath or embryo water only. Survival curves representing the PLGA-TZ/RIF bath combination treatment were significantly different from RIF bath treatment alone (p=0.0027). However, PLGA-TZ treatment alone was not significant compared to mock treated larvae (p=0.3483). Asterisks represent statistical significance, as determined by survival analysis in GraphPad Prism 6, ** $p < 0.01$, **** $p < 0.0001$.

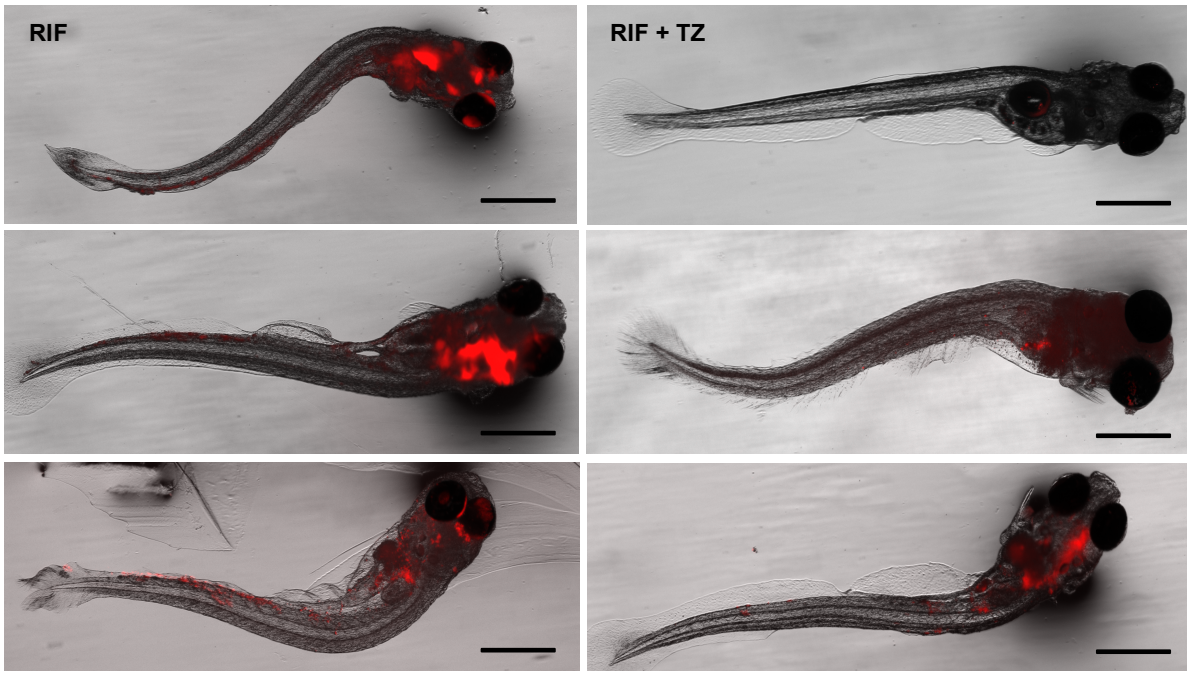

Figure 4.17: Zebrafish larvae at 9 dpt (11 dpf) infected with dsRed *M. m* and treated with either 200 µg/ml RIF bath only (left) or a combination treatment with 32 mg/kg PLGA-TZ injections and 200 µg/ml RIF bath (right). Larvae were imaged in the fluorescence microscope. Scale bar represents 0.5 mm.

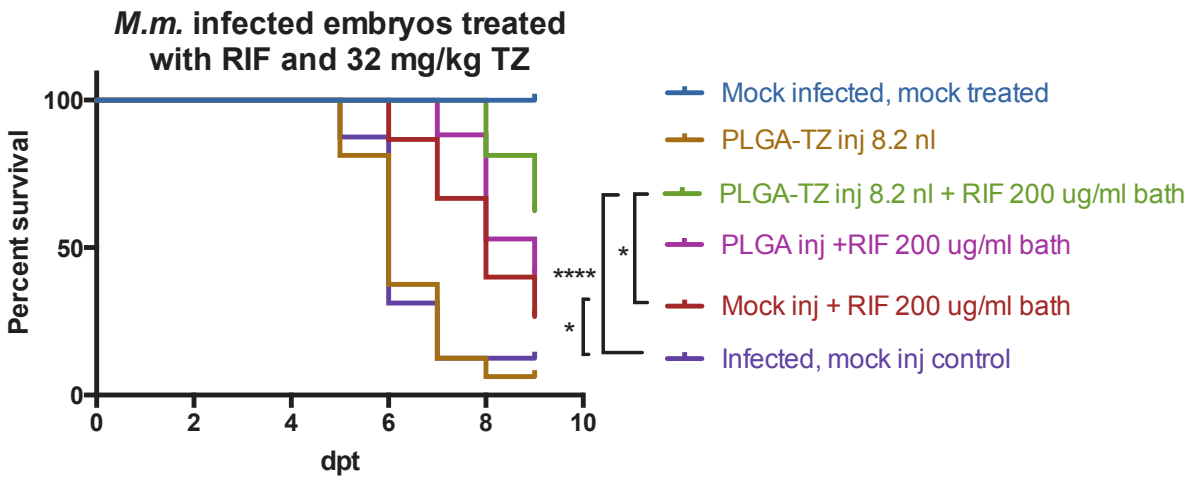

Figure: 4.18: Survival of zebrafish larvae (n=15-17) injected with 32 mg/kg PLGA-TZ in 2% PVP or mock injected with 2% PVP only, and treated with 200 µg/ml RIF bath or embryo water only. Survival curves representing the PLGA-TZ/RIF bath combination treatment were significantly different from RIF bath treatment alone (p=0.0146). Treatment with empty PLGA NPs and RIF bath was not significantly different from either PLGA-TZ and RIF bath (p=0.1452) or RIF bath alone (p=0.2386). PLGA-TZ treatment alone was not significant compared to mock treated larvae (p=0.8043). Asterisks represent statistical significance, as determined by survival analysis in GraphPad Prism 6, * $p < 0.05$, **** $p < 0.0001$

5 Discussion

5.1 Preparation of thioridazine nanoparticles

In order to efficiently encapsulate different drugs like RIF and TZ, the encapsulation procedure has to be carefully optimized to match their unique physical properties, such as their relative hydrophobicity. With this in mind, a protocol for the encapsulation of TZ in biodegradable PLGA NPs was established. For the PLGA NPs to efficiently function against *M. tb*, they must be able to reach intracellular bacteria, inside macrophages. Previous studies done in our group have shown that 90% of polymeric NPs can be found in phago-lysosomes, whereas BCG were located in early phagosomes inside the same cells [123]. It was expected from the outset that the physical characteristics of NPs can make a difference in how efficiently NPs are taken up. With this in mind, NPs are made small enough for phagocytosis, but also made to have a surface charge in order to be more easily recognized by the macrophages that take them up.

5.1.1 Optimization and characterization of PLGA-TZ

A protocol for the formulation of PLGA-RIF NPs has previously been established and tested [114, 123]. By following this protocol, PLGA-RIF NPs were formulated with similar drug loading to those prepared previously, approximately 32%. We had not yet optimized the formulation of PLGA-TZ NPs, however, and this prompted the evaluation of different parameters in order to establish the method best suited for TZ encapsulation.

TZ is more hydrophobic than RIF, and as might be expected the highest TZ loading was achieved with the more hydrophobic PLGA (75:25) polymer, with 1% PVA. However, like many of the other NPs, these particles were difficult to re-suspend in an aqueous solution. In order to take advantage of the higher loading efficiency achieved with this more hydrophobic variety of PLGA, the amount of PVA could be increased to make NPs with higher loading that are easier to resuspend in water. The addition of an emulsifier like PVA contributes reducing aggregation and lowering surface tension, which increases the solubility of the hydrophobic drug in the aqueous phase [143]. It follows that a higher amount of emulsifier could also aid the retention of drug in the aqueous phase during NP preparation, which may lead to a lower encapsulation. However, varying the amount of PVA from 1 to 4% in the different PLGA (50:50) NPs did not seem to affect the encapsulation significantly, as all the TZ-NPs we made had a loading of 25-27% (**Table 4.2**).

In the end, the TZ NPs with PLGA (50:50) and 4% PVA were chosen for continued characterization, as these had the highest loading (26.5%) of the NPs that could be re-suspended in water. Measurements using the Zetasizer (**Table 4.3**) revealed that both these NPs and the PLGA-RIF NPs had a size distribution range, quantified as PDI, below 0.7 [130], which indicates that they make up a relatively homogenous suspension and have a lower tendency to aggregate. One of the reasons for their lack of aggregation is likely their overall negative charge. High NP charge causes electrostatic repulsion between particles, making them less likely to aggregate and sediment. Surface charge therefore makes an important contribution to solution stability [130]. Furthermore, a negative surface charge also leads to increased opsonization (such as binding of IgG or complement factors from serum) and rapid macrophage uptake compared to neutral NPs, despite the negative charge of cell membranes [116]. In addition, PLGA's hydrophobic nature is also conducive to binding of opsonins [144]. Taken together, these physical properties of NPs make them favorable for macrophage uptake, which in turn promotes the bioavailability of the encapsulated drug [144].

The size of the PLGA-TZ NPs determined by the Zetasizer and EM (approximately 500 and 200 nm respectively) places them in the range for macrophage phagocytosis (100 nm-3μm) [116, 142]. In the Zetasizer, size is quantified as the hydrodynamic diameter of NPs, which reflects the fact that the measurement is dependent on their speed of diffusion through a given solvent. The hydrodynamic diameter depends on the NPs interaction with the solvent, which forms a discrete layer on the outside of the NP. In theory, the hydrodynamic diameter may therefore be larger than the NP's diameter in the absence of an aqueous environment. The measurement of NP diameter is inextricably linked to the solvent used, as the properties of the solvent can have a significant impact on the results. For instance, the hydrodynamic diameter of particles can be exaggerated if the medium has low conductivity. Conversely, a medium with high conductivity can underestimate the particle size. This is due to the conductivity of the medium affecting the diffusion speed of the particles in the solvent, which affects the degree of scattering and thus the diameter measurements [130]. The measurements reported in **Table 4.3** were taken in de-ionized water, which can explain why the diameters estimated by imaging in the EM are smaller than those reported by the Zetasizer. In addition to diameter, choice of solvent also affects the zeta-potential. This is because the zeta-potential represents *overall* NP charge, which takes into account the layer of solvent molecules around NPs in solution and is measured at a small distance from its surface. This overall charge can vary from the surface potential of the particle itself due to

interactions with the solvent in this discrete layer around the NP [130]. As the measurements presented in **Table 4.3** were taken in distilled water, a solvent that does not reflect the physiological environment, these values may be an inaccurate estimate of the physical characteristics *in vitro* or *in vivo*. To more realistically and accurately measure NP size and charge, it may be better to use a more physiologically relevant solvent, such as an isotonic, physiological salt solution (0.9 % w/v NaCl). As described above, size and charge are important for cell interaction with NPs in terms of uptake, immunogenicity and clearance from the blood stream.

The size and shape of NPs can also help to localize NPs to certain tissues. This would be interesting in the context of TB, as NPs can be made to preferentially accumulate in the lung, the main site of TB in humans. In the mouse model for instance, PLGA-NPs of approximately 200 and 500 nm injected into the circulation of mammals mostly end up in the liver and to a lesser extent in the lungs and spleen, without any active targeting [145]. However, increased homing of NPs to the lung can be achieved via actively targeting with antibodies, and increased phagocytosis by macrophages can be achieved by making rod-shaped NPs [146]. An alternative approach is to target NPs or microparticles to the lungs is via direct aerosol administration [147].

5.2 The encapsulation of thioridazine reduces toxicity

Toxicity is a major concern when it comes to the potential use of TZ for the treatment of TB [148]. The rate of sudden death due to heart failure is nearly twice as high in patients undergoing neuroleptic treatment with TZ compared to the general (untreated) population [85]. Using TZ to treat TB in humans will most likely necessitate even higher concentrations than those normally used for neurological disorders, which is typically around 8 mg/kg in chronically psychotic patients [90]. Judging from both *in vitro* and *in vivo* studies performed here, however, encapsulation can make TZ less toxic than the free form of the drug.

5.2.1 Thioridazine *in vitro* toxicity in macrophages

The results of the CCK-8 toxicity assay show that the encapsulation of TZ significantly decreased the toxic effects of free TZ on macrophages. The concentrations tested were the same as those used in previous *in vitro* treatment experiments in our group (2.5 and 5 μg/ml TZ). In these experiments, the most promising synergistic effects were seen using 5 μg/ml continuously added free TZ in combination with 8 μg/ml PLGA-RIF NPs,

which cleared the intracellular infection after 9 days (unpublished data by Raja Kalluru). However, there were some indications that this concentration was toxic, noticed both by our group and by our collaborators David Pires and Elsa Anes working on human macrophages and *M. tb*. In support of this, it has previously been established that 3 μg/ml free TZ is toxic to 50% of macrophages, whereas 10 μg/ml gives 100% toxicity after 72 hours [79]. We therefore decided to quantify cell survival using the CCK assay and to see whether high concentrations of the drug are less toxic when encapsulated. According to the data presented in **Figure 4.7**, we saw that 5 μg/ml is toxic in the free form but that this toxicity can be significantly reduced by encapsulation in concentrations up to (but not limited to) 7.5 μg/ml. This result fits well with the widely expressed advantage of NPs in reducing drug toxicity *in vivo* [149].

The lowest concentration of free drug used in this thesis (2.5 μg/ml) did not show any significant *in vitro* toxicity for the duration of the CCK8 assay. If anything, the macrophages seem to be stimulated by the low dose of TZ, as their dehydrogenase activity was slightly higher than in the untreated cells at the last two time-points, although this difference was not deemed significant. This issue is addressed in the product trouble-shooting guide of the commercial CCK8 assay, which states that low levels of drugs can activate the cells as enzymatic activity increases in an attempt to eliminate the toxic substance. This can result in higher readings, reflecting an increase in metabolic activity that can be mistakenly interpreted as cell proliferation. It is conceivable that this antibiotic-stimulated increase in metabolism could be masking any toxic effect from treatment with 2.5 μg/ml TZ. To test this, one could use a method that detects cell death as opposed to cell viability, for example the LDH (lactate dehydrogenase) assay, which detects LDH, a biomarker released from dying cells [150].

5.2.2 Thioridazine *in vivo* toxicity in zebrafish

Injections of free TZ and encapsulated PLGA-TZ caused dramatically different phenotypes in the zebrafish larvae in terms of cardiotoxicity, yolk discoloration, edemas, swim bladder inflation and overall survival (**Figures 4.11-4.14**). The cardiotoxic effect of free TZ was especially striking, as injection of 32 mg/kg free TZ caused the heart to immediately stop beating in all fish. In the larvae that re-gained a heartbeat, there was a significant decrease in heart-rate (**Figure 4.13**). This effect resembles the human symptoms of prolonged QT-interval and ventricular arrhythmia following TZ exposure [68, 151]. In fact, quantification of toxicity in terms of morphological indicators in zebrafish has

previously correlated well with human data [138, 140]. In particular, drugs that are cardiotoxic in humans, such as aspirin and verapamil, also induce cardiotoxicity in zebrafish, including changes in heart-rate and formation of pericardial edemas. Conversely, drugs that manifest their human toxicity in other ways, such as gentamicin and tetracycline, do not cause cardiotoxicity in zebrafish [140]. With this in mind, the zebrafish model has been deemed excellent for high-throughput screening and prediction of human cardiotoxicity [140]. In the case of TZ, encapsulation in NPs clearly reduces this cardiotoxicity, which is a prerequisite for the evaluation of TZ's treatment effect. In contrast to free TZ injections, which cause 60% of treated fish to die within four days of treatment, the PLGA-TZ NPs make a fair comparison of TZ therapy to other treatments possible. In addition to TZ's cardiotoxicity, another striking effect of injecting 32 mg/kg free TZ in zebrafish was the incidence of pericardial edemas. Pericardial edemas occur when an abnormal amount of fluid accumulates in the space around the heart chamber. This phenotype is often associated with toxicity and can be caused by heart failure or changes in the blood flow, among other things [138]. By encapsulating TZ, the incidence of edemas was no longer a problem, and the larvae were morphologically indistinguishable from mock-treated fish.

The inflation of the zebrafish swim bladder, normally used by the fish for generating the lift necessary for flotation [152], is also a commonly used toxicity indicator [153]. Lack of swim bladder inflation in larvae treated with toxic chemicals often correlates with other morphological defects, such as edemas [139]. In order to inflate the swim bladder, larvae must achieve "swim-up behavior", which means they need to reach the surface to gulp the air necessary for inflation [152]. In zebrafish larvae, the swim bladder normally inflates within 96 hpf, which corresponds to 4 dpf [154]. In the toxicity analysis presented here, 4 out of 13 larvae (or 31%) treated with PLGA-TZ had still not inflated their swim bladders at 4 dpt (6 dpf). However, this effect is comparable to the mock-treated group where 2 out of 6 larvae (or 33%) had still not inflated their swim bladders at 6 dpf. This could indicate a general developmental delay in this particular batch of embryos, or reflect that the injection itself had some effect in interfering with swim bladder inflation. This illustrates the importance of having mock-injected controls for the sake of comparison, but would need to be verified by also including a non-injected group in the experiment. On the other hand, none of the larvae injected with free TZ at 32 mg/kg were able to inflate their swim bladders. These larvae could be failing to inflate their swim bladders due to the direct physiological effects of the drug, or indirectly due their general weakened condition causing a lack of "swim-up behavior" necessary for the process of inflation.

In addition to the morphological changes discussed above, larvae injected with free TZ have an overall change in color, which does not occur in mock or PLGA-TZ injected larvae. They become darker and develop necrotic spots, especially in the yolk sac. In summary, the encapsulation of TZ in PLGA NPs protects zebrafish larvae from the toxic effects associated with free TZ, including dramatic morphological changes in zebrafish larvae. The PLGA-TZ-injected larvae were comparable to mock-injected larvae in terms of heart rate, swim bladder inflation, edemas and yolk discoloration.

5.3 Thioridazine can potentiate rifampicin treatment

The treatment of TB using TZ is often applied by monotherapy in the literature [74, 79, 90, 155]. In fact, TZ monotherapy has been suggested as a treatment for XDR-TB [155], supported by promising results in infected macrophages [74], in the mouse model [85, 90] and in humans receiving compassionate XDR-TB therapy [155]. However, much of the experimental data, including our own, on TZ's therapeutic effect alone and together with RIF suggest that, while TZ has a modest effect on its own *in vitro*, the key lies in using a synergistic combination treatment rather than using TZ alone.

5.3.1 *In vitro* combination treatment using CFU time-kill assay

Experiments quantifying BCG CFUs following TZ-RIF combination treatment have been carried out previously (unpublished data by Raja Kalluru). These showed a steady decrease in CFUs in all groups, including the controls, and a clear synergistic effect of RIF NPs with free TZ. However, as mentioned above, in these experiments the toxic concentration of 5 μg/ml free TZ was added continuously throughout the experiment. It is therefore possible that the reduction of CFUs seen in those experiments was partially due to the death of macrophages hosting the bacteria, as opposed to death of bacteria themselves. In addition, the bacteria used for those experiments were cultured differently, and they were most likely not in the logarithmic phase when harvested. We therefore decided to repeat this experiment, and the results presented here differ from those previous results in several important aspects.

Firstly, we did not see the characteristic steady decrease in CFUs in any of our conditions. Untreated control bacteria grew continuously, and although both free RIF and PLGA-RIF-treated bacteria experienced an initial drop, these also started growing at the final time point (**Figure 4.8**). In direct contrast to this result, it has previously been reported that

BCG in mouse primary macrophages do not grow intracellularly, but rather show a steady decrease in the absence of any drugs. However, in the same study BCG did grow intracellularly in RAW macrophages and human primary macrophages [156]. Previous results in our group behaved more like the former, whereas the BCG in the results presented here behaved more like the latter, exhibiting intracellular growth. This discrepancy could reflect differences in culture conditions that influence bacterial growth.

The conditions used for BCG culture are extremely important for bacterial growth-state and antibiotic susceptibility. For example, limiting oxygen-supply can induce a non-replicative, dormant state in *M. tb* [157] and BCG [158], which makes them less susceptible to bacteriostatic drugs, including RIF and INH [47, 48]. Culture conditions can also interfere with a recently identified capsular layer in mycobacteria, which aids in virulence and is lost if a culture is agitated too much [159]. Bacterial cultures that are agitated regularly, either by shaking or in the context of processing for OD measurement, also grow faster than cultures that are not agitated. The vessel and volume used for culturing also has an effect, and bacteria may sometimes collect at the bottom of the vessel as a pellet. In the end, *artificial in vitro* systems vary a lot, and even the smallest variation in the culture procedure can have a big impact on the result.

The combination treatment using PLGA-RIF and PLGA-TZ showed a synergistic effect between the two drugs, reducing BCG burden by 19- and 20-fold with TZ at 2.5 and 5 μg/ml respectively. This is not an additive effect, as PLGA-RIF NPs alone reduced the burden by nearly 10-fold, and PLGA-TZ NPs alone reduced it by 2.5- and 2.8-fold at 2.5 and 5 μg/ml respectively. However, the contribution of TZ to synergy with RIF was not as striking as we have seen in previous experiments. This implies that the PLGA-RIF NPs used here were a lot more effective on their own, despite that the parameters such as duration of treatment and drug concentrations were kept constant. This could be due to the fact that the batch of PLGA-RIF NPs used previously was different, although they had very similar loading (approximately 32%). Despite this, the amount of drug that is released from a given batch of NPs may be different, either because of different physical-chemical release characteristics or because of differences in how the NPs were processed before treatment. Release studies on previous batches of PLGA-RIF NPs have been done in our group, measuring how much of the drug escapes from the NPs at pH 4, mimicking a lysosomal environment, and pH 7, mimicking a physiological environment. These experiments have shown that a rapid initial “burst-release” occurs with loss of 60% of the encapsulated drug after one day at pH 4, and 80% at pH 7 [123]. The lower release at pH 4 is most likely due to

RIF's reduced solubility at acidic pH [160]. Initial burst release in our NPs is followed by a slower release of the remaining drug that lasts for at least 12 days [123].

Previously in our group, treatment with RIF NPs was shown to be significantly more effective than treatment with free RIF. This is the case both *in vitro* [123] and *in vivo* [114]. On the other hand, in our latest experiment (**Figure 4.8**), treatment with free TZ and free RIF had an unexpectedly potent effect, comparable to treatment with PLGA-RIF NPs. Interestingly, at day 3, free drug treatment lowers CFUs more efficiently than the corresponding amounts of encapsulated drugs, which might be expected as an initial effect of the high dose of free drugs, although this effect was not significant. However, this effect did not last beyond the initial time points, as the free drug disappeared when the cell media was changed. However, the PLGA-RIF-treated conditions, whether alone or in combination with PLGA-TZ, also had a similar drop in CFUs at 3 days, after which they all started growing again. This does not fit well with the hypothesis of a prolonged NP treatment relative to free drug treatment due to sustained release of drug. This could, however, also be explained by the initial burst release effect. If 60-80% of the drug in the NPs is being released as soon as they are re-suspended in water, the NP treated cells will also have a relatively high amount of free drug in the media, almost approaching the levels of drug in the free drug-treated cells. In addition, to properly re-suspend the NPs in treatment media, a brief sonication is necessary. This may cause more drug to escape from the NPs, which contributes to the burst release-effect. In comparison to previous experiments, it is conceivable that the free dose of RIF used here was too efficient against our particular strain of BCG under our specific growth conditions, and that the burst release caused the level of free RIF in the NP treatment condition to be comparable to this free dose.

While the RIF was being rapidly released from NPs, this is likely not the case with the TZ in PLGA-TZ NPs, as this would clearly manifest itself as morphologic toxicity. Since we did not see any significant toxicity in the PLGA-TZ-injected larvae, TZ was probably better retained in the NPs than RIF was. TZ is more hydrophobic than RIF, and this could explain why TZ interacts better with the hydrophobic PLGA polymer. To verify this, release studies analogous to those done on RIF NPs would have to be carried out.

In the literature, drug-susceptible *M. tb* cultures have a TZ MIC of 15 μg/ml, and complete clearance was achieved with 30 μg/ml TZ in the absence of macrophages [74]. However, Ordway *et al.* [74] showed complete clearance of both susceptible and MDR intracellular *M. tb* infections after just three days using TZ mono-therapy at the extremely low, non-toxic concentration of 0.1 μg/ml. This striking reduction at such low concentrations

of TZ was attributed to a concentrating effect of the drug inside macrophages [72]. However, in the results reported by Ordway *et al.*, macrophages were pre-pulsed with TZ for 1 hour before they were actually infected. Hence, it is difficult to say if the decrease in bactericidal concentration was due to intracellular residence alone, or if pre-pulsing of the drug had an additional effect. Although pre-treating macrophages with TZ before infection works efficiently *in vitro*, it does not reflect therapeutic situations *in vivo*. When comparing our results to those of Ordway *et al.*, it is important to remember that, where free drugs where used in our model, we used a longer, 3-hour treatment, with a higher concentration of TZ (5 μg/ml), which was administered after macrophage infection. Still, our treatment, which was 25 and 50 times higher than the concentrations used by Ordway *et al.*, and administered in combination with free RIF (at 8 μg/ml), did not lead to clearance of the infection. The big difference seems to lie in the pre-treatment of cells with TZ before they are infected, which greatly boosts bacterial killing.

To our knowledge, there is only one other published study by Adams *et al.* [74, 161] where the antimicrobial capacity of TZ against *M. tb* inside macrophages is tested without pre-loading. In this paper, TZ improved treatment with RIF (approximately 1.5 fold) and INH (approximately 2-fold) following a 48-hour treatment with TZ at 2 μg/ml. However, these bacteria were made phenotypically resistant by intracellular residence in macrophages, and then released prior to treatment with TZ and RIF. Despite this, the results presented by Adams were comparable to the data presented in **Figure 4.8**, where both NP combination treatments (using 2.5 and 5 μg/ml TZ) improved PLGA-RIF NP treatment by 2-fold. Similarly, in **Figure 4.8** free RIF and free TZ combination treatment were approximately 1.6 fold better than PLGA-RIF treatment alone, again illustrating the fact that there is little difference between the free and encapsulated drugs in terms of efficacy.

In summary, despite the fact that we were not able to completely clear the infection in our system with these higher concentrations of TZ, we did see a significant reduction of CFUs at the final time point using PLGA-TZ monotherapy. We also observed a significant improvement when using both free and encapsulated TZ/ RIF combination treatment in comparison to RIF NP treatment alone, even if this was not different between free and encapsulated forms of the drug. In order to improve this treatment, we should increase the dose or duration of PLGA-TZ NP treatment in future experiments. However, we will most likely not be able to compare these higher doses of PLGA-TZ NPs to their free drug counterparts *in vitro* because, as we saw in the CCK assay, concentrations above 2.5 μg/ml are toxic to macrophages when administered continuously. In this respect the encapsulation

of TZ is advantageous after all, as it allows us to bring up the concentration of TZ without increasing toxicity.

5.3.2 CFU time-kill assay with *M. tb* and human macrophages

Our collaborator David Pires, working in Elsa Anes's lab in Lisbon, Portugal, also tested our PLGA-RIF and PLGA-TZ NPs in human macrophages infected with *M. tb* (presented in **Figure 8.1** in the appendix, supplementary results). Unlike our BCG CFU data, the PLGA-TZ NPs only had a brief effect in killing bacteria on the first day of the assay, after which these bacteria grew as fast as the untreated controls, with no reduction in CFUs at the last time-point. Despite the fact that PLGA-TZ alone had no significant effect, it did improve treatment in combination with PLGA-RIF NPs after day 5, implying synergy between the two drugs. In fact, the low dose of PLGA-RIF NPs with the high dose of PLGA-TZ NPs (8 and 2.5 μg/ml by drug weight respectively) was comparable to the high dose of PLGA-RIF NPs alone (16 μg/ml RIF by drug weight) at the final time-point. However, the RIF treatment alone was very potent, and therefore reducing this dose may be helpful in determining the real contribution of TZ in potentiating RIF treatment.

We have previously collaborated with David Pires and Elsa Anes to test free TZ in combination with PLGA-RIF NPs. During these experiments, the high concentration we had tested on BCG in our lab, 5 μg/ml was too toxic to use on primary human macrophages. Therefore they used 1.25 and 2.5 μg/ml free TZ instead. When they received the new batch of PLGA-TZ NPs from our lab, the same low concentrations were used, which can explain the lack of effect in the lowest treatment with PLGA-TZ only. However, while we saw a significant reduction in CFUs at the final time-point with 2.5 μg/ml PLGA-TZ NPs against BCG, this was not the case for the *M. tb*-infected human cells, implying that a higher dose of TZ may be necessary against this pathogenic strain. In order to test this, the dose of TZ could be increased in the future, since the PLGA-TZ NPs provide an opportunity to increase the dose of TZ without inducing toxicity. Our collaborators are now working on repeating this experiment using a higher dose of PLGA-TZ NPs, and a lower dose of PLGA-RIF NPs to see if the synergistic effects can be highlighted.

5.3.3 *In vivo* combination treatment with TZ and antibiotics

In the survival experiments conducted herein, initial injection of TZ was done with approximately 12 mg/kg TZ encapsulated in NPs, comparable to the concentration used by

Dutta *et al.* [89] in the mouse model. These authors showed no improved effect when using free TZ at 10 mg/kg in combination with free RIF at 10 mg/kg, although this dose of TZ did have a moderate effect in improving INH therapy [89]. Our results are similar in that this dose of PLGA-TZ had no significant effect on its own or in combination with the RIF bath in the zebrafish model. In subsequent survival experiments, we therefore increased the dose to 32 mg/kg (**Figure 4.16 and 4.18**), which is comparable to what van Soolingen *et al.* [85] used in the mouse model. This group of authors was able to show that both TZ monotherapy and combination treatment using free TZ at 32 mg/kg and free RIF at 10 mg/kg significantly improved therapy [85]. We also saw this improved synergistic effect in the zebrafish model using combination treatment with 32 mg/kg PLGA-TZ in the RIF bath; while PLGA-TZ alone did not improve treatment efficiency, RIF bath treatment alone improved survival by 2-fold, and treatment with RIF bath and PLGA-TZ injections improved survival 5-fold compared to untreated controls (**Figure 4.18**). In **Figure 4.16**, there are no untreated fish left at the final time point (9 dpt, 11 dpf), but again, while PLGA-TZ alone did not improve embryo survival, the combination treatment was 2.3-fold better than RIF bath treatment alone.

Unlike the *in vitro* data, the survival of larvae treated with our PLGA-TZ particles alone at 32 mg/kg was not significantly different from that of untreated controls. These experiments were only monitored for 9 dpt, after which conditions were no longer optimal, and uninfected controls stared to die. However, in the mouse model, *in vivo* monotherapy with lower doses of free TZ (16 mg/kg) given daily for 300 days has shown an 8-fold decrease in bacterial loads, although residual bacteria remained [90]. This implies that TZ may be even more effective if we could renew the dose of PLGA-TZ periodically, and monitor larvae for longer. To do this we would have to optimize living conditions so uninfected control larvae do not start dying after 9 dpt.

Previous survival experiments in our group have shown an improved effect of injecting PLGA-RIF NPs rather than free RIF [114]. This comparison is impossible in the case of TZ, as injecting the high dose of free drug necessary for treatment of *M. m* infection is highly toxic to the fish. In order to study combination treatment in the zebrafish larvae, the optimal situation would have been to use separate injections of both PLGA-RIF NPs and PLGA-TZ NPs. However, this would also be technically difficult to achieve and could adversely affect the fish. Instead, we tested a combination of RIF bath with PLGA-TZ NP injections, which improved survival relative to RIF bath treatment only.

Interestingly, as seen in **Figure 4.18**, injecting empty PLGA NPs also seemed to improve survival in combination with RIF bath, although this was not statistically significant. Previous experiments in our group have also shown that empty PLGA NPs slightly (non-significantly) improved survival of infected embryos, although PLGA-RIF NP injections were much more efficient, significantly improving survival [114]. This suggests that PLGA itself has an immunogenic effect, and an important question in our experiments is whether this putative macrophage stimulation contributes more than the anti-microbial effect of TZ itself. In our experiment, PLGA-TZ NPs did not significantly improve survival when administered alone, which implies that the TZ component of the NPs has limited therapeutic effect beyond what PLGA alone already contributes to survival. On the other hand, based on our results and the literature, TZ is more potent in combination treatment; while PLGA-TZ injections and RIF bath is significantly better than RIF bath alone, empty PLGA injections and RIF bath showed no such improvement. However, it is difficult to make this conclusion unequivocally, as the combination treatments with either PLGA-TZ or empty PLGA injections were not significantly different from each other.

5.3.4 Can we really call thioridazine an efflux pump inhibitor?

It is often implied in the literature that TZ mainly functions as an EP inhibitor. This is supported by data showing that antibiotic-induced increase in efflux of ethidium bromide by BCG bacteria can be blocked by adding TZ [80]. However, TZ is a pleiotropic drug, and considering the many effects it has on both bacterial and eukaryotic cells, it is difficult to say how each putative target contributes to overall clearance. With this in mind, it may not be appropriate to refer to TZ as an EP inhibitor only. One of the major pieces of evidence supporting TZ's role as an EP inhibitor is its increased efficacy against intracellular bacteria; a hypothesized "self-concentrating" effect inside macrophages. This is often explained by EP blockage, which would lead to an increase in intracellular concentration of the drug [72, 86]. However, this has not been shown directly. On the other hand, it has also been hypothesized that TZ is able to stimulate the macrophage itself and increase its microbicidal capacity [86]. In support of this, TZ has been implicated in the increased acidification of the phago-lysosome (unpublished data by Elsa Anes's group, University of Lisbon, Lisbon, Portugal). This macrophage stimulation could explain the contribution of TZ to combination treatment with RIF just as well as the blockage of EPs, and the overall killing of bacteria is likely due

to both of these factors. In the end, more cell biological experiments should be preformed to accurately determine where TZ's antimicrobial capacity is rooted.

5.4 Methodological considerations

5.4.1 Optimization of primary macrophage culture

Macrophages are known to be heterogeneous cells, both in morphology and function [162]. During pilot experiments in macrophage culture, the cell morphology we saw was not that of typical primary murine macrophages, which tend to be more rounded with irregular projections [163]. Instead, our macrophages were elongated and more fibroblast-like when plated on cell-culture treated dishes. Interestingly, this was not the case on non-treated dishes, where they looked more like typical macrophages. Initially, we were concerned that this could be due to incomplete differentiation of the cells. However, the phenotype did not change when we varied the source of M-CSF from recombinant cytokine to L929 conditioned media. In addition, these elongated cells displayed typical macrophage characteristics, such as the ability to efficiently phagocytose NPs and to show positive labeling for CD14 (**Figure 4.5** and **4.6**).

In comparison to similar experiments in the literature, where 10-20 ng/ml of the growth factor M-CSF is common, we have been using relatively high levels of M-CSF (40 ng/ml) for the CFU time-kill assay. Reducing this value clearly changed the morphology of the cells to a more rounded shape, which could explain why our cells appeared so elongated. In addition, the higher levels of M-CSF increased the readings obtained from the CCK assay after six days (**Figure 4.3**). This increase could either be due to cell proliferation or cell activation, both of which have been associated with the effects of M-CSF [164].

In addition to plastic-ware surface treatment and concentration of M-CSF cytokine in the media, macrophage morphology can be affected by plating density [165]. This could also explain the differences we saw on treated dishes compared to non-treated dishes (**Figure 4.4**), as the non-treated dishes in the images were sparsely populated compared to the treated dishes. In other words, macrophages are very sensitive to their environments, and like in all cell culture, lab-to-lab variation is inevitable. This makes it all the more important to keep all the accessible parameters as reproducible as possible and to be detailed about documenting every technical aspect of the procedure. Taking this into consideration, we decided to continue using the high concentration of M-CSF, (40 ng/ml), in order to be able to make comparison with previous results more valid and maintain reproducibility, especially

considering that the cells showed classic macrophage characteristics at this concentration of M-CSF.

5.4.2 Establishing a luciferase assay

The CFU time-kill assay has long been the ”golden standard” in microbiology for quantification of bacterial loads. Among its advantages are its simplicity and its high sensitivity for even minute quantities of bacteria. In addition, this method yields absolute numbers of bacteria, and only the viable (non-dormant) ones will form colonies, allowing for the exclusion of debris and non-viable bacteria [166]. However, this method also has several inherent drawbacks. First of all, quantification relies on manual counting of visible colonies, which can often clump together, making it difficult to distinguish one CFU from a small cluster of CFUs. BCG colonies also require up to three weeks before they can be counted, which together with 9 days of *in vitro* treatment makes each experiment take a month before any results are obtained. Further, colonies vary in size, and very small ones can easily be missed. Lastly, the wide range of detection relies on dilutions of the sample, which often fail to follow a linear relationship.

In an attempt to increase the objectivity of *in vitro* BCG quantification following treatment with drugs, we attempted to establish a new protocol using firefly luciferase. This would not only give an unbiased reading of relative bacterial numbers, but it would also give results on the same day as bacteria are lysed, making the quantification quicker. When plating CFUs for BCG, two to three weeks are required before colonies become visible. With the luciferase quantification, sample processing is reduced, and results can be read immediately. However, unlike CFU quantification, the luciferase assay requires expensive reagents and specialized equipment.

Luciferase quantification is classified as a bioluminescence assay. As a rule, bioluminescence produces a weaker signal, and fluorescence is often preferred in its place. However, unlike fluorescence, bioluminescence has very little background, which makes it more sensitive to weaker signals [167]. In addition, the luciferase enzyme does not require any post-translational modification and can therefore emit luminescence as soon as it is produced. Its half-life is also very short in cells, lasting approximately 3 hours after translation [168] This means that unviable bacteria will not be detected, which can be a problem with fluorescently labeled bacteria.

Before we could implement the new method, it had to be directly compared to CFUs. The luciferase assay has been used for quantifying mycobacteria by others, with a linear correlation to CFUs [169]. Similarly for us, parallel CFU and luciferase experiments using cells infected with BCG-lux showed that the traditional CFU method had a strong linear correlation with the luciferase assay (R^2=0.998), although CFU values were consistently higher (**Figure 4.9**). This could be due to the fact that the luciferase assay requires more processing, which can lead to the loss of some sample material.

One important aspect in the establishment of the luciferase bacterial-quantification was to explore the limit of detection. High sensitivity is one of the important strengths of the CFU method, as one can technically measure reduction in CFUs down to a single colony. We were concerned that the luciferase assay would not be sensitive to low numbers of bacteria, which we regularly obtain in killing experiments. Pilot experiments using BCG-lux in liquid culture were discouraging, as the lowest amount of bacteria that could be detected over background was an OD_{600} of 0.05, corresponding to $5x10^6$ CFU. However, by increasing the concentration of the bacterial lysate by a factor of 50, we were able to go well below this limit, with the least amount of bacteria detected over background corresponding to 1300 CFU, a level rarely reached by our time-kill assays.

During the establishment of the protocol, an important aspect was the lysis of infected macrophages. Lysis of macrophages was carried out in the same way as for plating by CFU, but the extracted bacteria were in turn lysed to release all intracellular luciferase. A concern during pilot luciferase assay experiments was to ensure complete lysis of these bacterial cells, which is why samples were vortexed and sonicated twice during processing. Another concern was to remove as much as possible of the supernatant from macrophage lysis. If any of this supernatant were to carry over, it could dilute the sample, causing it to produce a lower signal. To avoid this as much as possible, macrophage lysate was spun down twice, and as much supernatant as possible was removed without disturbing the bacterial pellet. It remains to be seen, however, if this method can be reliably and reproducibly applied to the exploration of TZ and RIF combination treatment *in vitro*.

6 Conclusions

TZ is now beyond patent protection [85], and with its background in compassionate use, has been suggested for global trials against human TB [155]. However, it has been emphasized that patients treated with TZ should be screened for signs of cardiotoxicity before and during treatment. The results in this thesis indicate that the high concentrations of TZ needed to treat mycobacterial infection are toxic when administered as free drugs in both *in vitro* and *in vivo* models of TB. However, by encapsulating TZ in biodegradable PLGA NPs, these toxic side-effects can be greatly reduced. If TZ's toxicity is overcome, its addition to the traditional anti-TB regimen for human patients could be beneficial in several respects. First of all, the pleiotropic nature of TZ makes it less likely for any bacteria to become completely resistant to this drug. Furthermore, not only may TZ play a role in potentiating RIF efficacy, as shown by us in the zebrafish model and van Soolingen *et al.* in the mouse model [85], but it may also improve INH efficacy, as shown by Dutta *et al.* [89] at 3-fold lower concentrations of TZ than those used here for the potentiation of RIF. If TZ does indeed interact synergistically in humans with INH and RIF, two of the most potent anti-TB drugs, its addition to the traditional anti-TB regimen could contribute to shortening treatment-time [53]. Together with TZ's direct activity against both resistant and non-resistant bacteria [74, 76], this treatment-shortening effect could indirectly reduce patient non-compliance. In addition, encapsulating TZ in polymeric drug-carriers such as PLGA could not only reduce toxicity and facilitate local delivery, but also limit the frequency of drug administration due to sustained release of the drug from the NP. Taken together, these measures would both improve patient compliance and thereby help prevent the development of bacterial drug resistance in the first place.

7 Future perspectives

7.1.1 Further nanoparticle optimization

While we have conducted some optimization already, there are several aspects that can be tuned in NPs in order to more efficiently deliver drugs to their target sites. For instance, NP hydrophobicity and degradation time can be adjusted by varying the ratio of PLA to PGA in the PLGA copolymer formulation [124]. Chemical modification of PLGA end-groups can also increase or reduce degradation time of the polymer. For instance, PLGA that has terminal esters, as opposed to free, uncapped carboxylic acid has a longer degradation time *in vivo* [170]. Further, increasing the molecular weight of the copolymer can also decrease the rate of degradation; PLGA with a molecular weight of 10 kDa degrades twice as fast as PLGA with a molecular weight of 20 kDa [171]. A longer degradation time means that the drug encapsulated is released more slowly, potentially leading to more efficient TB therapy. Another possible improvement to the combined administration of RIF and TZ is to co-encapsulate the two drugs in the same NP [116]. This approach has been tried using another EP inhibitor, verapamil, by encapsulating it in PLGA NPs together with the cancer drug vincristine sulfate in an attempt to fight MDR in cancer cells [172]. However, this necessitates a relatively high loading of both drugs in the NP, which can be difficult to achieve if the drugs compete for encapsulation, especially since RIF and TZ have different degrees of hydrophobicity.

7.1.2 The role of eukaryotic efflux pumps

As briefly mentioned earlier, EPs are not just present in bacteria but are also common in eukaryotic cells. Here they have a similar function in that they pump out harmful substances from the cell [173]. In cancer cells, drug efflux is also closely associated with a drug resistant cell phenotype. For example, in cancer cells over-expressing P-glycoprotein (an ABC transporter), TZ is able to inhibit efflux of chemotherapeutics [174, 175]. In addition to blocking bacterial EPs, TZ has the potential to block these eukaryotic pumps. Macrophages have a lot less of the P-glycoprotein, but have several others EPs that could potentially be blocked by TZ [176]. If this is the case, TZ against intracellular bacteria could be concentrating not only at the bacterial level, but also the macrophage level, as suggested by Crowle *et al*. [72].

We have already initiated the process of exploring this question by high-pressure liquid chromatography coupled to mass spectrometry (HPLC-MS). For our application, this

method can separate TZ or RIF from cell lysates by HPLC and quantify the amount of intracellular drug by MS. Using this technique, we hope to quantify whether or not RIF (and TZ itself) can be concentrated in cells in the presence of the EP inhibitor TZ.

7.1.3 Alternative combinations of efflux pump inhibitors and antibiotics

Even if EP inhibition is central to TZ's function, it is important to remember that EP-mediated extrusion of drugs may be one of several mechanisms contributing to phenotypic resistance. Combination therapy using antibiotics and EP inhibitors may therefore only be efficient in those cases where efflux plays a major role [54]. In addition, even if pumps are promiscuous, if the antibiotic used for treatment is effluxed by a different pump than the one being blocked, it may still not have an effect in improving treatment. It follows that there is a need to explore the specific relationship between different pumps and their antibiotic substrates, as well as the EP inhibitors that interfere with their mechanism of action. If a given EP extruding a given antibiotic is not affected by TZ for instance, other compounds exist that can take TZ's place in that they have been shown to block efflux, such as verapamil or piperine or derivatives of these [161]. Apart from varying the type of EP inhibitor used, it would also be interesting to explore the potentiation of INH therapy, which according to Dutta *et al.* [89] requires only 10 mg/kg of TZ to achieve a significant improvement in comparison to INH monotherapy *in vivo*, a three-fold lower dose than what was needed to improve RIF therapy *in vivo* [85].

7.1.4 Thioridazine and mycobacterial resistance

TZ has been used against both genetically resistant and susceptible *M. tb* in bacterial culture [76] and inside macrophages [74, 161]. In addition, TZ has been shown to reduce macrophage-induced phenotypic resistance to INH and RIF using a 48-hour treatment of TZ at 2 μg/ml *in vitro* [161]. It would be interesting to explore TZ's effect against phenotypic resistance further *in vivo*. For example, experiments could be carried out in the zebrafish model, by exposing infected larvae to low levels of RIF in a bath, in theory leading to induced phenotypic resistance to RIF. This could be followed by treatment with RIF and TZ, or a higher dose of RIF alone, in order to compare their relative efficiency. This would give an insight as to whether or not TZ contributes to fighting phenotypic resistance *in vivo*.

8 Appendix

8.1 Supplementary methods

8.1.1 Poly-L Lysine coating

Coverslips (14 mm) were washed with 96% ethanol and lens paper to remove grease. For coating, 0.01% poly L-lysine (average molecular weight 150-300 kDa; Sigma-Aldrich, St. Louis, MO, USA) solution in water was prepared from a 10x stock. This was sterile filtered through a 0.2 mm filter and poured into a petri-dish. The coverslips were placed floating on this solution for 5 minutes using a pair of sterile tweezers, and washed by dipping it in autoclaved milliQ water three times, minding which side has the coating. The coated coverslips were placed in a 12-well plate, and left to dry at RT overnight under and UV-light for sterilization. To store the coated coverslips, a lid was secured in place with parafilm. The remaining poly L-lysine solution was stored at +4 °C.

8.1.2 Rotifer culture

Rotifers were cultured in 14 L buckets in 2% salt water with circulation of oxygen and daily feeding with pasteurized microalgae (Reed Marine culture, Campbell, CA, USA). Rotifers were harvested and kept in 2% salt water for up to one week at 4°C. Before feeding larvae, rotifers were strained using a 70 μm cell strainer and washed with embryo water to remove all salt water. The rotifers were then re-suspended in embryo water and a few drops were added to the plates with larvae. Any remaining rotifers were removed when embryo water was changed.

8.1.3 CFU time-kill assay using M. tb and primary human macrophages

The following procedure was carried out by our collaborator David Pires, working in Elsa Anes's group in Lisbon, Portugal. Primary human monocyte-derived macrophages were isolated and differentiated for 7 days with 20ng/ml M-CSF. On the day of infection, *M. tb* strain H37Rv was processed and added to cells at an MOI of 1 for 3 hours, followed by washing to remove extracellular bacteria. Treatment media was prepared with PLGA-RIF NPs at 25 and 50 μg/ml, which corresponds to 8 and 16 μg/ml free RIF, and PLGA-TZ NPs at 4.7 and 9.4 μg/ml, which corresponds to 1.25 and 2.5 μg/ml in free drugs. Treatment duration was 3 hours, followed by another wash. Bacterial load was quantified by CFU after 3 hours (before treatment), and on days 1, 3, 5 and 7 post-infection.

8.2 Supplementary results

Table 8.1: Summary of toxicity indicators recorded in 6 day-old zebrafish larvae treated with free TZ or encapsulated PLGA-TZ. All indicators were recorded at 4 dpt (6 dpf). (n= 6, 13 and 6 for free, NP and mock respectively)

	Edema (+/-)	Swim bladder inflation (+/-)	Yolk discoloration (+/-)	Survival (%)
Free TZ	(5/1)	(0/6)	(3/3)	40
PLGA-TZ NP	(2/11)	(9/4)	(2/11)	100
Mock	(1/5)	(4/2)	(1/5)	100

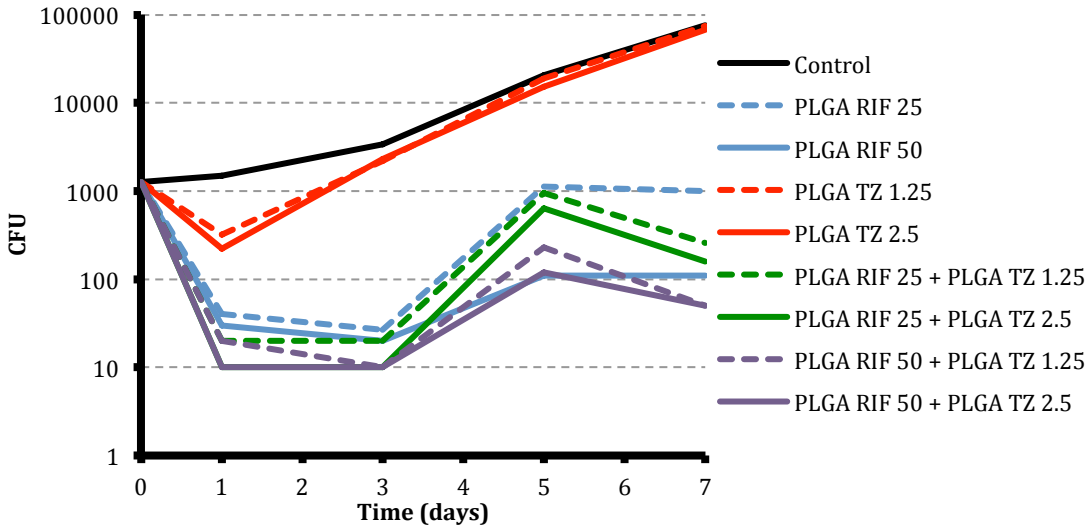

Figure 8.1: Results from CFU time-kill assay using *M. tb* strain H37Rv and human primary macrophages, carried out by our collaborator David Pires from Elsa Anes's lab in Lisbon, Portugal. Concentrations of RIF are given in weight of NPs of 25 and 50 µg/ml, which corresponds to 8 and 16 µg/ml free RIF. Concentrations of TZ are given in free drug weight.

8.3 Supplementary recipes

8.3.1 7H10 agar plates

The following was taken from [102]. Dissolve 19 mg 7H10 Difco Middlebrook 7H10 agar powder and 10 ml 50% glycerol in 900 ml sterile milliQ water. Autoclave this solution, and after it cools, add 10% OADC and 50 µg/ml Hygromycin. Fill in bacterial culture dishes under sterile conditions. Allow plates to cool and pack in sealed plastic bags, bottom-side up. Keep plates at 4 °C for up to two months, protected from light. Warm plates to 37°C before plating bacteria on them.

8.3.2 ADC/OADC growth supplement

ADC/OADC growth supplement are essential to the growth of slow-growing mycobacteria. Both of these contain sodium chloride to ensure osmotic equilibrium, albumin, which binds to toxic agents in the media, dextrose (glucose), an energy source for the bacteria and catalase which catalyzes the removal of hydrogen peroxide. In addition, OADC also contains oleic acid, a long chain fatty acid important to mycobacterial metabolism [177]. The following recipe is taken from [112]. Add 4.5 g NaCl, 25 g BSA, 10 g dextrose and 15 mg catalase to 400 ml sterile milliQ water under stirring at RT. Fill up with sterile milliQ water to a final volume of 500 ml, and adjust pH to 6.8-7.0 with 1 M NaOH. Sterilize by using a 0.22 µm filter. Store up to 1 month at 4 °C.

8.3.3 Tricaine stock solution

The following was adapted from [102]. For 100 ml tricaine stock solution, 400 mg Tricaine methanosulfonate MS-222 (Argent laboratories group Inc., Redmond, WA, USA) was dissolved in 97.9 ml water and 2.1 ml 1M TrisCl (pH 9). The solution was adjusted to pH 7.4. For sedation, add 300 µl of the stock solution to 5 ml embryo water, giving a final concentration of 226 µg/ml tricaine. Do not leave the embryos for more than half an hour in this solution, as they will eventually die.

8.3.4 Zebrafish embryo water

The following was taken from [102]. For 100 ml embryo water, mix 1.0 ml Hanks' stock solution #1, 0.1 ml Hanks' stock solution #2 , 1.0 ml Hanks' stock solution #4, 1.0 ml Hanks'

stock solution #5 and 1.0 ml Hanks' stock solution #6 in 95.9 ml water. Adjust pH to 7.2 (approx.10 drops 1 M NaOH) and autoclave or sterile filter. Can be stored indefinitely at 4°C

8.3.5 Hanks' stock solutions

The following was taken from [102].

Stock #1:
8.0 g NaCl
0.4 g KCl
100 ml H_2O

Stock #2:
0.358 g Na_2HPO_4 anhydrous
0.60 g KH_2PO_4
100 ml H_2O

Stock #4:
0.72 g $CaCl_2$
50 ml H_2O

Stock #5:
1.23 g $MgSO_4 \cdot 7H_2O$
50 ml H_2O

Stock #6:
0.35 g $NaHCO_3$
10 ml H_2O

Store indefinitely at 4°C.

References

1. Daniel, T.M., *The history of tuberculosis.* Respir Med, 2006. **100**(11): p. 1862-70.
2. Gutierrez M.C., B.S., Brosch R., Fabre M., Omaïs B., et al. , *Ancient origin and gene mosaicism of the progenitor of Mycobacterium tuberculosis.* PLoS Pathog 1(1): e5., 2005.
3. Gagneux, S., et al., *Variable host-pathogen compatibility in Mycobacterium tuberculosis.* Proc Natl Acad Sci U S A, 2006. **103**(8): p. 2869-73.
4. Sakula, A., *Robert Koch: centenary of the discovery of the tubercle bacillus, 1882.* Thorax, 1982. **37**(4): p. 246-51.
5. Calmette, A., *Preventive Vaccination Against Tuberculosis with BCG.* Proc R Soc Med, 1931. **24**(11): p. 1481–1490.
6. Sakula, A., *BCG: Who were Calmettte and Guerin?* Thorax 1983. **38**: p. 806-812.
7. Behr, M.A., et al., *Comparative Genomics of BCG Vaccines by Whole-Genome DNA Microarray.* Science, 1999. **284**(5419): p. 1520-1523.
8. Volkman, H.E., et al., *Tuberculous Granuloma Formation Is Enhanced by a Mycobacterium Virulence Determinant.* PLoS Biol, 2004. **2**(11): p. e367.
9. Mitchison, D. and G. Davies, *The chemotherapy of tuberculosis: past, present and future.* The International Journal of Tuberculosis and Lung Disease, 2012. **16**(6): p. 724-732.
10. Fox, W.S., Ian Daniels, Marc, *A five-year assessment of patients in a controlled trial of Streptomycin in pulmonary Tuberculosis: Report to the Tuberculosis Chemotherapy Trials Committee of the Medical Reasearch Council.* QJM, 1954. **23**(3): p. 347-366.
11. Cohn, M.L., G. Middlebrook, and W.F. Russell, Jr., *Combined drug treatment of tuberculosis. I. Prevention of emergence of mutant populations of tubercle bacilli resistant to both streptomycin and isoniazid in vitro.* J Clin Invest, 1959. **38**(8): p. 1349-55.
12. TB CARE I, *International Standards for Tuberculosis Care, Edition 3*, 2014, TB CARE I: The Hague.
13. Dye, C., *Doomsday postponed? Preventing and reversing epidemics of drug-resistant tuberculosis.* Nat Rev Microbiol, 2009. **7**(1): p. 81-7.
14. Andersen, P. and S.H.E. Kaufmann, *Novel Vaccination Strategies against Tuberculosis.* Cold Spring Harbor Perspectives in Medicine, 2014. **4**(6).
15. Kaufmann, S.H.E., *Is the development of a new tuberculosis vaccine possible?* Nat Med, 2000. **6**(9): p. 955-960.
16. World Health Organization, *Global Tuberculosis Report 2013*, 2013: Geneva
17. Dannenberg, A.M., Jr., *Immune mechanisms in the pathogenesis of pulmonary tuberculosis.* Rev Infect Dis, 1989. **11 Suppl 2**: p. S369-78.
18. Ernst, J.D., *Macrophage Receptors for Mycobacterium tuberculosis.* Infection and Immunity, 1998. **66**(4): p. 1277-1281.
19. Flynn, J.L. and J. Chan, *Immunology of tuberculosis.* Annu Rev Immunol, 2001. **19**: p. 93-129.
20. Armstrong, J.A., *Response of cultured macrophages to Mycobacterium tuberculosis, with observations on fusion of lysosomes with phagosomes.* The Journal of experimental medicine, 1971. **134**(3): p. 713-740.

21. Sturgill-Koszycki, S., et al., *Lack of acidification in Mycobacterium phagosomes produced by exclusion of the vesicular proton-ATPase.* Science, 1994. **263**(5147): p. 678-81.
22. Olakanmi, O., et al., *Intraphagosomal Mycobacterium tuberculosis acquires iron from both extracellular transferrin and intracellular iron pools. Impact of interferon-gamma and hemochromatosis.* J Biol Chem, 2002. **277**(51): p. 49727-34.
23. Brighenti, S. and M. Lerm, *How Mycobacterium Tuberculosis Manipulates Innate and Adaptive Immunity - New Views of an Old Topic*. 2012: INTECH Open Access Publisher.
24. Russell, D.G., *Mycobacterium tuberculosis: here today, and here tomorrow.* Nat Rev Mol Cell Biol, 2001. **2**(8): p. 569-586.
25. Flynn, J.L. and J. Chan, *Tuberculosis: Latency and Reactivation.* Infection and Immunity, 2001. **69**(7): p. 4195-4201.
26. Davis, J.M. and L. Ramakrishnan, *The role of the granuloma in expansion and dissemination of early tuberculous infection.* Cell, 2009. **136**(1): p. 37-49.
27. Ramakrishnan, L., *Revisiting the role of the granuloma in tuberculosis.* Nat Rev Immunol, 2012. **12**(5): p. 352-66.
28. Russell, D.G., et al., *Foamy macrophages and the progression of the human tuberculosis granuloma.* Nat Immunol, 2009. **10**(9): p. 943-8.
29. Chackerian, A.A., et al., *Dissemination of Mycobacterium tuberculosis is influenced by host factors and precedes the initiation of T-cell immunity.* Infect Immun, 2002. **70**(8): p. 4501-9.
30. Wolf, A.J., et al., *Initiation of the adaptive immune response to Mycobacterium tuberculosis depends on antigen production in the local lymph node, not the lungs.* J Exp Med, 2008. **205**(1): p. 105-15.
31. Scott Algood, H.M., P.L. Lin, and J.L. Flynn, *Tumor Necrosis Factor and Chemokine Interactions in the Formation and Maintenance of Granulomas in Tuberculosis.* Clinical Infectious Diseases, 2005. **41**(Supplement 3): p. S189-S193.
32. van der Werf, M.J., et al., *Multidrug resistance after inappropriate tuberculosis treatment: a meta-analysis.* European Respiratory Journal, 2012. **39**(6): p. 1511-1519.
33. Kjellsson, M.C., et al., *Pharmacokinetic evaluation of the penetration of antituberculosis agents in rabbit pulmonary lesions.* Antimicrob Agents Chemother, 2012. **56**(1): p. 446-57.
34. Nardell, E. and A. Dharmadhikari, *Turning off the spigot: reducing drug-resistant tuberculosis transmission in resource-limited settings.* Int J Tuberc Lung Dis, 2010. **14**(10): p. 1233-43.
35. Ramaswamy, S. and J.M. Musser, *Molecular genetic basis of antimicrobial agent resistance inMycobacterium tuberculosis: 1998 update.* Tubercle and Lung Disease, 1998. **79**(1): p. 3-29.
36. Kester, J.C. and S.M. Fortune, *Persisters and beyond: mechanisms of phenotypic drug resistance and drug tolerance in bacteria.* Crit Rev Biochem Mol Biol, 2014. **49**(2): p. 91-101.
37. Colijn, C., et al., *Spontaneous emergence of multiple drug resistance in tuberculosis before and during therapy.* PLoS One, 2011. **6**(3): p. e18327.
38. Gillespie, S.H., *Evolution of Drug Resistance in Mycobacterium tuberculosis: Clinical and Molecular Perspective.* Antimicrobial Agents and Chemotherapy, 2002. **46**(2): p. 267-274.

39. Migliori, G.B., et al., *First tuberculosis cases in Italy resistant to all tested drugs.* Euro Surveill, 2007. **12**(5): p. E070517 1.
40. Parida, S.K., et al., *Totally drug-resistant tuberculosis and adjunct therapies.* J Intern Med, 2014.
41. Kwon, Y.S., B.H. Jeong, and W.J. Koh, *Tuberculosis: clinical trials and new drug regimens.* Curr Opin Pulm Med, 2014. **20**(3): p. 280-6.
42. Wallis, R.S., et al., *Drug Tolerance in Mycobacterium tuberculosis.* Antimicrobial Agents and Chemotherapy, 1999. **43**(11): p. 2600-2606.
43. Ramaswamy, S.V., et al., *Single Nucleotide Polymorphisms in Genes Associated with Isoniazid Resistance in Mycobacterium tuberculosis.* Antimicrobial Agents and Chemotherapy, 2003. **47**(4): p. 1241-1250.
44. Telenti, A., et al., *Detection of rifampicin-resistance mutations in Mycobacterium tuberculosis.* The Lancet, 1993. **341**(8846): p. 647-651.
45. Tuomanen, E., *Phenotypic Tolerance: The Search for β-Lactam Antibiotics That Kill Nongrowing Bacteria.* Reviews of Infectious Diseases, 1986. **8**: p. S279-S291.
46. Hobby, G.L. and M.H. Dawson, *Effect of Rate of Growth of Bacteria on Action of Penicillin.* Experimental Biology and Medicine, 1944. **56**(2): p. 181-184.
47. Mitchison, D.A., *Basic mechanisms of chemotherapy.* CHEST Journal, 1979. **76**(6_Supplement): p. 771-781.
48. Herbert, D., et al., *Bactericidal action of ofloxacin, sulbactam-ampicillin, rifampin, and isoniazid on logarithmic- and stationary-phase cultures of Mycobacterium tuberculosis.* Antimicrob Agents Chemother, 1996. **40**(10): p. 2296-9.
49. Dartois, V., *The path of anti-tuberculosis drugs: from blood to lesions to mycobacterial cells.* 2014.
50. Wayne, L.G. and C.D. Sohaskey, *Nonreplicating persistence of mycobacterium tuberculosis.* Annu Rev Microbiol, 2001. **55**: p. 139-63.
51. Mitchison, D.A., *Understanding the chemotherapy of tuberculosis—current problems.* Journal of Antimicrobial Chemotherapy, 1992. **29**(5): p. 477-493.
52. Monedero, I. and J.A. Caminero, *MDR-/XDR-TB management: what it was, current standards and what is ahead.* Expert Rev Respir Med, 2009. **3**(2): p. 133-45.
53. Adams, K.N., et al., *Drug tolerance in replicating mycobacteria mediated by a macrophage-induced efflux mechanism.* Cell, 2011. **145**(1): p. 39-53.
54. Poole, K., *Efflux pumps as antimicrobial resistance mechanisms.* Annals of Medicine, 2007. **39**(3): p. 162-176.
55. Martinez, J.L., et al., *Functional role of bacterial multidrug efflux pumps in microbial natural ecosystems.* FEMS Microbiol Rev, 2009. **33**(2): p. 430-49.
56. da Silva, P.E., et al., *Efflux as a mechanism for drug resistance in Mycobacterium tuberculosis.* FEMS Immunol Med Microbiol, 2011. **63**(1): p. 1-9.
57. Balganesh, M., et al., *Efflux pumps of Mycobacterium tuberculosis play a significant role in antituberculosis activity of potential drug candidates.* Antimicrob Agents Chemother, 2012. **56**(5): p. 2643-51.
58. Pasipanodya, J.G. and T. Gumbo, *A new evolutionary and pharmacokinetic-pharmacodynamic scenario for rapid emergence of resistance to single and multiple anti-tuberculosis drugs.* Curr Opin Pharmacol, 2011. **11**(5): p. 457-63.
59. De Rossi, E., J.A. Aínsa, and G. Riccardi, *Role of mycobacterial efflux transporters in drug resistance: an unresolved question.* FEMS Microbiology Reviews, 2006. **30**(1): p. 36-52.
60. Jarlier, V. and H. Nikaido, *Mycobacterial cell wall: Structure and role in natural resistance to antibiotics.* FEMS Microbiology Letters, 1994. **123**(1-2): p. 11-18.

61. Niederweis, M., *Mycobacterial porins – new channel proteins in unique outer membranes.* Molecular Microbiology, 2003. **49**(5): p. 1167-1177.
62. Gupta, A.K., et al., *Microarray analysis of efflux pump genes in multidrug-resistant Mycobacterium tuberculosis during stress induced by common anti-tuberculous drugs.* Microb Drug Resist, 2010. **16**(1): p. 21-8.
63. Colangeli, R., et al., *The Mycobacterium tuberculosis iniA gene is essential for activity of an efflux pump that confers drug tolerance to both isoniazid and ethambutol.* Mol Microbiol, 2005. **55**(6): p. 1829-40.
64. Siddiqi, N., et al., *Mycobacterium tuberculosis Isolate with a Distinct Genomic Identity Overexpresses a Tap-Like Efflux Pump.* Infection, 2004. **32**(2): p. 109-111.
65. Piddock, L.J.V., *Multidrug-resistance efflux pumps ? not just for resistance.* Nat Rev Micro, 2006. **4**(8): p. 629-636.
66. Amaral, L. and M. Viveiros, *Why thioridazine in combination with antibiotics cures extensively drug-resistant Mycobacterium tuberculosis infections.* International Journal of Antimicrobial Agents, 2012. **39**(5): p. 376-380.
67. Li, X.Z. and H. Nikaido, *Efflux-mediated drug resistance in bacteria: an update.* Drugs, 2009. **69**(12): p. 1555-623.
68. Davis, J.C. and J.T. Bigger, *The effects of thioridazine on electrical and ischemic ventricular fibrillation in the dog heart in situ.* Journal of Pharmacology and Experimental Therapeutics, 1981. **216**(1): p. 39-44.
69. Purhonen, M., et al., *Outcome of patients after market withdrawal of thioridazine: a retrospective analysis in a nationwide cohort.* Pharmacoepidemiol Drug Saf, 2012. **21**(11): p. 1227-31.
70. Reilly, J.G., et al., *QTc-interval abnormalities and psychotropic drug therapy in psychiatric patients.* The Lancet, 2000. **355**(9209): p. 1048-1052.
71. van Noord, C., M. Eijgelsheim, and B.H. Stricker, *Drug- and non-drug-associated QT interval prolongation.* Br J Clin Pharmacol, 2010. **70**(1): p. 16-23.
72. Crowle, A.J., G.S. Douvas, and M.H. May, *Chlorpromazine: a drug potentially useful for treating mycobacterial infections.* Chemotherapy, 1992. **38**(6): p. 410-9.
73. Amaral, L., M. Viveiros, and J. Molnar, *Antimicrobial activity of phenothiazines.* In Vivo, 2004. **18**(6): p. 725-31.
74. Ordway, D., et al., *Clinical Concentrations of Thioridazine Kill Intracellular Multidrug-Resistant Mycobacterium tuberculosis.* Antimicrobial Agents and Chemotherapy, 2003. **47**(3): p. 917-922.
75. van Ingen, J., et al., *In vitro activity of thioridazine against mycobacteria.* Int J Antimicrob Agents, 2009. **34**(2): p. 190-1.
76. Bettencourt, M.V., S. Bosne-David, and L. Amaral, *Comparative in vitro activity of phenothiazines against multidrug-resistant Mycobacterium tuberculosis.* International Journal of Antimicrobial Agents, 2000. **16**(1): p. 69-71.
77. Elferink, J.G.R., *Fluorescence studies of membrane interactions of chlorpromazine and chlorimipramine.* Biochemical Pharmacology, 1977. **26**(6): p. 511-515.
78. Guth, P.S. and M.A. Spirtes, *The phenothiazinetranquilizers: biochemical and biophysical actions.* International review of neurobiology, 1964. **7**: p. 231-278.
79. Ordway, D., et al., *Intracellular activity of clinical concentrations of phenothiazines including thioridiazine against phagocytosed Staphylococcus aureus.* Int J Antimicrob Agents, 2002. **20**(1): p. 34-43.
80. Rodrigues, L., et al., *Contribution of efflux activity to isoniazid resistance in the Mycobacterium tuberculosis complex.* Infection, Genetics and Evolution, 2012. **12**(4): p. 695-700.

81. Yano, T., et al., *Steady-state Kinetics and Inhibitory Action of Antitubercular Phenothiazines on Mycobacterium tuberculosis Type-II NADH-Menaquinone Oxidoreductase (NDH-2).* Journal of Biological Chemistry, 2006. **281**(17): p. 11456-11463.
82. Sohaskey, C.D., *Nitrate Enhances the Survival of Mycobacterium tuberculosis during Inhibition of Respiration.* Journal of Bacteriology, 2008. **190**(8): p. 2981-2986.
83. Dutta, N.K., S. Mehra, and D. Kaushal, *A Mycobacterium tuberculosis sigma factor network responds to cell-envelope damage by the promising anti-mycobacterial thioridazine.* PLoS One, 2010. **5**(4): p. e10069.
84. Viveiros, M., et al., *Inhibitors of mycobacterial efflux pumps as potential boosters for anti-tubercular drugs.* Expert Rev Anti Infect Ther, 2012. **10**(9): p. 983-98.
85. van Soolingen, D., et al., *The antipsychotic thioridazine shows promising therapeutic activity in a mouse model of multidrug-resistant tuberculosis.* PLoS One, 2010. **5**(9).
86. Amaral, L. and J. Molnar, *Why and how thioridazine in combination with antibiotics to which the infective strain is resistant will cure totally drug-resistant tuberculosis.* Expert Rev Anti Infect Ther, 2012. **10**(8): p. 869-73.
87. Viveiros, M. and L. Amaral, *Enhancement of antibiotic activity against poly-drug resistant Mycobacterium tuberculosis by phenothiazines.* International Journal of Antimicrobial Agents, 2001. **17**(3): p. 225-228.
88. Szumowski, J.D., et al., *Antimicrobial Efflux Pumps and Mycobacterium Tuberculosis Drug Tolerance: Evolutionary Considerations.* Curr Top Microbiol Immunol, 2012.
89. Dutta, N.K., M.L. Pinn, and P.C. Karakousis, *Reduced Emergence of Isoniazid Resistance with Concurrent Use of Thioridazine against Acute Murine Tuberculosis.* Antimicrobial Agents and Chemotherapy, 2014. **58**(7): p. 4048-4053.
90. Martins, M., et al., *The Curative Activity of Thioridazine on Mice Infected with Mycobacterium tuberculosis.* In Vivo, 2007. **21**(5): p. 771-775.
91. Gupta, S., et al., *Acceleration of tuberculosis treatment by adjunctive therapy with verapamil as an efflux inhibitor.* Am J Respir Crit Care Med, 2013. **188**(5): p. 600-7.
92. Amaral, L., et al., *Thioridazine cures extensively drug-resistant tuberculosis (XDR-TB) and the need for global trials is now!* Int J Antimicrob Agents, 2010. **35**(6): p. 524-6.
93. Abbate, E., et al., *Successful alternative treatment of extensively drug-resistant tuberculosis in Argentina with a combination of linezolid, moxifloxacin and thioridazine.* J Antimicrob Chemother, 2012. **67**(2): p. 473-7.
94. Flynn, J.L., *Lessons from experimental Mycobacterium tuberculosis infections.* Microbes Infect, 2006. **8**(4): p. 1179-88.
95. Capuano, S.V., 3rd, et al., *Experimental Mycobacterium tuberculosis infection of cynomolgus macaques closely resembles the various manifestations of human M. tuberculosis infection.* Infect Immun, 2003. **71**(10): p. 5831-44.
96. Barry, C.E., 3rd, et al., *The spectrum of latent tuberculosis: rethinking the biology and intervention strategies.* Nat Rev Microbiol, 2009. **7**(12): p. 845-55.
97. Cosma, C.L., D.R. Sherman, and L. Ramakrishnan, *The secret lives of the pathogenic mycobacteria.* Annu Rev Microbiol, 2003. **57**: p. 641-76.
98. Barut, B.A. and L.I. Zon, *Realizing the potential of zebrafish as a model for human disease*. Vol. 2. 2000. 49-51.

99. van der Sar, A.M., et al., *A star with stripes: zebrafish as an infection model.* Trends Microbiol, 2004. **12**(10): p. 451-7.
100. Swaim, L.E., et al., *Mycobacterium marinum infection of adult zebrafish causes caseating granulomatous tuberculosis and is moderated by adaptive immunity.* Infect Immun, 2006. **74**(11): p. 6108-17.
101. Tobin, D.M. and L. Ramakrishnan, *Comparative pathogenesis of Mycobacterium marinum and Mycobacterium tuberculosis.* Cell Microbiol, 2008. **10**(5): p. 1027-39.
102. Cosma, C.L., et al., *Zebrafish and frog models of Mycobacterium marinum infection.* Curr Protoc Microbiol, 2006. **Chapter 10**: p. Unit 10B 2.
103. Davis, J.M., et al., *Real-Time Visualization of Mycobacterium-Macrophage Interactions Leading to Initiation of Granuloma Formation in Zebrafish Embryos.* Immunity, 2002. **17**(6): p. 693-702.
104. Herbomel, P., B. Thisse, and C. Thisse, *Ontogeny and behaviour of early macrophages in the zebrafish embryo.* Development, 1999. **126**(17): p. 3735-45.
105. Lam, S.H., et al., *Development and maturation of the immune system in zebrafish, Danio rerio: a gene expression profiling, in situ hybridization and immunological study.* Dev Comp Immunol, 2004. **28**(1): p. 9-28.
106. Saunders, B.M. and A.M. Cooper, *Restraining mycobacteria: role of granulomas in mycobacterial infections.* Immunol Cell Biol, 2000. **78**(4): p. 334-41.
107. Howe, K., et al., *The zebrafish reference genome sequence and its relationship to the human genome.* Nature, 2013. **496**(7446): p. 498-503.
108. Stinear, T.P., et al., *Insights from the complete genome sequence of Mycobacterium marinum on the evolution of Mycobacterium tuberculosis.* Genome Research, 2008. **18**(5): p. 729-741.
109. Carvalho, R., et al., *A high-throughput screen for tuberculosis progression.* PLoS One, 2011. **6**(2): p. e16779.
110. Decostere, A., K. Hermans, and F. Haesebrouck, *Piscine mycobacteriosis: a literature review covering the agent and the disease it causes in fish and humans.* Vet Microbiol, 2004. **99**(3-4): p. 159-66.
111. Tonjum, T., et al., *Differentiation of Mycobacterium ulcerans, M. marinum, and M. haemophilum: mapping of their relationships to M. tuberculosis by fatty acid profile analysis, DNA-DNA hybridization, and 16S rRNA gene sequence analysis.* J Clin Microbiol, 1998. **36**(4): p. 918-25.
112. Gao, L.Y. and J. Manoranjan, *Laboratory maintenance of Mycobacterium marinum.* Curr Protoc Microbiol, 2005. **Chapter 10**: p. Unit 10B 1.
113. van Ingen, J., et al., *Why Do We Use 600 mg of Rifampicin in Tuberculosis Treatment?* Clin Infect Dis, 2011. **52**(9): p. e194-9.
114. Fenaroli, F., et al., *Nanoparticles as Drug Delivery System against Tuberculosis in Zebrafish Embryos: Direct Visualization and Treatment.* ACS Nano, 2014. **8**(7): p. 7014-26.
115. Jalil, R. and J.R. Nixon, *Biodegradable poly(lactic acid) and poly(lactide-co-glycolide) microcapsules: problems associated with preparative techniques and release properties.* Journal of Microencapsulation, 1990. **7**(3): p. 297-325.
116. Kamaly, N., et al., *Targeted polymeric therapeutic nanoparticles: design, development and clinical translation.* Chem Soc Rev, 2012. **41**(7): p. 2971-3010.
117. Poznansky, M.J. and R.L. Juliano, *Biological approaches to the controlled delivery of drugs: a critical review.* Pharmacological Reviews, 1984. **36**(4): p. 277-336.

118. Dutt, M. and G.K. Khuller, *Therapeutic efficacy of Poly(DL-lactide-Co-Glycolide)-encapsulated antitubercular drugs against Mycobacterium tuberculosis infection induced in mice.* Antimicrob Agents Chemother, 2001. **45**(1): p. 363-6.
119. Dutt, M. and G.K. Khuller, *Chemotherapy of Mycobacterium tuberculosis infections in mice with a combination of isoniazid and rifampicin entrapped in Poly (DL-lactide-co-glycolide) microparticles.* J Antimicrob Chemother, 2001. **47**(6): p. 829-35.
120. Pandey, R., et al., *Poly (DL-lactide-co-glycolide) nanoparticle-based inhalable sustained drug delivery system for experimental tuberculosis.* J Antimicrob Chemother, 2003. **52**(6): p. 981-6.
121. Pandey, R., et al., *Nanoparticle encapsulated antitubercular drugs as a potential oral drug delivery system against murine tuberculosis.* Tuberculosis (Edinb), 2003. **83**(6): p. 373-8.
122. Sharma, A., et al., *Chemotherapeutic efficacy of poly (DL-lactide-co-glycolide) nanoparticle encapsulated antitubercular drugs at sub-therapeutic dose against experimental tuberculosis.* Int J Antimicrob Agents, 2004. **24**(6): p. 599-604.
123. Kalluru, R., et al., *Poly(lactide-co-glycolide)-rifampicin nanoparticles efficiently clear Mycobacterium bovis BCG infection in macrophages and remain membrane-bound in phago-lysosomes.* J Cell Sci, 2013. **126**(Pt 14): p. 3043-54.
124. Lu, J.M., et al., *Current advances in research and clinical applications of PLGA-based nanotechnology.* Expert Rev Mol Diagn, 2009. **9**(4): p. 325-41.
125. Athanasiou, K.A., G.G. Niederauer, and C.M. Agrawal, *Sterilization, toxicity, biocompatibility and clinical applications of polylactic acid/polyglycolic acid copolymers.* Biomaterials, 1996. **17**(2): p. 93-102.
126. Shive, M.S. and J.M. Anderson, *Biodegradation and biocompatibility of PLA and PLGA microspheres.* Adv Drug Deliv Rev, 1997. **28**(1): p. 5-24.
127. Cheng, J., et al., *Formulation of functionalized PLGA–PEG nanoparticles for in vivo targeted drug delivery.* Biomaterials, 2007. **28**(5): p. 869-876.
128. Sanderson, J.E., *Bone replacement and repair putty material from unsaturated polyester resin and vinyl pyrrolidone*, 1988, Google Patents.
129. Harris, J.R., *Negative staining of thinly spread biological samples.* Methods Mol Biol, 2007. **369**: p. 107-42.
130. Birgitta Loretz, C.S., Carolin Thiele, Hiroe Yamada, Tine Schroder, Christian Ruge, Babak Mostaghaci, Emad Malaeksefat, Patrick Hole, Thomas Jocks, Claus-Michael Lehr, *Biological Barriers 2012- Labcourse II, Pharmaceutical Nanomaterials*, S.U. Department of Biopharmaceutics and Pharmaceutical Technology, Editor 2012: Saarbruken, Germany.
131. Ryan, J., *Corning® Cell Culture Surfaces*, in *Sigma® Life Science: Cell Culture Manual*2011-2014, Sigma-Aldrich Biotechnology. p. 324-326.
132. Rollins-Raval, M.A. and C.G. Roth, *The value of immunohistochemistry for CD14, CD123, CD33, myeloperoxidase and CD68R in the diagnosis of acute and chronic myelomonocytic leukaemias.* Histopathology, 2012. **60**(6): p. 933-42.
133. Ishiyama, M., et al., *A combined assay of cell viability and in vitro cytotoxicity with a highly water-soluble tetrazolium salt, neutral red and crystal violet.* Biol Pharm Bull, 1996. **19**(11): p. 1518-20.
134. Yuan, Y., et al., *The 16-kDa alpha-crystallin (Acr) protein of Mycobacterium tuberculosis is required for growth in macrophages.* Proc Natl Acad Sci U S A, 1998. **95**(16): p. 9578-83.

135. Lee, M.H., et al., *Site-specific integration of mycobacteriophage L5: integration-proficient vectors for Mycobacterium smegmatis, Mycobacterium tuberculosis, and bacille Calmette-Guerin.* Proc Natl Acad Sci U S A, 1991. **88**(8): p. 3111-5.
136. Goude, R. and T. Parish, *Electroporation of Mycobacteria.* 2008(15): p. e761.
137. White, R.M., et al., *Transparent adult zebrafish as a tool for in vivo transplantation analysis.* Cell Stem Cell, 2008. **2**(2): p. 183-9.
138. D'Amico, L., et al., *Assessment of Drug-Induced Cardiotoxicity in Zebrafish*, in *Zebrafish*. 2011, John Wiley & Sons, Inc. p. 45-54.
139. Haldi, M., et al., *Developmental Toxicity Assessment in Zebrafish*, in *Zebrafish*. 2011, John Wiley & Sons, Inc. p. 15-25.
140. Zhu, J.J., et al., *Human cardiotoxic drugs delivered by soaking and microinjection induce cardiovascular toxicity in zebrafish.* J Appl Toxicol, 2014. **34**(2): p. 139-48.
141. Schindelin, J., et al., *Fiji: an open-source platform for biological-image analysis.* Nat Meth, 2012. **9**(7): p. 676-682.
142. Griffiths, G., et al., *Nanobead-based interventions for the treatment and prevention of tuberculosis.* Nat Rev Microbiol, 2010. **8**(11): p. 827-34.
143. Cooper, D.L. and S. Harirforoosh, *Design and Optimization of PLGA-Based Diclofenac Loaded Nanoparticles.* PLoS ONE, 2014. **9**(1): p. e87326.
144. Danhier, F., et al., *PLGA-based nanoparticles: An overview of biomedical applications.* Journal of Controlled Release, 2012. **161**(2): p. 505-522.
145. Mohammad, A.K. and J.J. Reineke, *Quantitative Detection of PLGA Nanoparticle Degradation in Tissues following Intravenous Administration.* Molecular Pharmaceutics, 2013. **10**(6): p. 2183-2189.
146. Kolhar, P., et al., *Using shape effects to target antibody-coated nanoparticles to lung and brain endothelium.* Proc Natl Acad Sci U S A, 2013. **110**(26): p. 10753-8.
147. Muttil, P., et al., *Inhalable microparticles containing large payload of anti-tuberculosis drugs.* Eur J Pharm Sci, 2007. **32**(2): p. 140-50.
148. Buckley, N.A., I.M. Whyte, and A.H. Dawson, *Cardiotoxicity More Common in Thioridazine Overdose than with Other Neuroleptics.* Clinical Toxicology, 1995. **33**(3): p. 199-204.
149. Couvreur, P. and C. Vauthier, *Nanotechnology: intelligent design to treat complex disease.* Pharm Res, 2006. **23**(7): p. 1417-50.
150. Korzeniewski, C. and D.M. Callewaert, *An enzyme-release assay for natural cytotoxicity.* J Immunol Methods, 1983. **64**(3): p. 313-20.
151. Clinical Pharmacy Team, M.H., NHS Lothian Pharmacy Services *Shared Care Protocol and information for GPs – thioridazine for treatment of schizophrenia*. 2012 [cited 2014 25.08.2014]; Available from: http://www.ljf.scot.nhs.uk/SharedCareofMedicines/SCP/scp/thioridazine v5.pdf.
152. Lindsey, B.W., F.M. Smith, and R.P. Croll, *From inflation to flotation: contribution of the swimbladder to whole-body density and swimming depth during development of the zebrafish (Danio rerio).* Zebrafish, 2010. **7**(1): p. 85-96.
153. McCollum, C.W., et al., *Developmental toxicity screening in zebrafish.* Birth Defects Research Part C: Embryo Today: Reviews, 2011. **93**(2): p. 67-114.
154. Lindsey, B.W., et al., *Effects of simulated microgravity on the development of the swimbladder and buoyancy control in larval zebrafish (Danio rerio).* Journal of Experimental Zoology Part A: Ecological Genetics and Physiology, 2011. **315A**(5): p. 302-313.

155. Amaral, L., et al., *Thioridazine cures extensively drug-resistant tuberculosis (XDR-TB) and the need for global trials is now!* International Journal of Antimicrobial Agents, 2010. **35**(6): p. 524-526.
156. Jordao, L., et al., *On the killing of mycobacteria by macrophages.* Cell Microbiol, 2008. **10**(2): p. 529-48.
157. Wayne, L.G. and L.G. Hayes, *An in vitro model for sequential study of shiftdown of Mycobacterium tuberculosis through two stages of nonreplicating persistence.* Infect Immun, 1996. **64**(6): p. 2062-9.
158. Boon, C., et al., *Proteins of Mycobacterium bovis BCG Induced in the Wayne Dormancy Model.* Journal of Bacteriology, 2001. **183**(8): p. 2672-2676.
159. Sani, M., et al., *Direct visualization by cryo-EM of the mycobacterial capsular layer: a labile structure containing ESX-1-secreted proteins.* PLoS Pathog, 2010. **6**(3): p. e1000794.
160. Makino, K., et al., *Efficient intracellular delivery of rifampicin to alveolar macrophages using rifampicin-loaded PLGA microspheres: effects of molecular weight and composition of PLGA on release of rifampicin.* Colloids and Surfaces B: Biointerfaces, 2004. **36**(1): p. 35-42.
161. Adams, K.N., J.D. Szumowski, and L. Ramakrishnan, *Verapamil, and its metabolite norverapamil, inhibit macrophage-induced, bacterial efflux pump-mediated tolerance to multiple anti-tubercular drugs.* J Infect Dis, 2014. **210**(3): p. 456-66.
162. Gordon, S. and P.R. Taylor, *Monocyte and macrophage heterogeneity.* Nat Rev Immunol, 2005. **5**(12): p. 953-964.
163. Petricevich, V.L., et al., *Macrophage activation, phagocytosis and intracellular calcium oscillations induced by scorpion toxins from Tityus serrulatus.* Clin Exp Immunol, 2008. **154**(3): p. 415-23.
164. Suzu, S., et al., *M-CSF-mediated macrophage differentiation but not proliferation is correlated with increased and prolonged ERK activation.* Journal of Cellular Physiology, 2007. **212**(2): p. 519-525.
165. Lee, C. and J. Hu, *Cell density during differentiation can alter the phenotype of bone marrow-derived macrophages.* Cell & Bioscience, 2013. **3**(1): p. 30.
166. Hazan, R., et al., *A method for high throughput determination of viable bacteria cell counts in 96-well plates.* BMC Microbiology, 2012. **12**(1): p. 259.
167. Fan, F. and K.V. Wood, *Bioluminescent assays for high-throughput screening.* Assay Drug Dev Technol, 2007. **5**(1): p. 127-36.
168. Promega Corporation *Protocols and Applications Guide. Chapter 8: Bioluminescent reporters*. 2011.
169. Zhang, T., et al., *Rapid assessment of antibacterial activity against Mycobacterium ulcerans by using recombinant luminescent strains.* Antimicrob Agents Chemother, 2010. **54**(7): p. 2806-13.
170. Kumbar, S., C. Laurencin, and M. Deng, *Natural and Synthetic Biomedical Polymers*. 2014: Elsevier Science.
171. Kamei, S., et al., *New method for analysis of biodegradable polyesters by high-performance liquid chromatography after alkali hydrolysis.* Biomaterials, 1992. **13**(13): p. 953-958.
172. Song, X.R., et al., *Reversion of multidrug resistance by co-encapsulation of vincristine and verapamil in PLGA nanoparticles.* Eur J Pharm Sci, 2009. **37**(3-4): p. 300-5.
173. Van Bambeke, F., J.M. Michot, and P.M. Tulkens, *Antibiotic efflux pumps in eukaryotic cells: occurrence and impact on antibiotic cellular pharmacokinetics,*

pharmacodynamics and toxicodynamics. J Antimicrob Chemother, 2003. **51**(5): p. 1067-77.
174. Akiyama, S., et al., *Circumvention of multiple-drug resistance in human cancer cells by thioridazine, trifluoperazine, and chlorpromazine.* J Natl Cancer Inst, 1986. **76**(5): p. 839-44.
175. Spengler, G., et al., *Thioridazine induces apoptosis of multidrug-resistant mouse lymphoma cells transfected with the human ABCB1 and inhibits the expression of P-glycoprotein.* Anticancer Res, 2011. **31**(12): p. 4201-5.
176. Cao, C.X., *J774 macrophages secrete antibiotics via organic anion transporters.* The Journal of infectious diseases, 1992. **165**(2): p. 322-328.
177. BD Diagnostics, *Difco & BBL Manual of Microbiological Culture Media, Second edition*, Mary Jo Zimbro, et al., Editors. 2009.